DEVELOPMENT OF A METHOD TO CREATE SUBJECT SPECIFIC COCHLEAR MODELS FOR ELECTRIC HEARING

by

Tiaan Krynauw Malherbe

Submitted in partial fulfilment of the requirements for the degree

Master of Engineering (Bio-Engineering)

in the

Faculty of Engineering, the Built Environment and Information Technology

UNIVERSITY OF PRETORIA

April 2009

And He said to me,

"My grace is sufficient for you, for My strength is made perfect in weakness."…

2 Corinthians 12:9

UNIVERSITEIT VAN PRETORIA
UNIVERSITY OF PRETORIA
YUNIBESITHI YA PRETORIA

DEVELOPMENT OF A METHOD TO CREATE SUBJECT SPECIFIC COCHLEAR MODELS FOR ELECTRIC HEARING by

Tiaan Malherbe

Supervisor: Prof T Hanekom

Co-supervisor: Prof JJ Hanekom

Department of Electrical, Electronic and Computer Engineering

Master of Engineering (Bio-Engineering)

Summary

Cochlear implants are electronic devices intended for restoring hearing to the profoundly deaf. Unfortunately the degree of restored hearing varies greatly between subjects. To investigate some of the mechanisms that determine this variability, mathematical models of the auditory system are used. The level of detail that these models incorporate varies greatly. The present study describes the development of a method to create high detail, subject specific cochlea models. µ-CT scans and photomicrographs were used to obtain the morphology and histology of a specific guinea pig cochlea. A 3D model was constructed from this data and the finite element method was used to determine the potential distribution inside the cochlea. The potential distribution was calculated for different stimulus protocols applied to different modelled electrodes. A neuron model was then used to obtain neural excitation profiles.

The modelled excitation profiles were compared to data from literature and it was found that this model is valid and can be used as a tool in electric hearing research. The model output was also compared to brainstem response data from the specific subject to assess the degree to which this model can predict brain stem data from a specific subject. Possible improvements to the model were also discussed.

Keywords: 3D model, brain stem response data, cochlear model, EABR, FEM model, neural model, subject specific, µ-CT scan.

UNIVERSITEIT VAN PRETORIA
UNIVERSITY OF PRETORIA
YUNIBESITHI YA PRETORIA

ONTWIKKELING VAN 'N METODE OM GEBRUIKER SPESIFIEKE KOGLEÊRE MODELLE VIR ELEKTRIESE GEHOOR TE SKEP deur

Tiaan Malherbe

Leier: Prof T Hanekom

Medeleier: Prof JJ Hanekom

Departement Elektriese, Elektroniese en Rekenaar-Ingenieurswese

Meester van Ingenieurswese (Bio-Ingenieurswese)

Opsomming

Kogleêre inplantings is elektroniese toestelle wat bedoel is om gehoor te herstel aan persone met ernstige doofheid. Die graad van herstelde gehoor verskil ongelukkig baie tussen gebruikers. Wiskundige modelle word gebruik om die meganismes wat hierde verskille veroorsaak te ondersoek. Die graad van detail wat hierdie modelle inkorporeer wissel baie. Die huidige studie beskryf die ontwikkeling van 'n metode om gebruiker spesifieke kogleêre modelle te skep. Mikrorekenaartomografie aftasbeelde en mikrofotos is gebruik om die morfologie en histologie van 'n spesifieke marmot koglea te verkry. 'n Drie dimensionele model is geskep vanaf hierdie data en die eindige element metode is gebruik om die spanningsverspreiding in die koglea te verkry. Die spanningsverspreiding is uitgewerk vir verskillende stimulasie protokolle wat op verskillende gemodelleerde elektrodes toegepas is. 'n Neuron model is gebruik om die neurale aktiveringsprofiele te verkry.

Die gemodelleerde aktiveringspatrone is vergelyk met data vanaf ander studies en dit was gevind dat die model geldige resultate lewer en dat dit as 'n navorsingsinstrument gebruik kan word. Die uitsette van die model was ook vergelyk met breinstam respons data vanaf die spesifieke gebruiker. Dit is gedoen om die mate waarin die model breinstam respons data kan voorspel te ondersoek. Moontlike verbeterings wat aan die model gemaak kan word is ook bespreek.

Sleutelwoorde: 3D model, breinstam respons data, eindige element model, kogleêre model, Mikrorekenaartomografie, neuron model.

List of abbreviations

BP	Bi-polar
CF	Characteristic Frequency
CI	Cochlear implant
CT	Computed tomography
EABR	Electrically evoked auditory brainstem response
FE	Finite element
FEM	Finite element method
IC	Inferior colliculus
MP	Monopolar
STC	Spatial tuning curve
TP	Tri-polar
µ-CT	Micro computed tomography

Table of contents

CHAPTER 1 INTRODUCTION

1.1 PROBLEM STATEMENT

1.1.1 Background and Context

Cochlear implants are electronic devices that are able to restore hearing to profoundly deaf persons. Research in the development of these devices has been active since the 1970's. Since the first commercial device became available in the mid 1980's, more than 100 000 people have had implants worldwide (Middlebrooks and Snyder, 2008).

Cochlear implants differ from normal hearing aids. Normal hearing aids simply amplify sounds whereas cochlear implants stimulate the acoustic nerves electrically. An electrode array is implanted into the cochlea in the inner ear of a person through a complex surgical procedure. Sounds are picked up by an external microphone connected to a speech processor that digitally encodes the sound signal. This is worn behind a user's ear, much like a normal hearing aid. This signal is then transmitted through the skin to an implanted processor. This processor sends current pulses to the electrode array implanted in the cochlea. These current pulses cause the cochlear neurons to fire and these firings are perceived by the brain as sound.

Although most implant users can hear again, the quality of what they hear varies dramatically between users. Speech perception performance is especially varied (Kunisue, Fukushima, Kawasaki, Maeda, Nagayasu, Kataoka, Kariya, Fukutomi, Takami and Nishizaki, 2007). Some of the factors that contribute to this variability are the duration of cochlear implantation and duration of deafness (Blamey, Arndt, Bergeron, Bredberg, Brimacombe, Facer, Larky, Lindström, Nedzelski, Peterson, Shipp, Staller and Whitford, 1996; Bouchard, Ouellet and Cohen, 2009; Dawson, Blamey, Rowland, Dettman, Clark, Busby, Brown, Dowell and Rickards, 1992; Friedland, Venick and Niparko, 2003; Geers, Tobey, Moog and Brenner, 2008; Mosnier, Sterkers, Bebear, Godey, Robier, Deguine, Fraysse, Bordure, Mondain, Bouccara, Bozorg-Grayeli, Borel, Ambert-Dahan and Ferrary, 2009; Rubinstein, Parkinson, Tyler and Gantz, 1999), age of implantation (Hassanzadeh, Farhadi, Daneshi and Emamdjomeh, 2002), speech perception before implantation (Friedland et. al., 2003; Rubinstein et. al., 1999), speech processing algorithm used (Kim, Shim, Chung, Chang and Choi, 1997; Loizou, Stickney, Mishra and Assmann, 2003; Skinner, Holden, Whitford, Plant, Psarros and Holden, 2002a), design of the electrode

array (Rebscher, Hetherington, Snyder, Leake and Bonham, 2007) and position of the electrode array in the cochlea (Finley, Holden, Holden, Whiting, Chole, Neely, Hullar and Skinner, 2008).

One way to investigate the effect that electrode design and electrode position has on speech perception is to implant different users with different arrays and measure their speech perception quantitatively. This is, however, not viable as implantation involves a complex and high risk surgical operation which is expensive and may cause damage to the cochlea if it is repeated. An alternative to using human subjects is to use animal subjects as models of the human auditory system. Speech perception cannot be measured using animals, but electrically evoked auditory brain stem responses (EABR) can be measured to give a gross indication of the cochlear neurons that are activated. Most of the research being done on the effects of electrode design and location are conducted using cats and guinea pigs (Rebscher et. al., 2007; Shepherd, Hatsushika and Clark, 1993; Snyder, Middlebrooks and Bonham, 2008; Van Den Honert, Finley and Xue, 1997). Experiments using these animals also require surgical implantation of electrode arrays. The cost of these surgeries is minimal compared to human surgeries, but still requires time. Specialized hardware is also needed to stimulate and record responses. To simplify the research process and to reduce the time it takes to obtain results, especially from a large number of experiments, computer models of the cochlea have been developed (Choi, Lai and Chen, 2004; Frijns, Briaire and Grote, 2001; Frijns, Briaire and Schoonhoven, 2000; Frijns, de Snoo and Schoonhoven, 1995; Girzon, 1987; Hanekom, 2001a; Hanekom, 2001b; Rattay, Leao and Felix, 2001).

These models vary in detail and are based on generic cochleae of guinea pigs and humans. In reality the geometry of the cochlea varies between subjects of the same species. This is seen in the slight differences in volume of cochlear fluid spaces of different guinea pigs (Salt, Henson, Gewalt, Keating, DeMott and Henson, 1995). The aforementioned models do not accommodate these variances and are thus not ideally suited to investigate the factors that determine variability in implant efficacy between specific implanted subjects. To investigate this, subject specific models are required. A method to rapidly develop such a subject specific model is needed.

1.1.2 Research Gap

To investigate the factors that determine variability in implant performance between subjects, subject specific models are required. Current cochlear models do not incorporate the morphological detail of specific cochleae. They rather use a model with a generalized morphology and place the electrode array in approximately the same location as the electrode array of the subject determined by imaging techniques.

Other areas of cochlear implant research such as the areas of current focussing and beam steering also require knowledge of the precise spatial spread inside the cochlea of a subject (Bonham and Litvak, 2008; Van Den Honert and Kelsall, 2007). Subject specific models could aid in determining this spread.

This study aims to develop a method to construct a high detail cochlear model based on the geometry and electrode configuration of a specific subject. An animal model (guinea pig) will be used to facilitate the development process. The purpose of this model is to simulate electrical current spread inside the cochlea so that the neural response of a specific user as a result of a certain stimulus may be estimated.

1.2 RESEARCH OBJECTIVE AND QUESTIONS

The objective of this study is to construct a subject specific cochlear model that is capable of estimating the neural response as a result of specific electrical stimulus. An animal model (guinea pig) will be used to facilitate the development process. The modelling method developed in the construction of this model may then be used in research where models based on the general morphology of a species are not adequate in describing inter subject differences.

This study will aim to answer the following research questions:

1. Is it possible to construct a subject specific cochlear model using available technology?

2. Is such a subject specific model able to predict neural responses in more detail than generic models?
3. To what extent does the output of this model compare to brain stem response data obtained from the same guinea pig subject?

1.3 HYPOTHESIS AND APPROACH

The hypotheses are that it is possible to develop a subject specific cochlear model, that it is a viable research tool and that it will be able to predict responses in more detail than generic models because of the increase in morphologic detail it incorporates.

To investigate these hypotheses, and to answer the research questions, a 3D model of a specific guinea pig subject will be developed. This model will incorporate the geometric detail of the implanted cochlea of the specific subject.

To assess if this model is a viable research tool, it will be determined if it is capable of predicting outcomes commonly found using generic models. This will validate the model and show that it is capable of at least the same level of performance as generic models commonly used in research. This will be done by employing a generic electrode array and not the array of the specific subject. To investigate if it is capable of predicting responses in more detail than generic cochlear models, the subject specific array will be employed. The results will be screened for trends not predicted by generic models. If these differing trends can be explained in the light of the increase in geometric detail of the model, the hypothesis will be proved.

To investigate a potential use of such a subject specific model, the output of the model will be compared to acoustic brain stem response data obtained from the specific guinea pig. This will assess the measure to which such a model may be used to predict EABR responses and where improvements may be made for more accurate results.

1.4 OVERVIEW OF THE STUDY

The following section briefly describes the steps taken to conduct this study. Figure 1.1 shows a diagram of these steps.

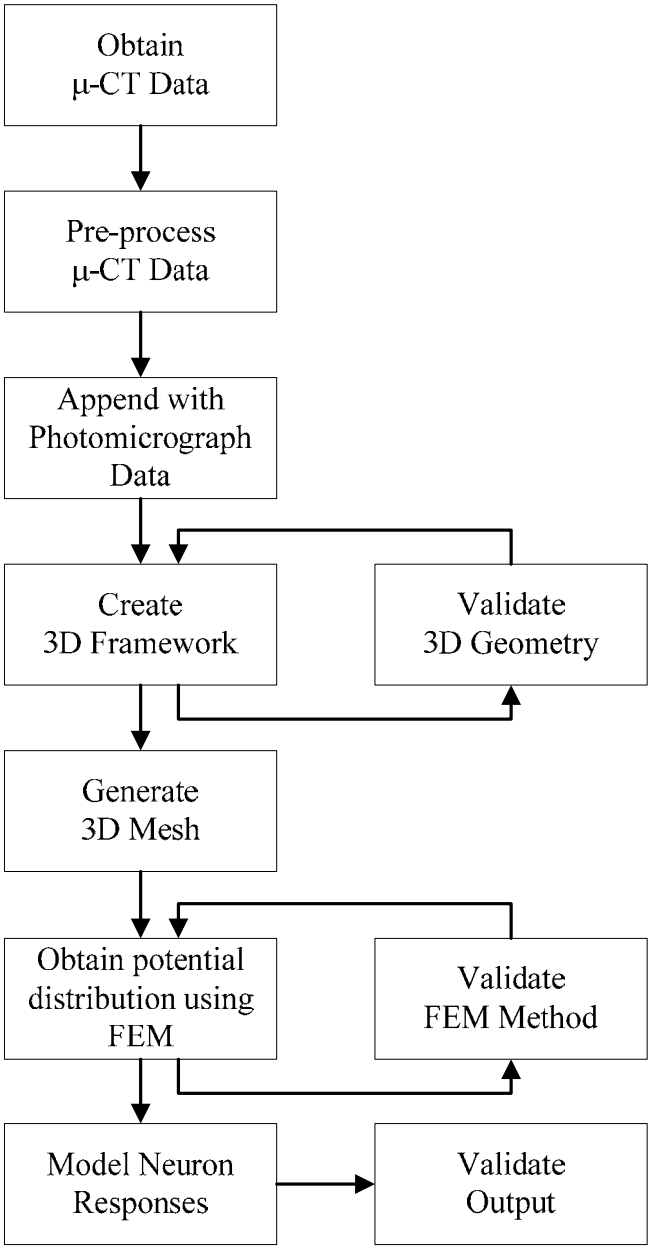

Figure 1.1. Steps taken to develop subject specific cochlear model.

A micro computer tomography (µ-CT) scanner was used to obtain the geometry of the cochlea of a specific subject. µ-CT imaging, although best suited for this application, still posed problems in obtaining an accurate geometry. µ-CT images have sufficient detail to describe the morphology of the cochlear bone, but lack the detail to describe the finer inner cochlear structures. The positions of the inner structures were estimated using data from photomicrograph data. The metal of the electrode contacts also caused artefacts on the µ-CT images. Image processing had to be done to obtain clear images of the cochlea.

A 3D framework model was constructed from this data. The geometry was validated by comparing it to guinea pig cochlea data found in literature before continuing to the next step. A mesh was then generated from the framework and finite element modelling (FEM) software was used to determine the potential distribution inside the cochlea. The FEM method was validated and the potentials at the locations of the neuron nodes were then obtained and used as an input to a cochlear neuron model developed by Frijns *et. al.* (1995). The neuron model was used to obtain the stimulus threshold currents of each cochlear neuron.

First the response to stimulation using a generic electrode array was modelled and the model output was compared to outcomes found in literature. This aided in validating the model. The subject specific electrode array was then modelled. The threshold curves obtained from the model were then compared to data from the guinea pig subject and conclusions as to the extent to which the model can predict brainstem data from the specific subject was investigated. This data came in the form of electrically evoked auditory brainstem responses (EABR) and was obtained by Bonham *et. al.*[1] using an electrode array inserted into the central nucleus of the inferior colliculus of the animal.

[1] Unpublished data via personal communication with Ben H. Bonham – Epstein Laboratory, Department of Otolaryngology – HNS, Box 0526, U490, University of California, San Francisco, CA 94143-0526, United States

1.5 OUTLINE

This dissertation is divided into six chapters.

Chapter 1 is the current chapter and describes the background to the research problem and the hypothesis.

Chapter 2 includes a study of the literature pertaining to the various aspects of modelling a subject specific cochlea.

Chapter 3 describes the steps taken to develop such a model.

Chapter 4 summarizes the output data obtained from the model.

Chapter 5 discusses these results in the context of the research questions asked.

Chapter 6 lists the references to literature used in this document.

CHAPTER 2 LITERATURE STUDY

2.1 INTRODUCTION

The efficacy of cochlear implants varies greatly between individual users. The mechanisms responsible for this variability are not fully understood. To effectively investigate the mechanisms that influence this variability, mathematical models are used. This chapter summarizes the literature pertaining to the development of such a model.

2.2 BACKGROUND ON COCHLEAR IMPLANTS

Cochlear implants are prosthetic devices that allow persons with little or no hearing to hear to a certain extent. This is achieved by stimulating surviving cochlear neurons via an electrode array implanted into the cochlea. The pulses applied to the electrodes are provided by an external speech processor which encodes sound picked up by an external microphone into short pulses. The external speech processor communicates with the implanted electronics via a transcutaneous link.

Some of the seminal work on cochlear implants was done by Simmons in 1966 (Simmons, 1966). He was of the first to investigate the effect that artificial nerve stimulation could have on hearing. The electrodes he implanted near the modiolus of a patient did not succeed in enabling the patient to perceive speech, but did pave the way for further research.

Since then numerous advances in this field have been made. Some of the first single channel implants allowed users to perceive environmental sounds and identify a few words, but speech perception was poor (Brackmann, 1976; Michelson, Merzenich, Pettit and Schindler, 1973). Today, multichannel electrode arrays with advanced speech encoding and stimulation strategies allow some users to perceive speech without visual cues and enable them to use the telephone. In some cases implants have allowed pre-lingually deaf children to learn language skills at close to the same rate as normal hearing children (Bouchard et. al., 2009) and have provided a large improvement in the quality of life of the users (Klop, Briaire, Stiggelbout and Frijns, 2007; Schorr, Roth and Fox, 2009).

Despite these advances there still remains large variability in speech perception performance between individual subjects (Kunisue et. al., 2007). Some of the factors that contribute to this variability are the duration of cochlear implantation and duration of deafness (Blamey et. al., 1996; Bouchard et. al., 2009; Dawson et. al., 1992; Friedland et. al., 2003; Geers et. al., 2008; Mosnier et. al., 2009; Rubinstein et. al., 1999), age of implantation (Hassanzadeh et. al., 2002), speech perception before implantation (Friedland et. al., 2003; Rubinstein et. al., 1999), speech processing algorithm used (Kim et. al., 1997; Loizou et. al., 2003; Skinner et. al., 2002a), design of the electrode array (Rebscher et. al., 2007) and position of the electrode array in the cochlea (Finley et. al., 2008).

In this study a model is developed to investigate the effect that electrode position has on neural excitation profiles.

Studies have shown that cochlear neurons start to degenerate if they are not stimulated for a prolonged period of time (Nadol Jr., 1990; Schuknecht, 1993; Vollmer, Beitel, Snyder and Leake, 2007). Another study has shown that neural degeneration is dependent on the cause of deafness (Teufert, Linthicum and Connell, 2006). The hearing performance of a subject, including speech perception, is directly dependent on the state of the neurons and the ability of the electrodes to excite them. In order for an electrode to excite a neuron, the neuron has to fall within the voltage distribution area of the electrode. This voltage distribution is determined by the geometry of the cochlea as well as the geometry and position of the electrode array in the cochlea (Rebscher et. al., 2007). It is thus necessary to develop a cochlear model that accurately models the geometry and conductive properties of the cochlea (also referred to as a volume conduction model in some literature).

2.3 VOLUME CONDUCTION TECHNIQUES

2.3.1 Introduction

A variety of volume conduction models have been developed for use in cochlear implant research. These models vary in complexity and scope of problems they can be used for. The following techniques may be used to determine the conduction patterns in a volume.

- Lumped parameter models
- Boundary element method (BEM)
- Finite element method (FEM)
- Finite difference method (FDM)
- Finite volume method (FVM)

2.3.2 Lumped parameter models

Lumped parameter models represent the geometric properties of a volume conductor with a resistor and capacitor network (Briaire and Frijns, 2000). This method has the advantage that capacitive effects are relatively easy to incorporate because of the network structure. Another advantage is that computer simulations are faster and less complex than finite element and finite difference methods (Suesserman and Spelman, 1993).

The lumped parameter modelling technique may be applied to find the potential distribution in a cochlea (Strelioff, 1973). This is done by dividing the unrolled cochlea into sections and modelling each section as a network of resistors, capacitors and voltage sources. These sections are then joined together to form a circuit that represents the potential distributions across the entire cochlea. The potential at any point in the cochlea may then be obtained by analyzing this circuit using a computer circuit simulation program such as SPICE.

These models are, however, not refined because circuit elements represent large areas of tissue and fluids (Suesserman and Spelman, 1993). They are thus more suited to modelling global effects in biomedical applications and not effects on a neuron level (Briaire and Frijns, 2000).

2.3.3 BEM

The boundary element method (BEM) is used to solve linear partial differential equations that have been formulated as integral equations (Cheng and Cheng, 2005). In this method only the boundary values are calculated instead of the values of the entire space described by the partial differential equation. This makes it a more computer resource efficient method than volume discretisation methods for some problems (FEM, FDM and FVM) (Cheng and Cheng, 2005). In some instances the BEM becomes less efficient. This is because BEM results in fully populated matrices that cause storage requirements and computing time to grow according to the square of the problem size. Volume discretisation methods result in banded matrices that cause storage requirements and computing time to rise linearly to the problem size.

To obtain the potential distribution caused by a current source in a piece-wise homogeneous volume conductor, Green's second theorem is used in the BEM (Briaire and Frijns, 2000). This results in a differential equation to be solved.

A mesh is then generated in the shape of the volume conductor. The BEM requires that only the boundaries between volumes with different conductivities be used in calculations. Equations describing these boundaries are then solved simultaneously.

2.3.4 FEM

To apply the finite element method (FEM), a continuous domain is discretized into a set of smaller sub domains (Clough, 1990) that can be described by their own partial derivative equations. The finite element method is then used to find approximate solutions to these equations. A disadvantage of this method is that mesh generation may be difficult and the entire volume has to be rediscretized when a small change is made to the geometry. The advantage of this method is that capacitive effects and anisotropic materials may be incorporated in a biological model (Briaire and Frijns, 2000).

To solve a FEM problem the following operations have to be completed (Burnett, 1987):

- construction of a trial solution,
- application of an optimizing criterion and
- estimation of accuracy.

A trial solution $\overline{U}$ is a solution that approximately satisfies solution. It is generally in the following form:

$$\overline{U}(x;a) = \phi_0(x) + a_1\phi_1(x) + a_2\phi_2(x) + ... + a_N\phi_N(x) \tag{2.1}$$

where x represents the independent variables in the problem, $\phi_0(x)$ to $\phi_N(x)$ are known functions called *trial* or *basis* functions and the coefficients a_0 to a_N are undetermined parameters called *degrees of freedom*.

An optimizing criterion determines the best values of the undetermined parameters a_0 to a_N. There are two types of optimizing criterion namely *Method of weighted residuals* (MWR) which is used when the governing equations are differential equations and the *Ritz variational method* (RVM) which is used when the governing equations are integral equations.

An estimation of accuracy is needed to determine how close the approximate solution is to the exact solution. In most theoretical cases the exact solution is not known. The accuracy may then be estimated by comparing the solutions obtained from different optimizing criteria. The closeness and convergence of these results may give insight into the accuracy of the obtained solution (Burnett, 1987).

Powerful commercial software like COMSOL and ANSYS that employ FEM to solve volume conduction problems are readily available. FEM is used in this study because of its ease of implementation and because the COMSOL software package is readily available.

2.3.5 Finite difference method (FDM)

The finite difference method is similar to the finite element method but has distinct differences. The FDM is an approximation to the differential equation where the FEM is an approximation to the solution. The advantage of FDM is that it is easy to implement. The disadvantage is that it is restricted to simple rectangular shapes and simple alterations thereof. This makes it undesirable for use in complex biomedical modelling. When modelling a cochlea using FDM, a very small mesh has to be used to avoid leakage from the modelled membranes (which are very thin). This leads to large memory requirements and long computation times (Briaire and Frijns, 2000).

To implement the FDM, it can be considered as a subset of FEM with its basis functions chosen as piecewise constant functions or Dirac delta functions. To calculate the potential distribution in a biomedical application, the Taylor expansion of the Poisson equation along a fixed structure of points is calculated and then solved via an iterative process (Briaire and Frijns, 2000).

2.3.6 Finite volume method (FVM)

The finite volume method is used to represent partial differential equations as algebraic equations and to evaluate them (Rübenkönig, 2007). A mesh is created around a geometry just as in the FDM. The value of each node of the mesh is then calculated. The volume around each node is known as a finite volume.

To implement this method, a mesh is firstly created. Governing partial differential equations are then used to describe each node. If a volume integral in a partial differential equation contains a divergence term, it is converted to a surface integral using the Divergence theorem. The values of the nodes are then determined by estimating solutions to the partial differential equations.

2.4 COCHLEAR MODELS

2.4.1 Introduction

The aforementioned volume conduction techniques have been employed in various cochlear models to predict potential distributions inside the cochlea.

The seminal work on cochlear volume conduction modelling was conducted by Strelioff (Strelioff, 1973) in 1973 when he constructed a lumped parameter model that represents the geometric properties of an unrolled cochlea. This model and subsequent lumped parameter cochlea models (Black, Clark, Tong and Patrick, 1983; Jolly, Spelman and Clopton, 1996; Kral, Hartmann, Mortazavi and Klinke, 1998; O'Leary, Black and Clark, 1985; Suesserman and Spelman, 1993) model an unrolled cochlea where the conductance between turns is not taken into account.

The first 3D cochlear model was that of Girzon in 1987 (Girzon, 1987). This model used the Finite difference method. A 3D model of a rotationally symmetric cochlea was developed by Frijns et. al. (Frijns et. al., 1995). A more realistic spiralling 3D model of the second turn of the guinea pig cochlea was developed by Frijns et. al. (Frijns et. al., 2000) this method employed the BEM method. Later they developed a 3D model of the human cochlea (Frijns et. al., 2001) also employing the BEM method. Hanekom developed a detailed spiralling 3D model of the human cochlea and employed FEM (Hanekom, 2001a; Hanekom, 2001b). These models are used for determining the effect of electrode position in a generic cochlear shape. The development of a model that is subject specific with regard to histology and exact electrode placement has not been reported.

Lim et. al. (Lim, Park, Kim, Oh and Kim, 2005) modelled the mechanical behaviour of the electrode array inside the cochlea using FEM. Numerous other cochlear models that are not of direct use in cochlear implant research have been developed for use in other hearing related research fields. The techniques used to developed them are, however, useful in developing a cochlear implant model (Ghiz, Salt, DeMott, Henson, Henson and Gewalt, 2001; Koizuka, Seo, Murakami, Seo and Kato, 1997; Liu, Gao, Yin, Luo and Lu, 2007; Poznyakovskiy, Zahnert, Kalaidzidis, Schmidt, Fischer, Baumgart and Yarin, 2008; Salt et.

al., 1995; Sun, Chang, Dormer, Dyer and Gan, 2002; Thorne, Salt, DeMott, Henson, Henson and Gewalt, 1999; Voie and Spelman, 1995; Voie and Spelman, 1990; Wada, Sugawara, Kobayashi, Hozawa and Takasaka, 1998; Wang, Northrop, Burgess, Liberman and Merchant, 2006; Yin, Zhao, Liu, Shu, Huang, Gao, Zhu, Wu and Luo, 2007). Obtaining accurate geometric and morphological features of a subject specific cochlea is a challenge because of its small size. The imaging techniques used in the generation of these other models may be used to obtain clear images of inter cochlear structures and their dimensions.

2.5 OBTAINING COCHLEAR DIMENSIONS

2.5.1 Introduction

To construct a model of a subject specific implanted cochlea, the dimensions of the cochlea and position of the electrodes have to be estimated accurately. This is challenging because of the small size and intricate geometry of the cochlea and its internal structures. Reissner's membrane is approximately 1.7 µm thick and requires an imaging method with sufficient resolution to determine its position in the cochlea. The type of technique also plays a role in the visibility of structures. A study by Poznyakovskiy *et. al.* (2008) was only able to image Reissner's membrane when they used a computed tomography (CT) scanner with a resolution of 4 µm. When using a 10 µm resolution the membrane was not visible. Whereas using magnetic resonant imaging (MRI) techniques, Koizuka *et. al.* (1997) managed to image Reissner's using an MRI scanner with a resolution of only 25 µm.

The internal structures and ducts of the cochlea have different conductivities. Complex admittances of these tissues were not taken into account in this model as tissue impedances may be well approximated as pure resistivities (Black, Clark and Patrick, 1981). This will influence the potential distribution. It is thus important that the dimensions of these structures be estimated accurately. The following techniques have been used to obtain geometric data of cochleae.

- Physical dissection

- Histologic sectioning
- Video Fluoroscopy
- Orthogonal-plane Fluorescence Optical Sectioning (OPFOS)
- Radiography
- Magnetic Resonant Imaging (MRI)
- Computed tomography (CT)

2.5.2 Physical dissection

In 1952 Fernández (Fernandez, 1952) dissected six guinea pig cochleae and measured the dimensions of the cochlear structures. Measurements were done by magnifying the structures with a camera lucida. This method required that each specimen be stained with hematoxylin-eosainn to highlight histological features. One disadvantage of this method is that small structures such as Reissner's membrane cannot be studied because it gets damaged during dissection because of its thin and fragile membranous structure. Another disadvantage is that measurements from physical dissection cannot be obtained from living subjects. Obtaining measurements from living subjects may be advantageous in future research for constructing subject specific models to optimize implant parameters in a computational environment which may save time.

2.5.3 Histologic Sectioning

Histologic sectioning involves segmentation of the cochlea into thin slices. Before slicing the cochlea it undergoes a chemical preparation which includes decalcification and dehydration. It is then sliced into slices about 25 µm thick and observed using light microscopy (Nadol Jr. and Eddington, 2004). This method provides highly detailed images with a very high resolution of the internal cochlear structures. The disadvantage is that measurements cannot be obtained *in vivo*. Also the Reissner's membrane can sometimes be damaged during dehydration making the boundary between the scala media and scala vestibuli unresolvable. This method is time consuming and requires considerable technical expertise.

2.5.4 Video Fluoroscopy

Video fluoroscopy has been used in the imaging of cadeveric cochleae (Balkany, Eshraghi and Yang, 2002; Roland, Fishman, Alexiades and Cohen, 2000). This method also involves extensive chemical preparation of the cochlea. The resolution obtained using this method is insufficient to distinguish fine cochlear structures and is more suited to determining the position of the electrode contacts relative to the cochlear wall.

2.5.5 Orthogonal-plane Fluorescence Optical Sectioning (OPFOS)

Orthogonal-plane fluorescence optical sectioning was used by Voie (2002) to obtain detailed images of the inner ear and small cochlear structures such as Reissner's membrane. Hofman et. al. (2009) used OPFOS to create a three dimensional model of the guinea pig inner ear. This method also involves fixation, decalcification and dehydration of the cochlea and is not suited for *in vivo* applications.

2.5.6 Radiography

The position of an electrode array inside an implanted cochlear array may be determined using conventional radiography (Cohen, Saunders and Richardson, 2003; Skpizner, Holliday, Roland, Cohen, Waltzman and Shapiro, 1995). This method is commonly used during implant surgery to assess the insertion depth and placement of the array (Chen, Farb, Hanusaik, Shipp and Nedzelski, 1999; Cohen, Xu, Xu and Clark, 1996; Xu, Xu, Cohen and Clark, 2000). The position of individual electrodes relative to the cochlear walls are clearly visible on radiographs (Skpizner et. al., 1995) but smaller 3D structures are not clearly distinguishable (Verbist, Frijns, Geleijns and van Buchem, 2005). Phase-contrast radiography (Xu, Stevenson, Gau, Tykocinski, Lawrence, Wilkins, Clark, Saunders and Cowan, 2001) is a modality of conventional radiographs that produces more detail of the bony structure of the cochlea but still lacks the ability to distinguish between internal cochlear structures.

By using these methods it only takes a few seconds to obtain an image and is suitable for *in vivo* imaging. *In vivo* imaging using radiography does however expose the patient to radiation.

2.5.7 Rotational Tomography (RT)

Rotational tomography (also referred to as Digital Volume Tomography) is based on 3D digital subtraction angiography (Aschendorff, Kubalek, Turowski, Zanella, Hochmuth, Schumacher, Klenzner and Laszig, 2005). This technique has been successfully used post-operatively in imaging the electrode array placement of patients (Aschendorff et. al., 2005). A study by Aschendorff (Aschendorff, Kubalek, Hochmuth, Bink, Kurtz, Lohnstein, Klenzner and Laszig, 2004) suggests that this method predicts the position of the electrode array in the scala tympani and scala vestibuli more accurately than using a 16-slice CT scanner. The disadvantage of this method is that it exposes the patient to radiation.

2.5.8 Magnetic Resonant Imaging (MRI)

Magnetic resonant imaging has been used to image structures inside the guinea pig cochlea (Ghiz et. al., 2001; Koizuka et. al., 1997; Thorne et. al., 1999). Presently the best MRI scanners can achieve a resolution in the order of 3 µm. Studies by Thorne et. al. (1999) and Koizuka et. al. (1997) used a 25 µm scanner to image the scala vestibuli, scala tympani and cochlear duct. The boundaries between these structures were used to estimate the position of Reissner's membrane. Ghiz et. al. have successfully imaged the round window membrane in temporal bones of six specimens.

When imaging implanted ears using MRI, large artefacts arise due to the presence of the magnet in the implant. This magnet is used to keep the external processor worn by the patient in alignment with the implanted coil transcutaneously. This artefact can be in the order of 7 cm wide and totally obstructs the cochlea (Vincent, Ruzza, Vaneecloo and Dubrulle, 2008). Some implants allow the magnet to be removed surgically before an MRI scan. These implants include the HiRes90K from Advanced Bionics (Advanced Bionics, Sylmar, CA) and the CI24M, CI24R (CS) Nucleus Freeform and CI24ABI devices from Cochlear Corporation (Cochlear Corporation, Melbourne, Australia) (Majdani, Leinung, Rau, Akbarian, Zimmerling, Lenarz, Lenarz and Labadie, 2008).

MRI can also cause the implant to heat up. Tests have shown that this temperature rise is below 0.5 °C and within safety limits using 1.5 T and 3 T MRI scanners (Chou, 2007;

Majdani et. al., 2008). Serious demagnetization of the magnet can also occur during 3 T MRI scans which can lead to the external processor not lining up properly with the internal coil (Majdani et. al., 2008).

MRI has successfully been used in the pre-operative imaging of cochleae to assess implant feasibility. Studies have however shown that in some cases CT scans provide superior results (Bettman, Beek, Van Olphen, Zonneveld and Huizing, 2004; Chaturvedi, Mohan, Mahajan and Kakkar, 2006) due to the difficulty of displaying bony structures using MRI.

2.5.9 Computed tomography (CT)

CT scanners work by passing x-rays through a patient where they are attenuated and subsequently measured by detectors. The x-ray tube and detectors rotate around the scanned area while scanning. The signals measured by the detectors are then passed to a computer where image reconstruction takes place (Seeram, 2001).

Current CT scanners provide sufficient resolution to image cochlear structures and has been successfully used by Poznyakovskiy *et. al.* (2008), Shibata *et. al.* (2009) and Postnov *et. al.* (2006) to accurately image the guinea pig cochlea.

2.6 COMPUTED TOMOGRAPHY (CT)

2.6.1 Introduction

Computed tomography (CT) was used to image the guinea pig cochlea in this study. This was done because a 20 µm µ-CT scanner was readily available. This scanner provided sufficient resolution to image the larger bony structures of the cochlea and also provided a cost effective technique to image multiple cochleae.

The seminal work on CT scanning was done by Dr. Godfrey Hounsfield and Allan MacLeod Cormack in the late 1960’s (Seeram, 2001). Dr. Hounsfield is commonly referred as the inventor of the CT scanner. Hounsfield Units (HU) which is used to describe radiation in CT scanning was named after him.

There are different types of CT scanners two of which are direct CT and spiral CT scanners. Direct CT scanners work by scanning a single slice at a time and then moving on to the next slice. Each slice is scanned by rotating the x-ray tube and detectors through 360 degrees. Spiral CT continually rotates the x-ray tube and detectors while it is moved along the axis of the scanned subject (Seeram, 2001). This result in faster scanning times for high volume subjects and lower radiation dosages.

High resolution thin-section direct CT scanners are commonly used for temporal bone imaging (Sorn and Curtin, 1996; Swartz, 1989). These type of scans often require extensive neck extension by the patient which is not always possible (Caldemeyer, Sandrasegaran, Shinaver, Mathews, Smith and Kopecky, 1999). Spiral CT scans, however, is less dependent on the body position of the patient (Kaste, Young, Holmes and Baker, 1997; Luker, Lee and Erickson, 2007). A study conducted by Caldemeyer et. al. (Caldemeyer et. al., 1999) compared spiral CT with conventional direct CT scans of temporal bones. They concluded that using spiral CT scans resulted in higher detailed representations of temporal structures.

Newer methods that produce higher resolution scans with smaller inherent artefacts have also been developed. These involve the use of more advanced scanners and include Tuned Aperture Computed Tomography (TACT) (Sakata, Hareyama, Heil, Henson, Henson Jr., Webber, Nair and Smith, 2007), high-resolution spiral computed tomography (HRSCT) (Seemann, Seemann, Bon, Suckfüll and Englmeier, 1999), flat panel CT scanners (Gupta, Bartling, Basu, Ross, Becker, Pfoh, Brady and Curtin, 2004), Multisection CT (Verbist et. al., 2005) and Microcomputed Tomography (µ-CT) (Lane, Driscoll, Witte, Primak and Lindell, 2007).

Microcomputed Tomography scanners provide high resolution slices that can attain voxel sizes as small as 1 μm^3. This is sufficient for imaging small cochlear structures such as Reissner's membrane which is about 4 µm thick. Poznyakovskiy et. al. (Poznyakovskiy et. al., 2008) obtained highly detailed slices of a guinea pig cochlea using µ-CT and constructed an accurate 3D model of the cochlear ducts. Shibata et. al. successfully imaged Reissner's membrane of human foetal cochleae (Shibata, Matsumoto, Agishi and Nagano,

2009). Postnov et. al. (Postnov, Zarowski, De Clerck, Vanpoucke, Offeciers, Van Dyck and Peeters, 2006) used µ-CT to accurately determine the position of an implanted electrode array.

The metal electrodes cause artefacts on CT scans of cochlear implants and causes the resulting images to be blurred (Ketten, Skinner, Wang, Vannier, Gates and Neely, 1998; Whiting, Bae and Skinner, 2001; Yang, Wang, Skinner, Rubinstein and Vannier, 2000). This makes the determination of the electrode position difficult. A technique to enhance the image quality of the CT scan should be applied to be able to extract the exact position on the electrode array. Such methods are investigated in the following section.

2.6.2 Deblurring techniques

Numerous techniques are used to improve the image quality of CT scans of implanted cochleae. Wang et. al. (Wang, Vannier, Skinner, Cavalcanti and Harding, 1998; Xu et. al., 2000) developed an expectation-maximization (EM)-like iterative deblurring algorithm to achieve super-resolution CT images. This technique is based on the assumption that blurring of the images occurs according to a 3D separable Gaussian point spread function (PSF). This statistical approach produces images with a resolution gain of up to 40% resulting in a CT image with a resolution of 0.1 mm cubic voxels.

A study by Jiang et. al. (Jiang, Wang, Skinner, Rubinstein and Vannier, 2003) uses a blind deblurring method to enhance the resolution of CT scans. This method assumes that an oblique CT image can be approximated as the convolution of an isotropic Gaussian PSF and the actual cross section. Their study focused on the estimation of the PSF parameters so that this method may be applied in a fully automatic basis. Their results indicate a deblurring of up to 24% in implanted cochlear CT images.

Another method developed by Wang et. al. (Wang, Vannier, Skinner, Kalender, Polacin and Ketten, 1996) simply used the level of x-ray absorption of the CT scanner to determine the position of the electrodes. They found that the x-ray absorption coefficient of the platinum electrodes and lead wires is approximately 25000 HU. By only considering voxels with HU values above a certain threshold, the electrode positions could be found.

Because the HU values of the artefact streaks generated by the electrodes are much lower than the HU values of the electrodes, they will not appear after thresholding. This method is used in the present study to obtain the positions of the electrode contacts.

A study by Whiting et. al. (Whiting et. al., 2001) combined CT scans and radiographs to determine the position of the electrode array and anatomical structures. They developed an algorithm to map the points on the CT scans to points on the radiographs. This technique allowed them to determine the position of electrodes relative to inner ear structures to sub millimetre accuracy. This study combines µ-CT scans and photomicrographs to estimate positions of the internal cochlear structures.

2.6.3 Estimating electrode location

The methods used in the previous section focus on extracting clear images from temporal CT scans. To accurately construct a model from these images, the position of the electrode array relative to the inner ear structures should be clear.

Since small structures such as the basilar membrane, organ of Corti and Reisners membrane may not be resolvable on a CT image (Skinner, Ketten, Holden, Harding, Smith, Gates, Neely, Kletzker, Brunsden and Blocker, 2002b), their positions have to be estimated using known geometric data of the cochlea. This was done in a study of the human cochlea by Skinner et. al. (Skinner et. al., 2002b) where the position of these structures were estimated using data obtained by Ketten et. al. (Ketten et. al., 1998).

2.7 NEURON MODELS

The 3D volume conduction methods are capable of estimating the voltage distribution in the cochlea but not capable of estimating the highly non-linear response of nerve fibres. A separate neural model has to be used to translate the voltage distribution patterns of the 3D model into neural responses.

The seminal work on neural modelling was done by Hodgkin and Huxley (Hodgkin and Huxley, 1952). The Hodgkin-Huxley (HH) equations were derived through experimental work done on giant squid axons during the 1950's. Since that time various other neural models such as the Frankenhaeuser-Huxley (Frankenhaeuser and Huxley, 1964), Fitzhugh (Fitzburg, 1969), Chiu et. al. (Chiu, Richie, Rogart and Stagg, 1979), Sweeney et. al. (Sweeney, Mortimer and Durand, 1987) and Schwarz-Eikhof (Schwartz and Eikhof, 1987) models have been developed. The Hodgkin-Huxley model is however still widely used as it is one of the few models that can produce multiple spikes during low frequency sinusoidal stimulation (Hartmann, Topp and Klinke, 1984) as well as produce an action potential when successive sub-threshold pulses are applied (Rattay, Lutter and Felix, 2001). It is especially used when modelling human cochlear neurons where it has been found that a warmed Hodgkin-Huxley model (where gating has been accelerated to more closely match mammilian neurons) matches the behaviour of a cochlear neuron the closest out of all the above mentioned models (Rattay et. al., 2001).

These models however only model the dynamics of a single membrane patch of a neuron. To model complex cochlear neurons that consist of various nodes with different properties, a neural cable model should be used. Models incorporating such cable equations include a cochlear neuron model developed by Rattay (Rattay et. al., 2001) and the Generalized Schwarz-Eikhof-Frijns (GSEF) model (Frijns et. al., 1995).

2.8 IN VIVO MEASUREMENTS

To validate the response obtained from the neuron model, it has to be compared to actual measured neural responses. The aim is to determine which auditory neurons are activated, however current technology does not permit this for large numbers of neurons. A good alternative to direct measurement is used where responses are measured in a tonotopically arranged nucleus in the brain that seems to have tuning similar to the auditory nerve. The hope is that these measurements directly reflect activity of auditory nerve neurons at a specific frequency.

Recording the neural response from the inferior colliculus is common practice in auditory

nervous research (McCreery, Lossinsky and Pikov, 2007; Middlebrooks and Snyder, 2007; Rebscher, Snyder and Leake, 2001; Shivdasani, Mauger, Rathbone and Paolini, 2008; Snyder et. al., 2008; Vollmer et. al., 2007) . This structure is tonotopically arranged so that higher frequency neurons are accessed as the electrode depth increases (Rose, Greenwood, Goldberg and Hind, 1963). A single multi channel electrode array may thus be implanted to infer the activity of a wide range of frequency areas in the cochlea.

The position of these frequency areas in the cochlea may be obtained using Greenwood's equation (Greenwood, 1990). This equation gives the position of characteristic frequencies along the basilar membrane. This will allow the determination of the spatial spread inside the cochlea caused by the current elicited by the electrode array configuration.

2.9 SPATIAL SELECTIVITY OF ELECTRODE ARRAY CONFIGURATION

The extent of the area inside the cochlea that is stimulated is called the spatial spread. This spread has an influence on the effectiveness of the stimulation strategy which ultimately has an effect on hearing performance. Spatial spread also has a direct influence on pitch perception which influences musical perception (Spahr, Litvak, Dorman, Bohanan and Mishra, 2008) and the ability to discriminate between numerous voices speaking at the same time (Drullman and Bronkhorst, 2004).

The electrode configuration and stimulation parameters have an influence on spatial spread. Monopolar stimulation results in broad spatial spread (Cohen et. al., 2003; Snyder et. al., 2008; Van Den Honert and Stypulkowski, 1987), whereas bi-polar and tri-polar stimulation results in narrower spread (Rebscher et. al., 2001; Snyder et. al., 2008). Other field steering techniques employing multiple electrodes have been developed to focus and steer electric fields inside the cochlea. Techniques employing all the electrodes in the array to steer current to a specific location have been developed (Van Den Honert and Kelsall, 2007). Modelling these techniques is difficult because subject specific data is needed. Bonham et. al. (Bonham and Litvak, 2008) investigated current steering techniques that utilize multiple electrodes. They concluded that it is possible to steer the peak activity to locations between the peaks of the individual stimulating electrodes.

Spatial spread is also influenced by the position of the electrode array in the cochlea. Studies have shown that electrode arrays placed closed to the modiolus results in smaller current spread (Cohen, Saunders, Knight and Cowan, 2006; Hanekom, 2001a).

2.10 SUMMARY

This literature study investigated the steps involved in developing a subject specific cochlear model. The current knowledge surrounding these steps was also summarized. This knowledge will be used as a basis for developing a subject specific cochlear model.

CHAPTER 3 METHODS

3.1 CHAPTER OBJECTIVES

This chapter discusses the methods and implementation thereof to develop a cochlear model of a specific guinea pig subject.

3.2 INTRODUCTION

A subject specific model of a guinea pig was developed. A single guinea pig was deafened and implanted with a custom 12 electrode array in the left cochlea by Bonham *et. al.* Cochlear nerve responses were estimated using an electrode array implanted into the central nucleus of the inferior colliculus. Before deafening and implanting the cochlear array, responses to acoustic stimulation of the undeafened ear were recorded to obtain a frequency map of the electrodes implanted into the inferior colliculis. After the physiological study, the cochlea was removed and imaged digitally. This data was then used to create the present model.

To accurately model the guinea pig cochlea the following steps were taken.

1. Obtained subject specific cochlea data
2. Pre-processed µ-CT scan data
3. Extracted key geometric features from µ-CT scan data
4. Generated 3D geometry
5. Verified 3D geometry
6. Determined current distribution inside cochlea
7. Modelled neuron responses
8. Verified neuron responses

These steps are discussed in the subsequent sections.

3.3 DEVELOPMENT OF 3D GUINEA PIG MODEL

3.3.1 Obtaining subject specific cochlea data

Images of the cochlear geometry of a specific guinea pig subject were obtained by Bonham et. al. This was done by obtaining µ-CT scans of the left cochlea of a guinea pig implanted with a 12 electrode array. The µ-CT scanner used produced CT images with a 20 µm voxel size.

The CT-scan data was converted to a 1024 × 1024 × 244 matrix of raw voxels. The intensity of the voxels corresponds to the linear attenuation experienced by the CT source. Different material properties inside the cochlea cause the CT source to be attenuated differently. These attenuation values were used to distinguish between different cochlear structures.

The raw CT matrix was visualized using ImageJ (Wayne Rasband, NIH, public domain software). The Volume Viewer plug-in allows planar slices of the 3D volume to be viewed at any angle. To simplify analysis, the matrix was orientated so that the modiolus of the cochlea lies parallel to the z-axis. The coordinate system was also adjusted so that the center line of the modiolus runs through the origin.

Using the raw CT data, the contrast between cochlear structures is not very clear as seen in Figure 3.1. More definition was obtained by further image processing.

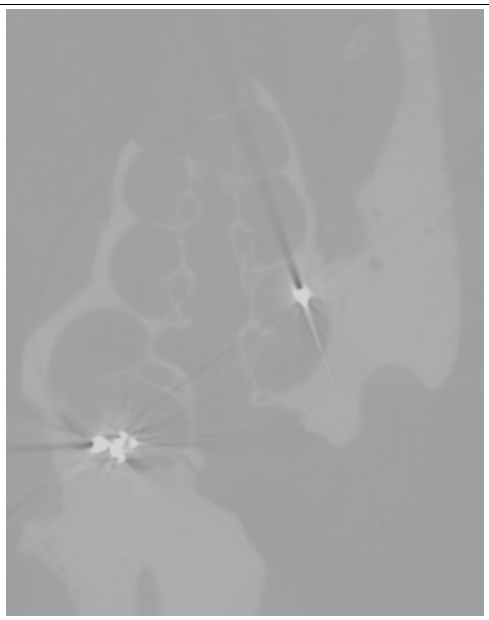

Figure 3.1. Raw µ-CT slice of guinea pig cochlea. Note that contrast between cochlear structures is not optimal.

3.3.2 Pre-processing of µ-CT-scan data

To better visualize different cochlear structures, further image processing is required. To enhance the contrast between structures, a HCA3 colour map was applied using ImageJ (Figure 3.2).

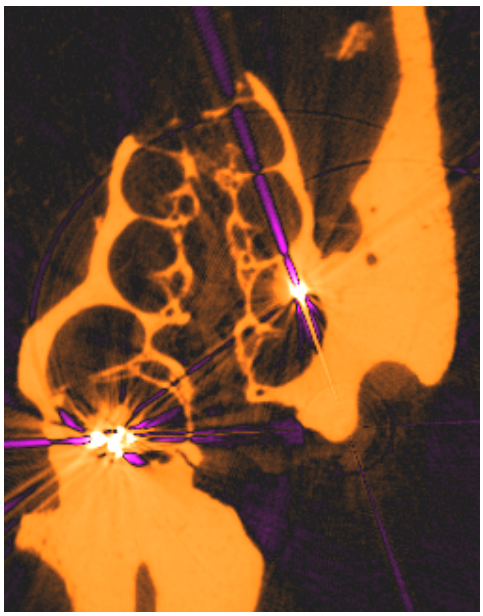

Figure 3.2. µ-CT cochlear slice with colour map applied to enhance contrast between cochlear structures.

To further enhance the boundaries between structures, the "Enhance Contrast" feature in ImageJ was applied (Figure 3.3).

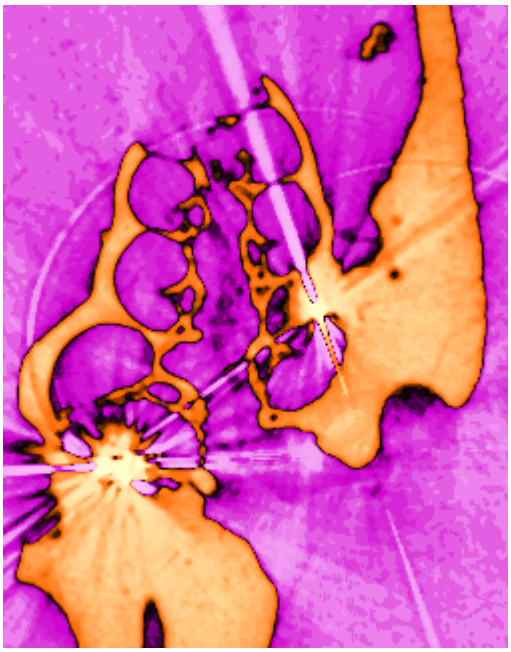

Figure 3.3. µ-CT cochlear slice with enhanced contrast applied in ImageJ. This clarifies the boundaries between structures further.

This enhanced the boundaries between cochlear structures especially the bony structures without any visible detrimental effects to the visibility of smaller structures. Some of the smaller cochlear structures like Reissner's membrane and the organ of Corti are, however, not visible because of the relatively low resolution of the scanner (20 µm voxels) and the inherent limitations that CT scans have on imaging soft tissue. The artefacts caused by the metal electrodes and wires also make the determination of cochlear geometry difficult.

To develop a highly detailed model, these detailed geometry features have to be incorporated into the model. This is done by appending the µ-CT data with data obtained using photomicrographs.

3.3.3 Appending µ-CT data

A mid-modiolar photomicrograph of the guinea pig cochlea was used to obtain the positions of the fine inter cochlear structures such as the organ of Corti and Reissner's

membrane. A photomicrograph of the specific guinea pig from which the µ-CT data obtained was not available. Instead, a photomicrograph of another healthy guinea pig was used (Figure 3.4).

Figure 3.4. Example of mid-modiolar photomicrograph of guinea pig cochlea used to obtain the dimensions and locations of cochlear structures not visible in µ-CT image (Fankhauser, 2008).

Care was taken to ensure that the photomicrograph matched the angle of the CT slice around the modiolus. Individual turn openings of the photomicrograph were then scaled and superimposed on the CT data to obtain the positions of the structures not visible on the CT data (Figure 3.5). The photomicrograph sections were scaled linearly in vertical and horizontal directions independently and positioned to ensure that the bony boundaries of the turn openings line up with the bony boundaries on the µ-CT slice. This allowed the geometry to be estimated even in cases where metal artefacts severely obscure the boundaries of the cochlear ducts. The helicotrema of the subject cochlea under investigation was damaged before µ-CT scanning after the physiological study was completed (Figure 3.3). This region was imaged using photomicrographs. This should not have a profound effect on the accuracy of the results as the stimulating electrodes are implanted near the basal area of the cochlea and are relatively far away from the helicotrema.

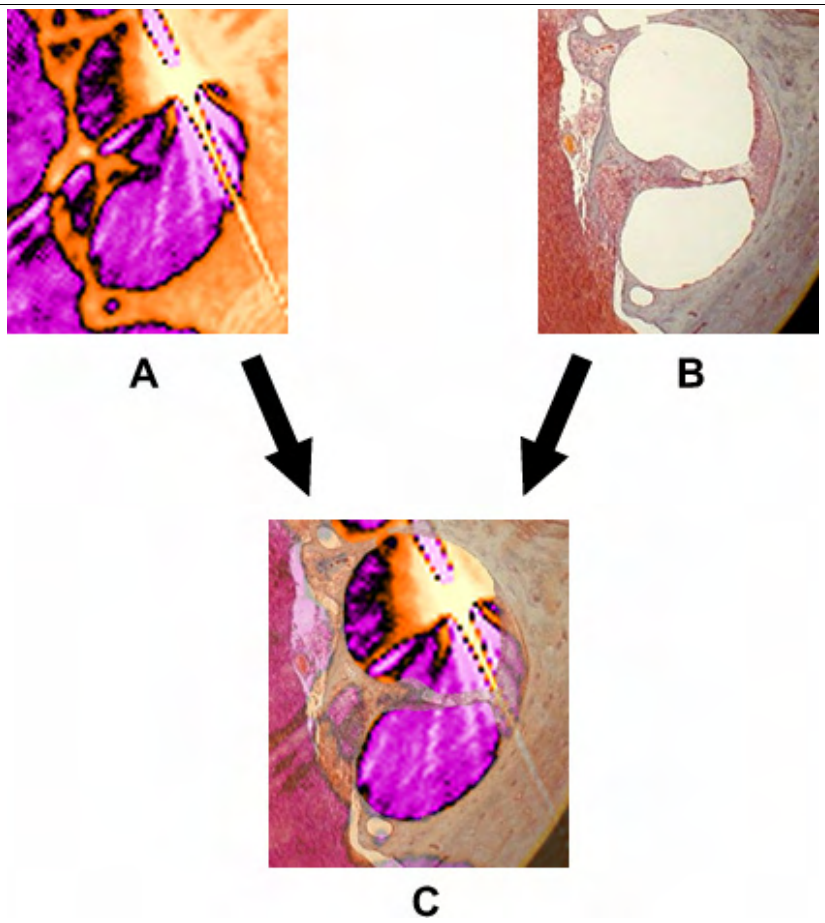

Figure 3.5. Photomicrograph (B) laid over µ-CT image (A) to obtain position of intercochlear structures not visible on µ-CT (C).

Using data from different subjects will also have an influence on the accuracy of the model. The positions of Reissner's membrane, the basilar membrane, organ of Corti and the spiral ligament were obtained mainly from the photomicrograph. These structures are smaller in size than the larger cochlear ducts the sizes of which were accurately obtained from the CT images. The effect of structural errors on volume conduction should thus be small as they take up a smaller percentage of the volume. The position of the nerve fibres is very important for accuracy of the model as the nerve fibre response is required. Fortunately the osseous spiral lamina, which is the bony shelf projecting from the modiolus, is clearly visible on the µ-CT images (Figure 3.6). The cochlear neurons protrude through the osseous spiral lamina (Figure 3.7). Their position can thus be accurately estimated directly from µ-CT data.

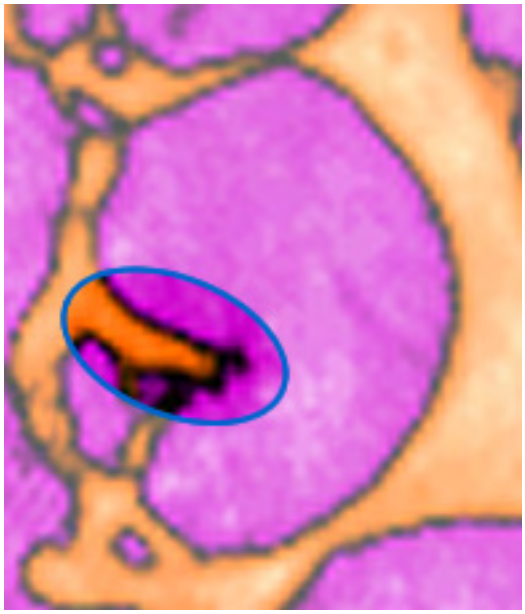

Figure 3.6. Osseous spiral lamina visible in µ-CT image. The Osseous spiral lamina is crucial in estimating cochlear neuron positions.

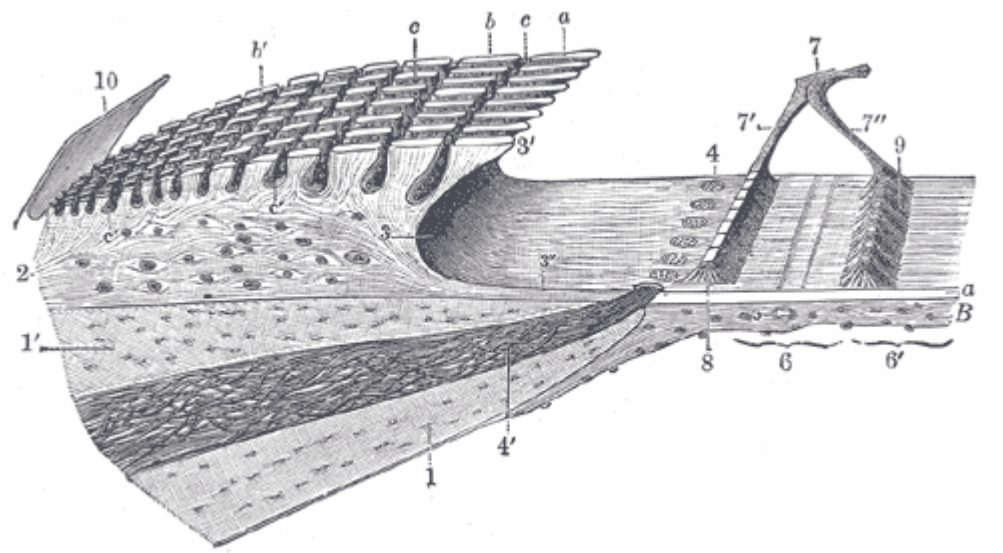

Figure 3.7. Anatomy of the osseous spiral lamina. Cochlear neurons (4' and 4) protrudes through the upper and lower lamellae (1' and 1). (Gray and Lewis, 1918)

The positions and dimensions of the cochlear structures obtained using these techniques were then used to construct a framework of the 3D model.

3.3.4 Creating model framework from cochlear data

The data obtained in the previous section was used to create a framework around which the model was built.

To construct this framework, a mid-modiolar slice was sectioned into the respective cochlear structures. The following cochlear structures were modelled.

- Scala Vestibuli
- Scala Tympani
- Scala Media
- Stria Vascularis
- Spiral Ligament
- Reissners Membrane
- Basilar Membrane
- Organ of Corti
- Nerve
- Osseus Labyrinth (bone case)

Structures not modelled were considered too small to have a significant effect on the current conduction in the model. Also incorporating more detail into the model will increase the mesh complexity and increase computation time of the results. Figure 3.8 shows the sections of a single opening of a mid-modiolar slice.

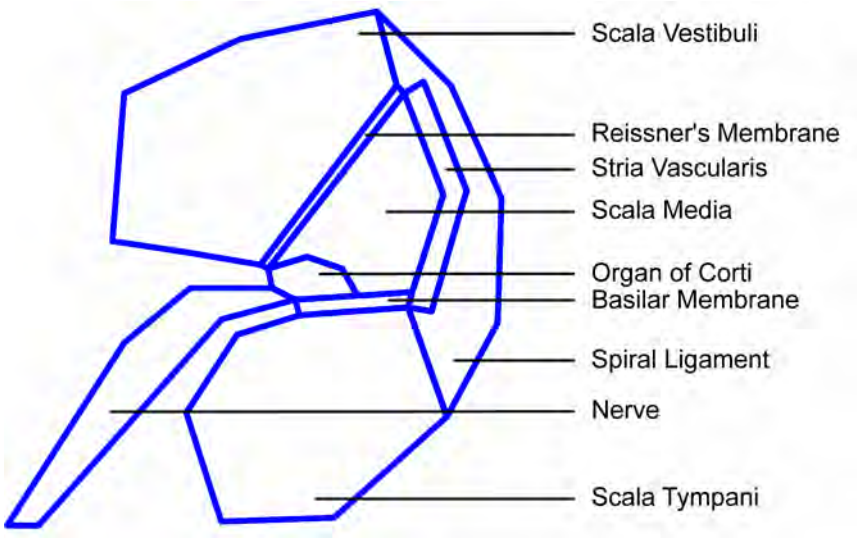

Figure 3.8. Sectioned areas of one cochlear opening in a mid-modiolar slice.

Software was written in Matlab that allows the user to pick points on the boundaries of the cochlear structures from the cochlear image using a mouse. This simplified the segmentation process. The software also automatically adjusted the thickness of the basilar membrane and Reissner's membrane as these structures were made thicker than they are histologically to ease mesh generation (Table 3.1). The new thickness was compensated for by adjusting the resistivities of the structures. This is described in section 3.4.

Table 3.1. Adjusted thicknesses of thin membranes to ease mesh generation.

Structure	**Original thickness**	**Modelled thickness**
Basilar membrane	4 µm	30 µm
Reissner's membrane	1.7 µm	20 µm

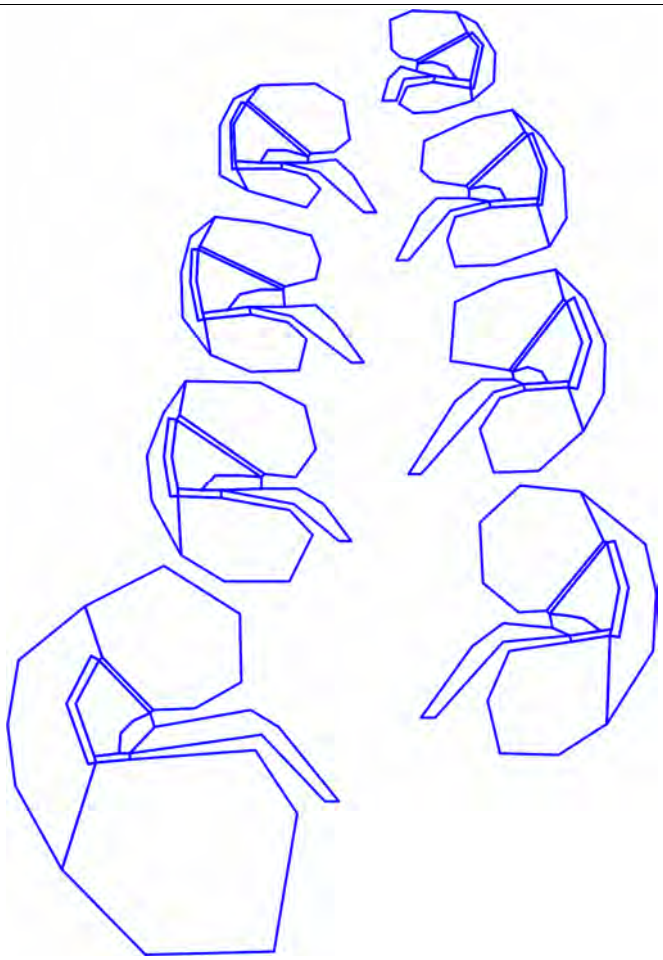

Figure 3.9. Sectioned cochlea used to generate 3D geometry.

Figure 3.9 shows the sections of the all the openings in a mid-modiolar slice. To simplify the modelling process, only one mid-modiolar slice was sectioned. Due to the spiralling nature of the cochlea, the rest of the geometry was generated by interpolating the data from this slice in a spiralling fashion. It was however found that this single slice was insufficient in describing the geometry accurately in the basal region. This is because the start of the base is found at a different angle than the mid-modiolar slice was taken. The mid-modiolar slice was made at an angle where it includes the part of the cochlea just before the helicotrema (Slice A-A in Figure 3.10). The base is not located at the same angle because the cochlea has three and three-quarter turns. The basal part also tapers sharply before the hook area. Two more slices of the basal part of the cochlea were obtained and segmented to accurately describe the geometry. The first slice was made just before the hook area starts (Slice C-C in Figure 3.10); the other slice was made 36° from the first slice measured in an anti-clockwise direction around the modiolus (Slice B-B in Figure 3.10).

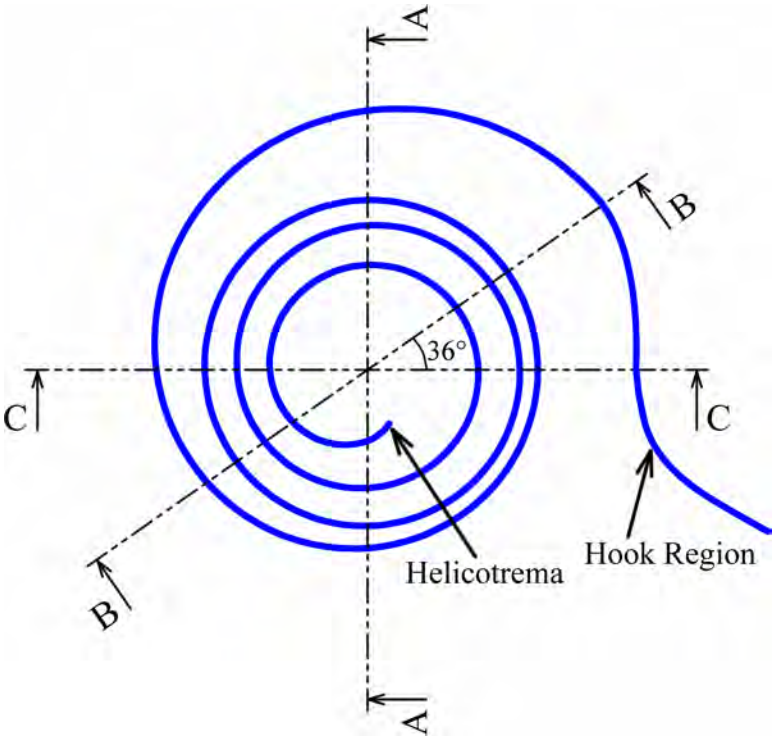

Figure 3.10. Top view of cochlea with positions of imaged slices indicated. Three slices were used to model the geometry. One full slice (A-A) was used in combination with two slices of the basal duct (B-B and C-C) to accurately describe the geometry.

The 3D cochlea geometry was generated by joining the corners of the sections with spirals. These spirals were generated using the middle of the modiolus as centre line. The discrete points on the spirals are characterized by cylindrical coordinates. ρ is the distance from the modiolus centre line, φ is the angle of the point measured in an anticlockwise direction and z is the height of the point. Figure 3.11 illustrates a single spiral generated through a point belonging to the boundary between the scala vestibuli and the spiral ligament. The coordinates of an arbitrary point on the spiral (A) are shown.

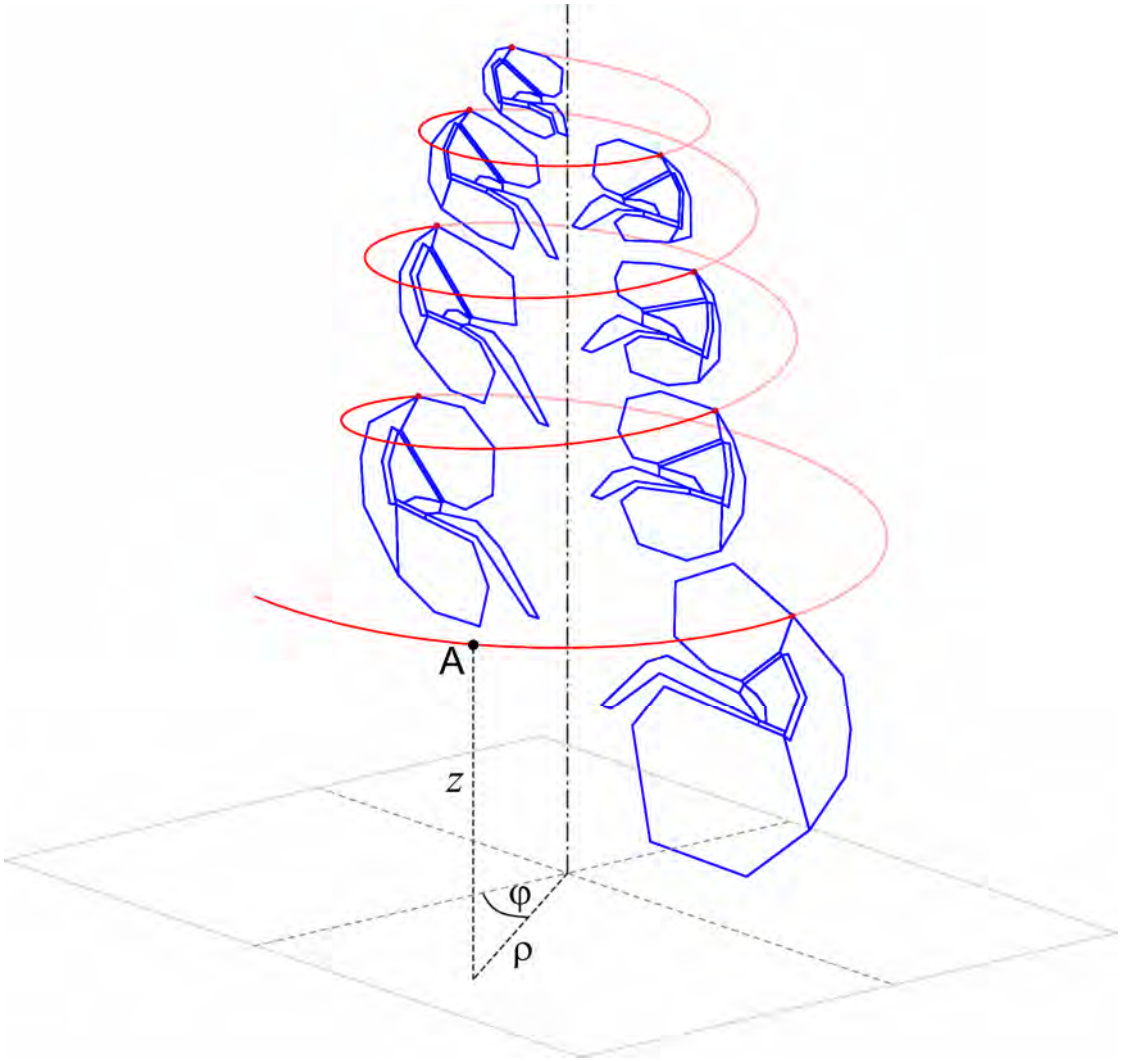

Figure 3.11. Example of a generated spiral to connect sectioned points. Each point on the spiral (A) is characterized using cylindrical coordinates (ρ, φ and *z*).

To generate the spirals, the ρ and z parameters were interpolated between the points on the sectioned slices using spline interpolation (*interp1* function in Matlab). Figure 3.12 and Figure 3.13 indicate the interpolated values of ρ and z of a single spiral. The blue markers indicate the ρ values of the segments obtained from the cochlear images. The red line indicates the interpolated values for the points not obtained from cochlear images.

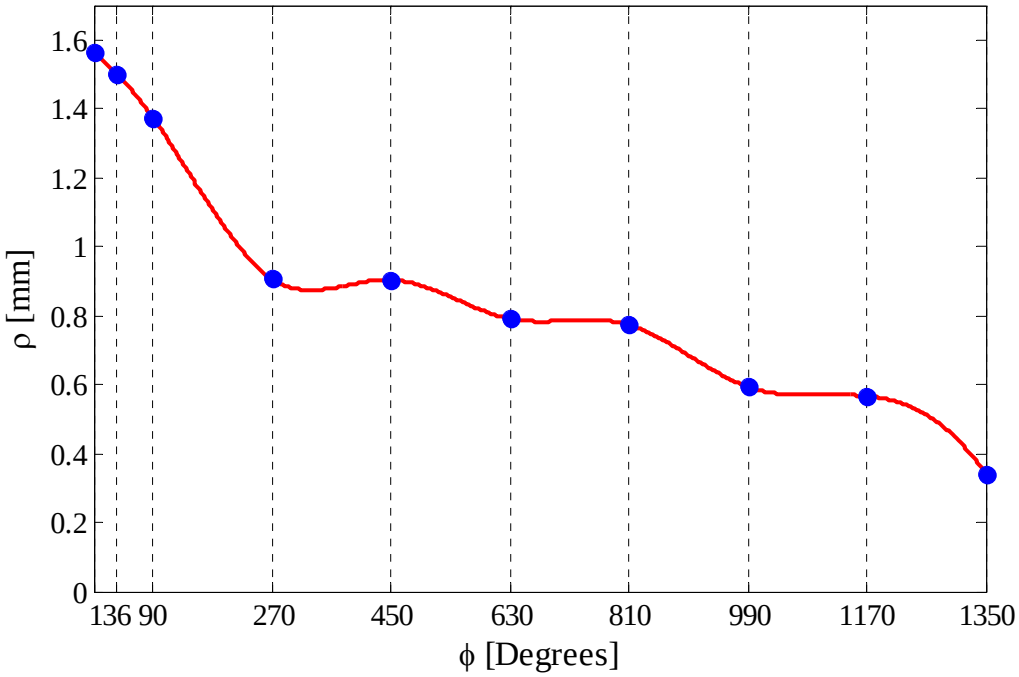

Figure 3.12. Extrapolated values of ρ of a single spiral. The blue markers indicate the positions of the segments obtained from the cochlear images. The red line indicates the interpolated distances.

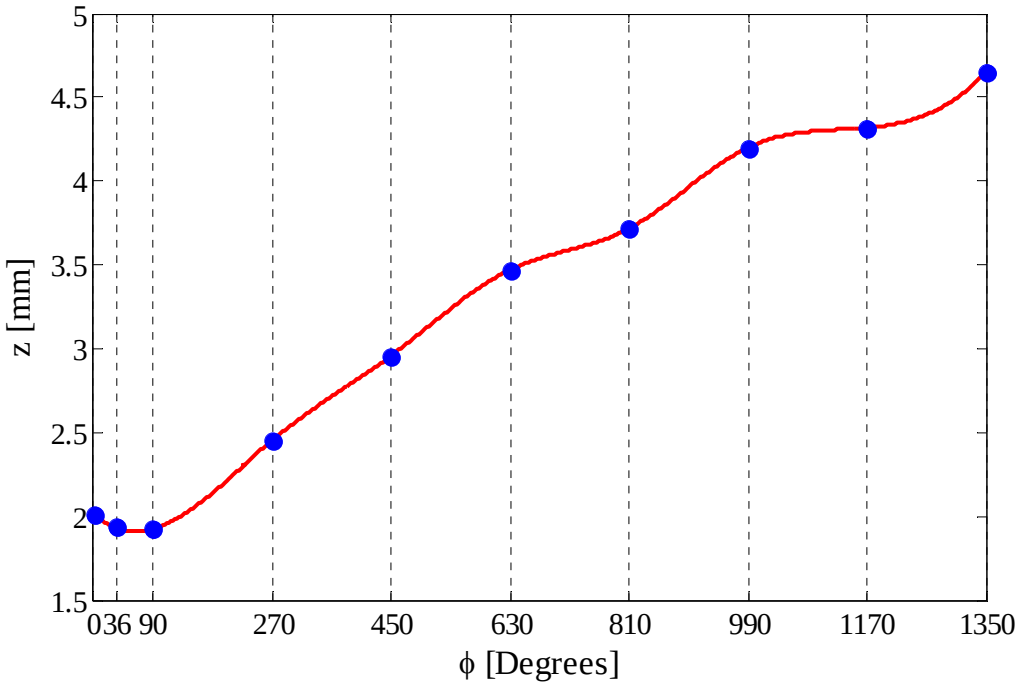

Figure 3.13. Extrapolated values of z of a single spiral. The blue markers indicate the positions of the segments obtained from the cochlear images. The red line indicates the interpolated distances.

This same interpolation technique was followed for all the spirals. Figure 3.14 shows the generated spirals that make up the scala vestibuli.

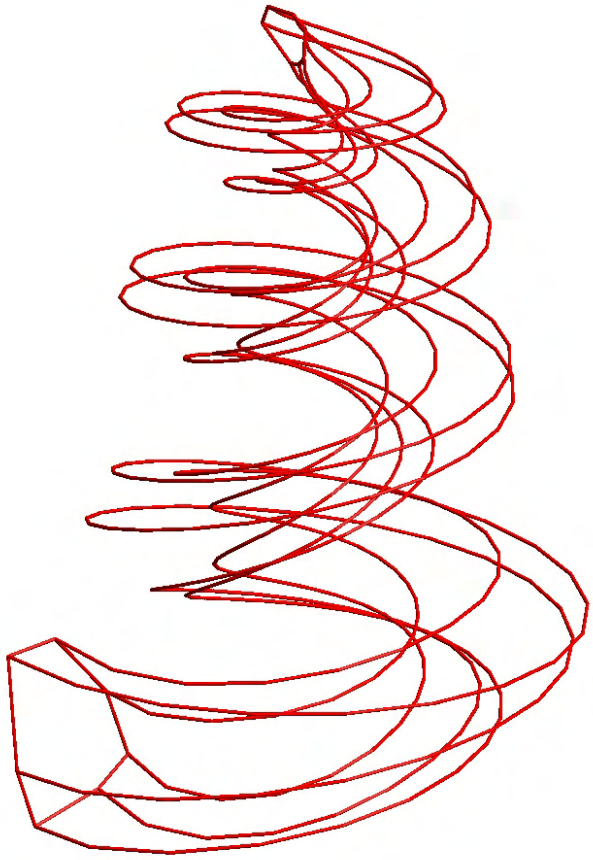

Figure 3.14. Generated spirals of the scala vestibuli.

Each section of the cochlea was generated in the same manner (Figure 3.15).

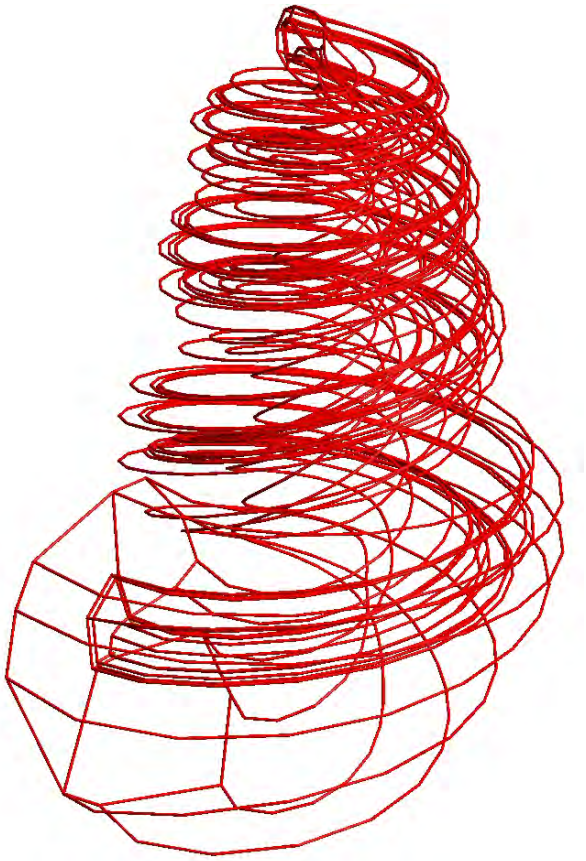

Figure 3.15. Generated spirals for most cochlear structures. Note than the cochlear nerve stem and bone encasing are not present and was added later.

The cochlear nerve stem was added by generating spirals around a tapering cylinder that fits between the existing nerve stem spirals. The bone around the cochlea was modelled as a cylinder around all cochlear structures. The actual guinea pig cochlea has a thin bone layer around the cochlea and an air-filled bulla on one side and relatively conductive neural tissue on the other side. The present model totally encases the cochlea in bone. This is similar to a human cochlea. This was done to simplify the modelling process. A study by Briaire et. al. (2000) found that a volume conduction model with an air filled bulla led to almost identical neural responses compared to a cochlea without the bulla. Figure 3.16 shows the full framework of the cochlea including the nerve stem and bone encasing. Figure 3.17 shows a 3D rendering of this framework with the bone casing removed. Cochlear structures are clearly visible in different colours.

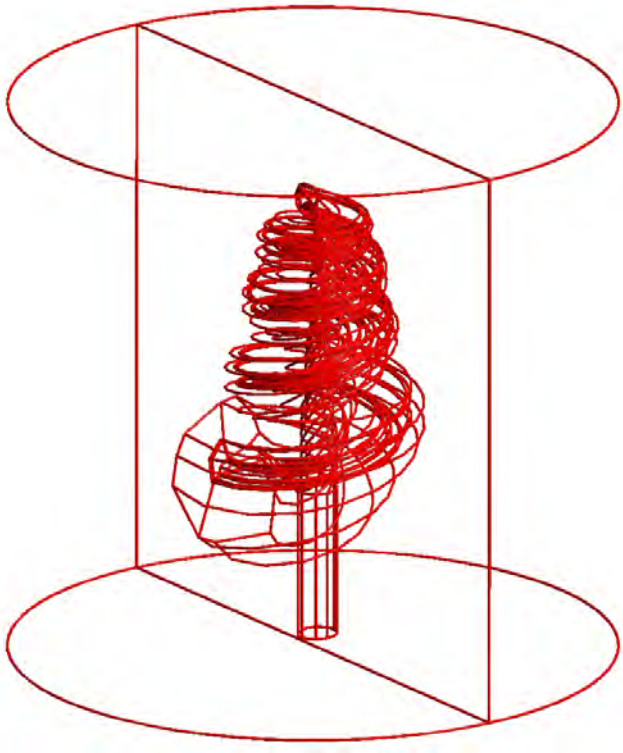

Figure 3.16. Generated framework for all the cochlear structures. The nerve stem and bone encasing are included.

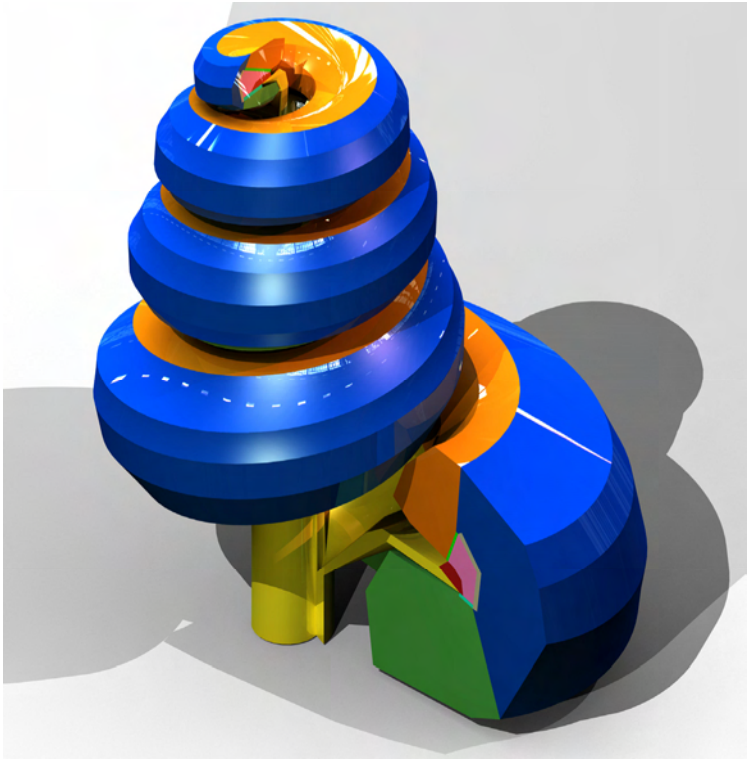

Figure 3.17. 3D rendering of all the cochlear structures with the cochlear bone removed. The cochlear structures are shown in different colours.

3.3.5 Validation of the model geometry

The accuracy of the inner structures of the cochlea that were not visible on the µ-CT scan was verified. This was done by comparing the geometry of the inner structures to data obtained from other studies. The cross sectional areas of the scala tympani, scala media and scala vestibuli were obtained from a study by Thorne et. al. (1999). The basilar membrane width data was obtained by Wada et. al. (1998). The cross sectional area data of the organ of Corti was obtained from a study by Fernandez (1952). The data from these studies was converted and plotted as the distance along the basilar membrane measured from the helicotrema. Figure 3.18 shows the histologic data from these studies in blue. The red indicates the measured data from the present model. The data from the scala tympani, scala media and scala vestibuli closely matches histologic data. The present model does not include the hook area, which explains why the histologic data shows data for longer ducts. The hook area was not included in the model to simplify the modelling process, the effect that this has on the elicited excitation spread is not known. The basilar membrane width closely matches the histologic data whereas the organ of Corti has a smaller cross sectional area than histologic data suggests. This was assumed as the optimal size of the organ of Corti because increasing its size would result in the other structures becoming smaller.

This verifies that the geometry of the modelled cochlea accurately resembles the geometry of an actual guinea pig cochlea. The positions of the electrode contacts were then estimated and inserted into the cochlear geometry.

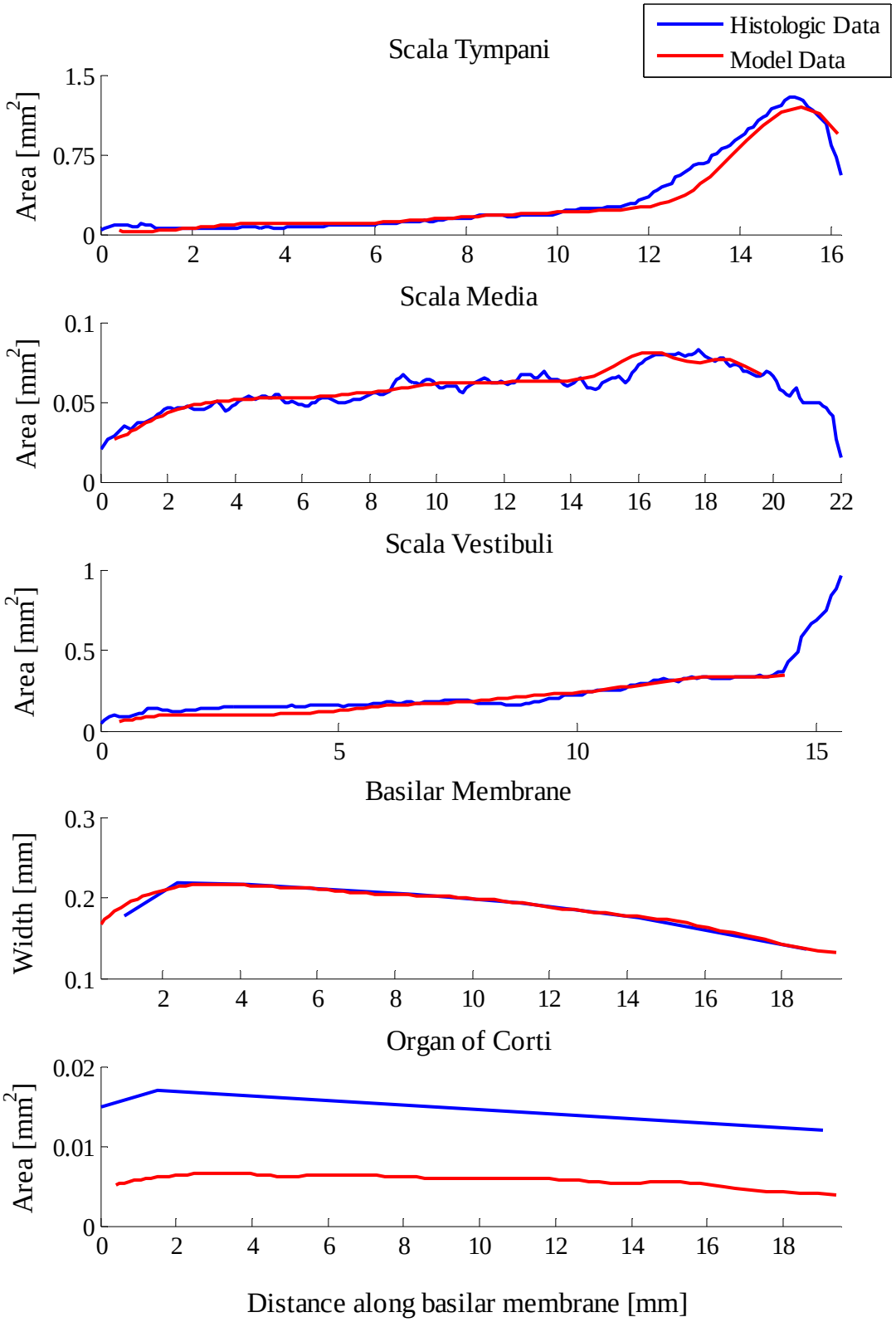

Figure 3.18. Comparison of model geometry (red) to histologic data from other studies (blue).

3.3.6 Electrode modelling

The positions of the electrode contacts relative to the cochlear neurons are crucial in obtaining accurate neuron responses from the model. Obtaining their positions from the µ-CT data is discussed here.

The metallic parts of the electrode array such as the electrode contacts and connecting wires have the highest exposure on the µ-CT scan image. This is because metal has a higher absorption rate than the surrounding cochlear tissue. To estimate the position of the electrode array, the voxels with the highest values were extracted. Figure 3.19 shows the extracted voxels of the electrode array. The electrode contacts and connecting wires are clearly visible.

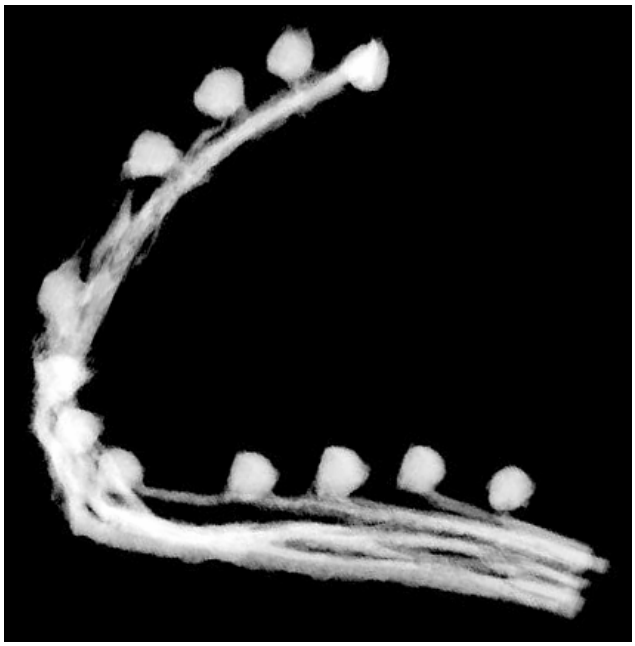

Figure 3.19. Image of electrode array obtained from µ-CT scan by extracting the brightest voxels. These belong to the 12 metallic electrode contacts and wires in the array.

The electrode contacts were modelled in the positions as these voxels. The contacts from the µ-CT image are not perfect spheres. This is because the metal artefact warps the image. The electrodes were modelled as perfect spheres with radii of 110 µm. Figure 3.20 shows the modelled electrode contacts in the locations obtained from the µ-CT scans. The electrode wires were not modelled as they are encased in a non-conductive silastic

electrode carrier and do not contribute to low frequency current flow in the model. The effect of carrier capacitance caused by these wires may come into play when using short stimulus pulses but was not investigated in this study. The non-conductive silastic electrode carrier was also not modelled because it is not distinguishable on the µ-CT image. Its geometry is also not known as this is a custom made electrode array.

Figure 3.20. Illustration of the modelled electrode contacts. The contacts were modelled as perfect spheres positioned in the same locations as the electrode contacts in the µ-CT scan image.

To validate that the electrode contacts are in the correct positions relative to the cochlear neurons and other cochlear structures, slices of the model were made through the electrode contacts and compared to µ-CT images sliced at the same angles. Figure 3.21 indicates the angles at which the electrodes are found.

Due to the interpolation of the spirals that define the boundaries of the cochlear ducts, it can be assumed that the geometry will not be perfectly accurate. This is especially true at angles far from where the imaged slices were obtained. Increasing the number of slices will reduce this error, but will increase the modelling time. The number of slices required to achieve near perfect accuracy is an area that needs further investigation.

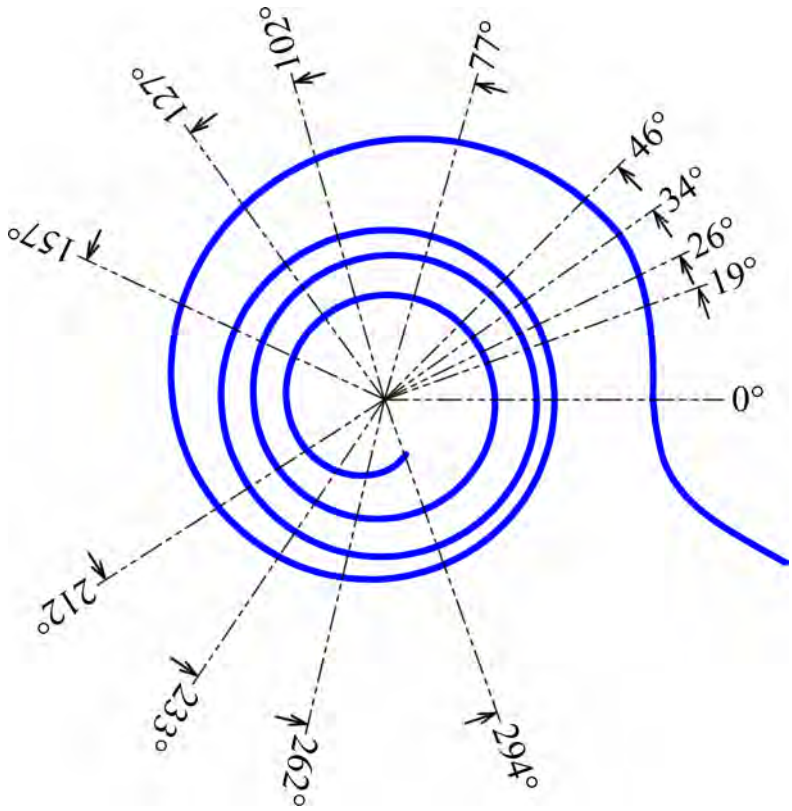

Figure 3.21. Top view of cochlea the arrows indicate the arrows where each electrode is found.

It was found that some of the modelled electrodes did not perfectly match their positions relative to the walls of the cochlear structures. Their positions were then adjusted so that their positions were in the same positions as shown in the µ-CT images relative to the cochlear walls.

The following procedure accomplished this:

1. A mid-modiolar µ-CT slice was made through a specific electrode contact.
2. Markers were placed on the extreme edges of the cochlea (in other words, the maximum and minimum edges in x and y directions). A marker was also placed at the centre of the electrode contact. Figure 3.22 shows the µ-CT slice through the fourth electrode from the apex with the extreme markers indicated in blue and the electrode marker indicated in green.

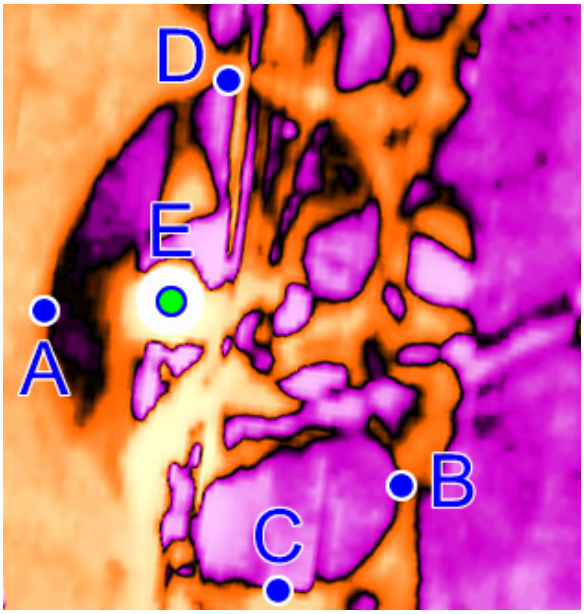

Figure 3.22. µ-CT slice through an electrode contact used in adjusting the modelled electrode position. Markers A, B, C and D are placed on the extreme edges of the segment. Marker E is placed at the centre of the electrode contact.

3. A slice of the model was then made through the same electrode. The extreme positions of the modelled segment were then marked similarly to the µ-CT image (Figure 3.23).

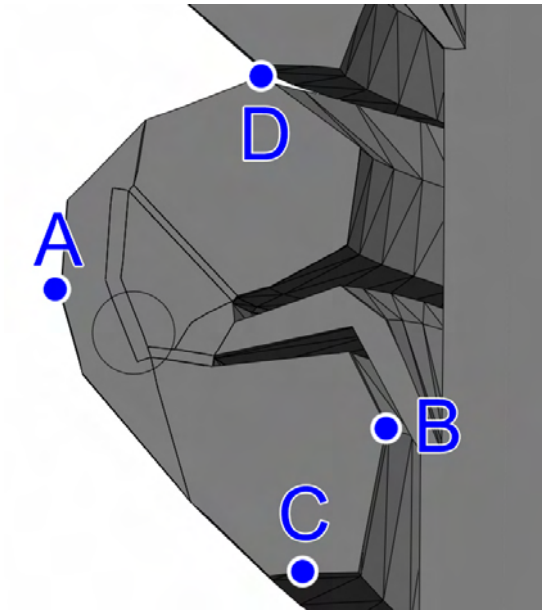

Figure 3.23. A slice through the model at the angle of the electrode. Markers were placed in the same manner as the µ-CT slice.

4. The height and the width of the µ-CT segments were calculated as follows.

$$\begin{aligned} Width_{CT} &= B_{CT,x} - A_{CT,x} \\ Height_{CT} &= D_{CT,y} - C_{CT,y} \end{aligned} \tag{3.1}$$

Where *CT* denotes the values obtained from the µ-CT image and *x* and *y* denotes the x and y coordinates of the points respectively.

The height and the width of the Model segments were calculated as follows.

$$\begin{aligned} Width_{M} &= B_{M,x} - A_{M,x} \\ Height_{M} &= D_{M,y} - C_{M,y} \end{aligned} \tag{3.2}$$

Where *M* denotes the values obtained from the model and *x* and *y* denotes the x and y coordinates of the points respectively.

5. The distance that the electrode is from the right (marker B) and top (marker D) boundary of the cochlea in the µ-CT image was obtained as follows.

$$\begin{aligned} Right_{CT} &= B_{CT,x} - E_{CT,x} \\ Top_{CT} &= D_{CT,y} - E_{CT,y} \end{aligned} \tag{3.3}$$

Where *CT* denotes the values obtained from the µ-CT image and *x* and *y* denotes the x and y coordinates of the points respectively.

6. The new vertical position of the electrode in the model was calculated by ensuring that the ratio between the height of the cochlear segment and the distance that the electrode is from the top is the same as it is in the µ-CT image:

$$E_{M,y} = D_{M,y} - \frac{Top_{CT}}{Height_{CT}} \times Height_{M} \tag{3.4}$$

7. The new distance that the modelled electrode is from the right was calculated by ensuring that the ratio between the width of the cochlear segment and the distance that the electrode is from the right is the same as it is in the µ-CT image:

$$E_{M,x} = B_{M,x} - \frac{Right_{CT}}{Width_{CT}} \times Width_{M} \tag{3.5}$$

8. The centre of the modelled electrode was then relocated to the new calculated position of E_M.

Figure 3.24 shows a slice of the model through the fourth electrode from the apex. The red is the location of the electrode contact obtained directly from the µ-CT scan. The green indicates the new adjusted position of the electrode contact to compensate for inaccuracies in the generated spirals.

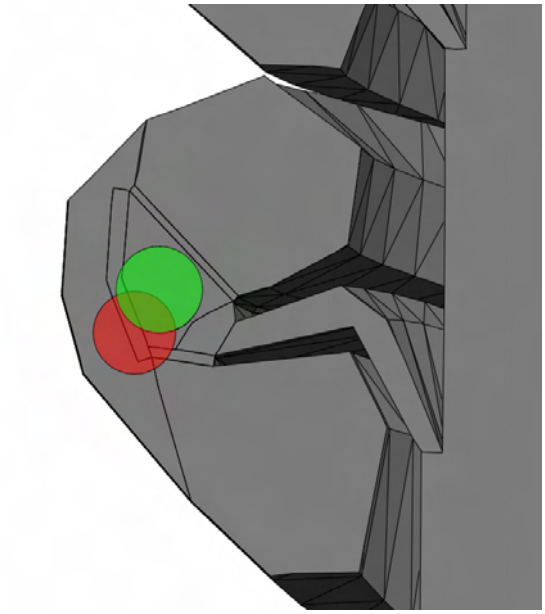

Figure 3.24. A slice of the model indicating old (red) and new (green) electrode placements.

Figure 3.25 shows the final positions of the electrodes. Each image was obtained by slicing the model at the angles indicated in Figure 3.21. Electrodes are numbered from the apex (electrode 1) to the base (electrode 12).

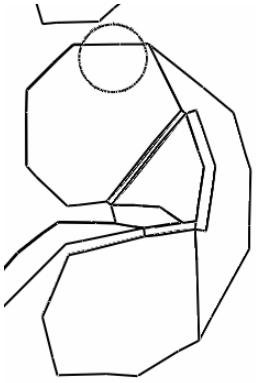

Electrode 1

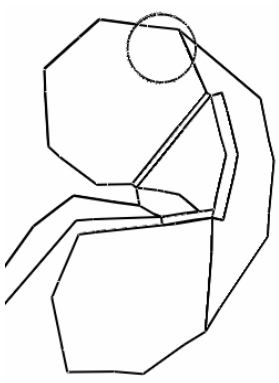

Electrode 2

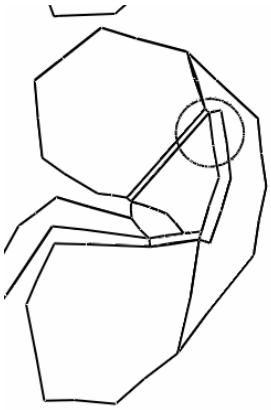

Electrode 3

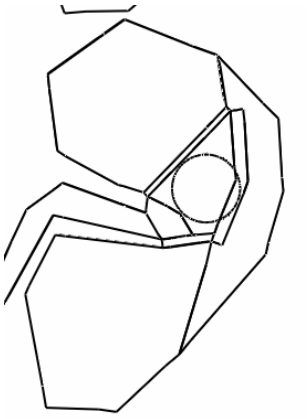

Electrode 4

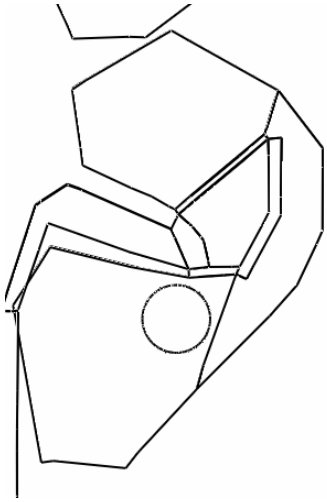

Electrode 5

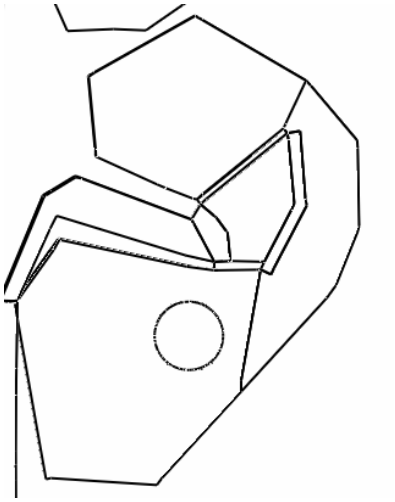

Electrode 6

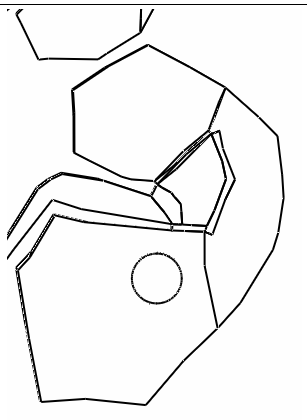

Electrode 7

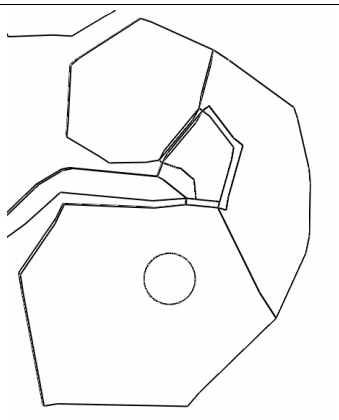

Electrode 8

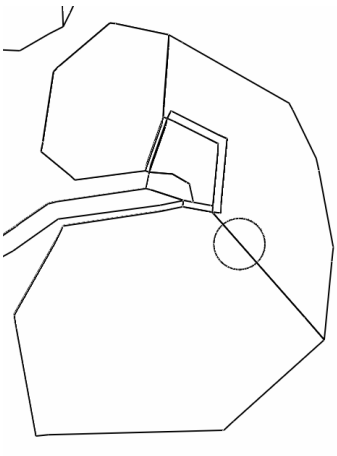

Electrode 9

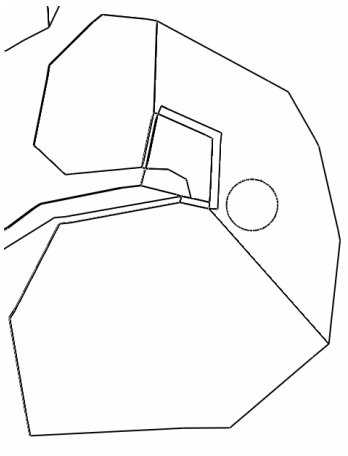

Electrode 10

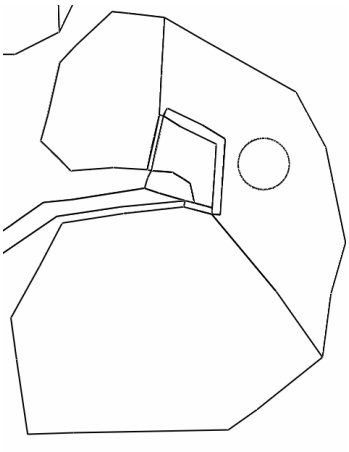

Electrode 11

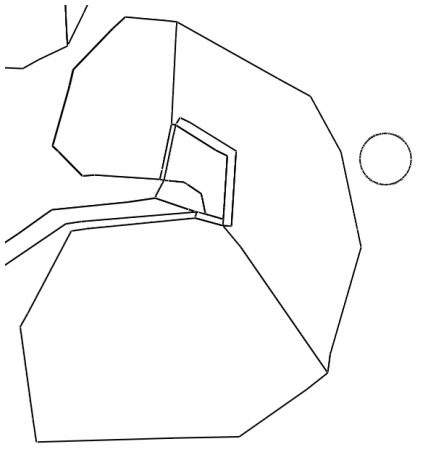

Electrode 12

Figure 3.25. Positions of the electrode contacts of the modelled cochlea.

During the implantation operation, the electrode array was inserted through the side wall at the basal end of the cochlea. As seen in Figure 3.25, electrode 12 is situated just outside the cochlea in the air-filled bulla. Electrodes 11 and 10 are situated in the spiral ligament and electrode 9 sits between the spiral ligament and the scala tympani. This may not be the case in the actual cochlea as the electrode carrier would push aside the spiral ligament forcing the electrode to be inside the scala tympani. As the spiral ligament is not visible on the µ-CT data, it was positioned as in the photomicrograph. The damage caused to the cochlear wall and spiral ligament at the time of insertion was not included in the model as it could not be estimated from the µ-CT data. Electrodes 5 to 8 are located in the scala tympani, where the electrode array was intended to be. It seems that during the insertion, the tip of the electrode array perforated the top part of the scala tympani and ended up in the scala vestibuli. Electrodes 1 to 4 are thus located in the scala media, and scala vestibuli.

With the electrode contacts in position, the model was then meshed to be used in the FEM software package.

3.3.7 Generation of 3D mesh

To perform FEM analysis on the model, the framework developed in the previous sections has to be converted into a 3D volume and be meshed into smaller tetrahedra.

Because of the complexity of the geometry, meshing was not done using the FEM software package Comsol but was done using the open source meshing program GMSH 2.3.0. (Geuzaine and Remacle, 2009). To model the geometry in GMSH, the generated spirals and electrode spheres were reconstructed using GMSH code. The geometry and meshing parameters that were used are listed in Addendum A. Because the geometry narrows from the base to the apex, the size of the mesh was adjusted to be smaller near the apex to still achieve the same geometric resolution. Figure 3.26 shows the mesh generated for the entire model. The full mesh consists of 88210 elements. Figure 3.27 shows the mesh generated for the cochlear structures with the bone cylinder removed.

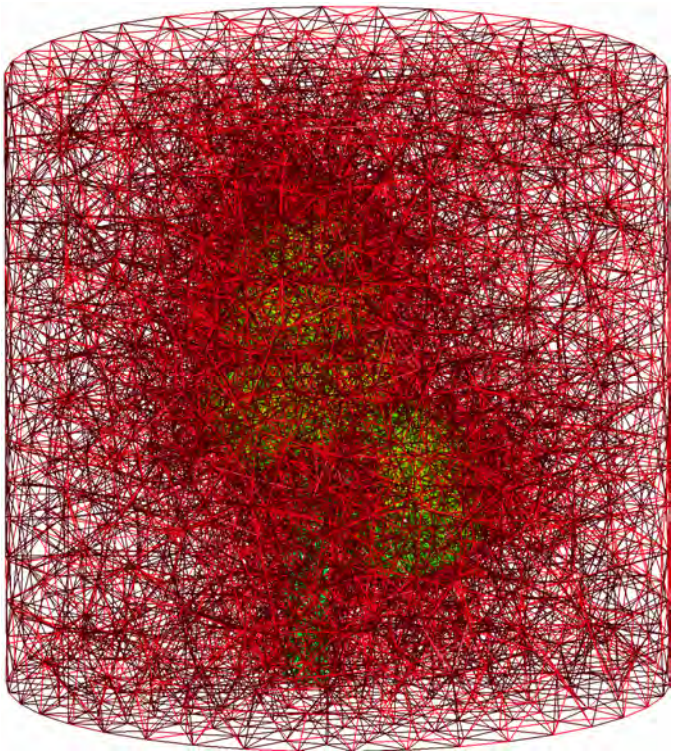

Figure 3.26. Full mesh of entire model. The mesh includes 88210 elements.

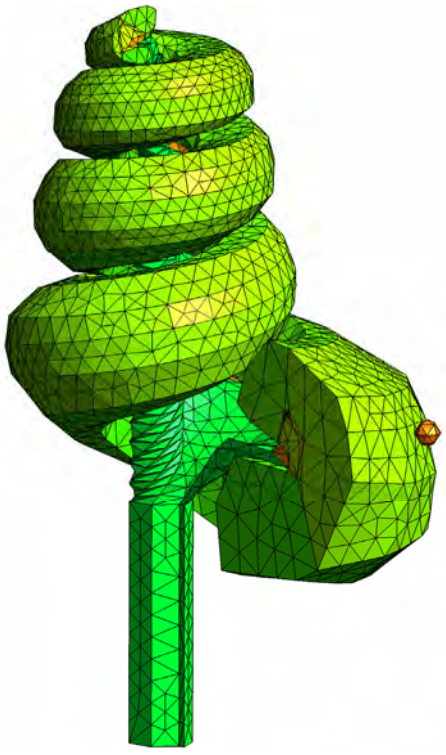

Figure 3.27. Mesh of cochlear structures with bone cylinder removed. Note that one electrode (shown in orange) is located outside of the cochlear structure in the cochlear bone.

The mesh was then saved in Nastran format for use in the FEM software package Comsol where the current distribution inside the cochlea was determined.

3.4 DETERMINING CURRENT DISTRIBUTION INSIDE THE COCHLEA

3.4.1 Comsol analysis

To determine the current distribution inside the cochlea as a result of a specific stimulation protocol, the 3D geometry developed in the previous section was imported into the finite element modelling software package Comsol 3.5a. The import settings used are listed in Addendum A. Comsol is a commercial software package designed to solve multiphysics problems using FEM. FEM was used to solve the volume conduction problem in this study because of its ease of implementation in readily available software and the accuracy it provides when used with the present geometry. The following steps were taken to set up the stimulation environment in Comsol.

First, the mesh generated in the previous section was imported into Comsol. Comsol was set up using the conductive media DC toolbox in the AC/DC module. Next, the material properties of the cochlear structures were defined. Table 3.2 lists the conductivities of the cochlear structures used in the model (Frijns et. al., 2000). Reissner's membrane and the basilar membrane were modelled thicker that they are histologically. This was done to avoid mesh elements that are too small. To compensate for this modelling error, the conductivities of Reissner's membrane and the basilar membrane were enlarged by factors of 11.765 and 7.5 respectively (enlarged values are shown in the table).

The inner boundaries of the cochlear structures were set to have a "continuity" boundary condition. This is the condition used by Comsol to indicate that two surfaces are connected. The outer boundaries of the bone cylinder were set to ground for monopolar stimulation and set to electric shielding for other stimulation protocols. The electric shielding condition was used to simulate the high resistance of the air-filled middle ear space of the guinea pig.

Table 3.2. Conductivities of cochlear structures used in model. Note that the conductivities of Reissner's membrane and the basilar membrane were enlarged.

Cochlear Structure	Conductivity [S/m]
Scala Tympani	1.43
Scala Vestibuli	1.43
Scala Media	1.67
Bone	0.156
Stria Vascularis	0.0053
Spiral Ligament	1.67
Reissner's Membrane	0.00115297
Basilar Membrane	0.09375
Organ of Corti	0.012
Nerve Tissue	0.3
Metal electrodes	1×10^7

A current was applied to various electrodes and the solver was run to obtain the potential distribution inside the cochlea. The solver parameters used are listed in Addendum A. Figure 3.28 shows an example of the potentials obtained after solving the case where current was applied to the ninth electrode from the apex in monopolar stimulation. The electrodes to which current was applied varied for different stimulation protocols.

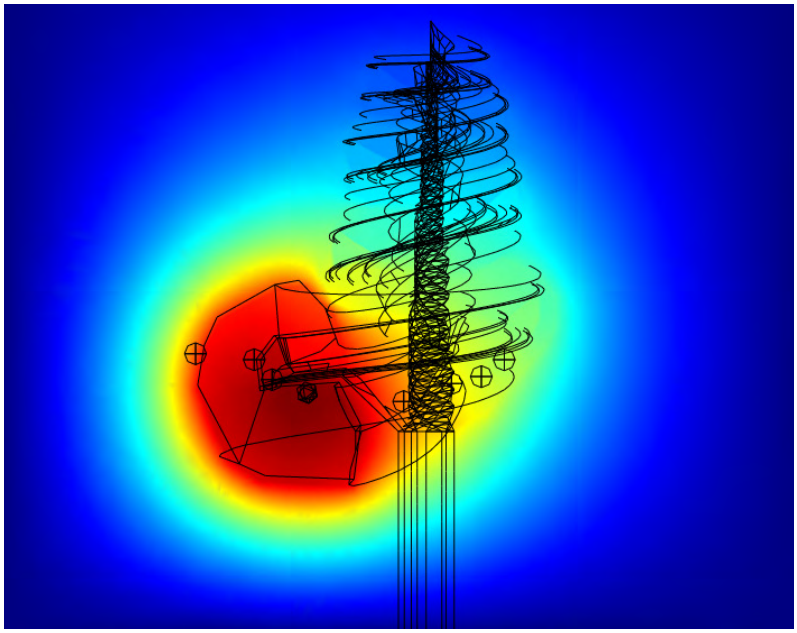

Figure 3.28. Example of potential distribution obtained after solving with Comsol. Illustrated here are the potentials caused by monopolar stimulation of the ninth electrode from the apex.

3.4.2 Stimulation protocols

In this study, three stimulation protocols were investigated namely, monopolar, bi-polar and tri-polar stimulation.

Monopolar stimulation involves the application of a current to a single electrode and connecting the ground to a structure outside the cochlea. In this case the outer boundaries of the bone cylinder were used as the ground. Bipolar stimulation applies a current to one electrode and applies the same current but with an opposite sign to a neighbouring electrode. In this case, the neighbouring electrode was connected to ground to ensure that the model has a ground reference. Tri-polar stimulation applies a current to one electrode and applies half the current but with opposite sign to electrodes on either side of the main electrode. The amplitudes of the current on the adjacent electrodes are equal because balanced stimulation is used. In this case, both the adjacent electrodes were set to ground to ensure a reference voltage for the model.

3.4.3 Location of data points

Once the potential distribution patterns were obtained, the potential at the location of the neurons were required. This was done by extracting the potentials at the locations of the neuron nodes. The neuron nodes correspond to the nodes of Ranvier of a model cochlear neuron (Frijns et. al., 2000). This is where current will enter the neuron and cause it to react. The first node was positioned at the periphery of the modelled 3D neuron region as shown in Figure 3.29 and the rest of the nodes positioned to fall within the modelled 3D neuron region whilst maintaining the internodal lengths given in Table 3.3. Nodes N9 to N16 are not shown but continue in a straight line down the modelled neuron region. The nodal positions were determined for 505 neurons in total each angled 2.5° apart measured around the modiolus. Full neurons were modelled spaced evenly along the cochlear turns. In a real cochlea, Rosenthal's canal is abbreviated in the apical turn (human cochlea) where there are very few spiral ganglion cells. This was not incorporated in the model to simplify the modelling process.

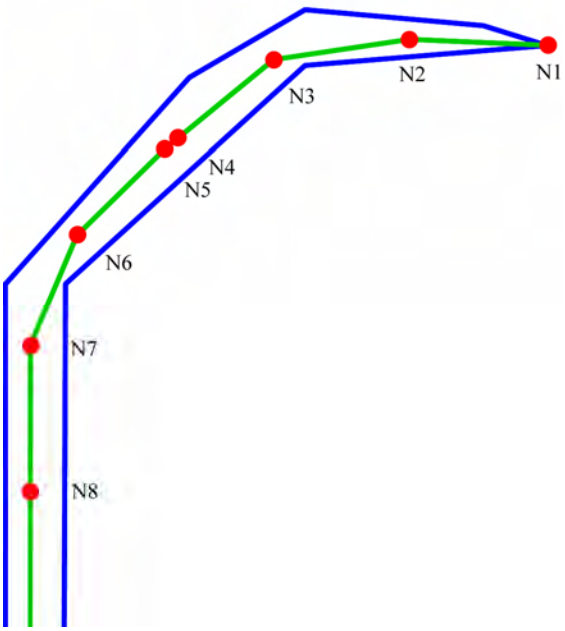

Figure 3.29. Neuron node locations (red) inside the modelled neuron region (blue). The internodal sections of the nerve fibre are shown in green. Note that N9 to N16 are not shown and continue in a straight line down the modelled neuron region.

Table 3.3. Internodal lengths of a modelled neuron.

Internode	**Length [µm]**
N1 – N2	175
N2 – N3	175
N3 – N4	175
N4 – N5	20
N5 – N6	150
N6 – N7	200
N7 – N8	250
N8 – N9	300
N9 – N10	350
N10 – N11	350
N11 – N12	350
N12 – N13	350
N13 – N14	350
N14 – N15	350
N15 – N16	350

Figure 3.30 shows the positions of the modelled neurons. Comsol was then used to obtain the potential at each node as a result of the specific stimulation criteria.

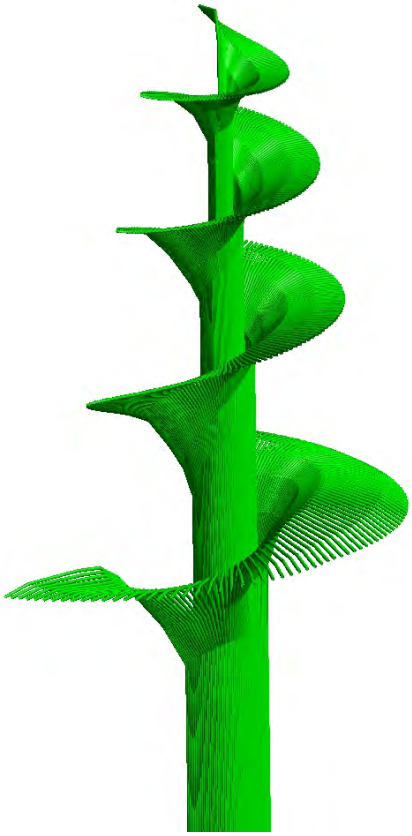

Figure 3.30. Illustration of modelled cochlear neurons. A total of 505 neurons were modelled.

3.4.4 Validation of FE method

To verify that the FE (Finite Element) method employed to obtain the potential distributions in the cochlea was implemented correctly, a simple geometry was modelled and solved using Comsol as well as solved analytically. The solutions were then compared to determine the accuracy of the FEM process.

To create a simple model of an electrode contact, a sphere was modelled in Comsol with a radius of 100 µm and placed inside a sphere with a radius of 50 mm. The electrode was made of platinum and the large sphere of bone. A current source of 1 mA was applied to the centre sphere and the outer boundary of the large sphere was set to ground. The large radius of the outer sphere compared to the dimensions of the modelled electrode will make

the large sphere resemble a dielectric infinitely far away. The problem was meshed and solved using Comsol. The sizes of the mesh elements are comparable to the element sizes of the cochlear model. Figure 3.31 shows the potential distribution obtained from this simulation. The centre of the image is enlarged so that the electrode (shown in dark red) is clearly visible.

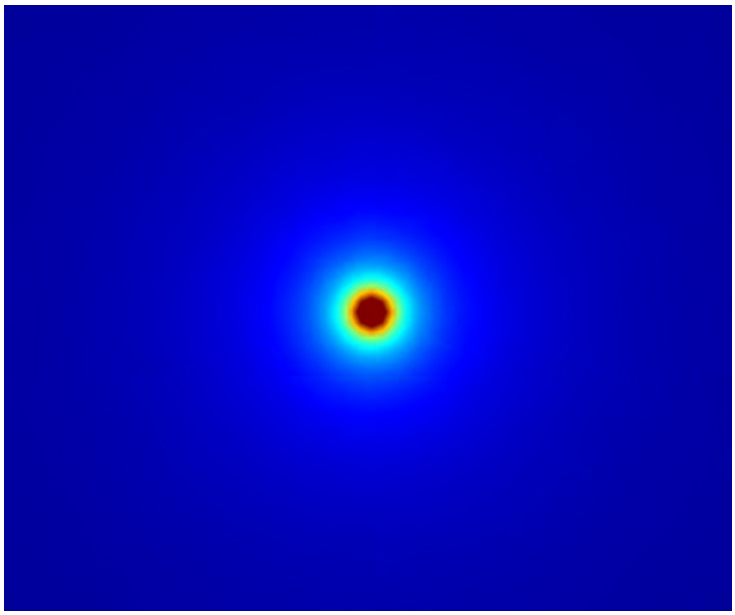

Figure 3.31. Illustration of potential distribution obtained from applying a 1 mA current to a 100 µm platinum sphere placed in a sphere made of bone. Dark red indicates a high potential on the electrode contact whereas dark blue indicates ground nearer to the model boundary.

The potential at a distance of 1 mm from the centre of the sphere was determined from the simulation as 0.5157 V. The same problem was solved analytically by determining the potential in a volume caused by a point source as follows (Plonsey and Barr, 2000; Rattay, 1990):

$$\begin{aligned} V_e &= \frac{\rho I}{4\pi r} \\ &= \frac{6.4103 \times 0.001}{4\pi \times 0.001} \\ &= 0.5101\,V \end{aligned} \tag{3.6}$$

Where $\rho = \frac{1}{\sigma}$ (ρ is the resistivity and σ is the conductivity of bone), I is the injected current and r is the distance from the source.

This value is comparable to the value of the Comsol simulation. This verifies that the method the FEM was implemented is correct. By decreasing the size of the mesh elements a more accurate value of 0.512 V was obtained. Decreasing the element sizes increases the total number of elements and the total degrees of freedom to be solved. This increases computation time of Comsol.

3.4.5 Analysis of mesh size

By increasing the number of mesh elements, the time it takes to solve the model in Comsol increases. Two simulations with different numbers of elements were solved to investigate this time difference.

Both simulations were run on a computer with a 2659 MHz 8-core AMD 64 processor and 8.2 GB of RAM running a Linux operating system and Comsol 3.5a.

First, a model with approximately 88200 elements was solved and had a solving time of 45 s. The amount of elements was then increased to 820 000 and solved and resulted in a solving time of 20395 s. This is a time increase of 453 times. The maximum error in the resulting potential distributions between the two simulations was found to be 0.332 %. This is not a significant increase in accuracy and therefore does not merit the use of more elements. All further simulations were run with a mesh size of about 88200 elements.

3.4.6 Potential distributions

The potential distribution inside the cochlea obtained using the FEM method is different for each stimulus protocol. The potential distributions of the unrolled neurons around electrode 5 are shown in Figure 3.32 to Figure 3.34. The node number of the neuron is given on the horizontal axis, whereas the number of the neuron (neuron 1 is located at the base) is given on the vertical axis.

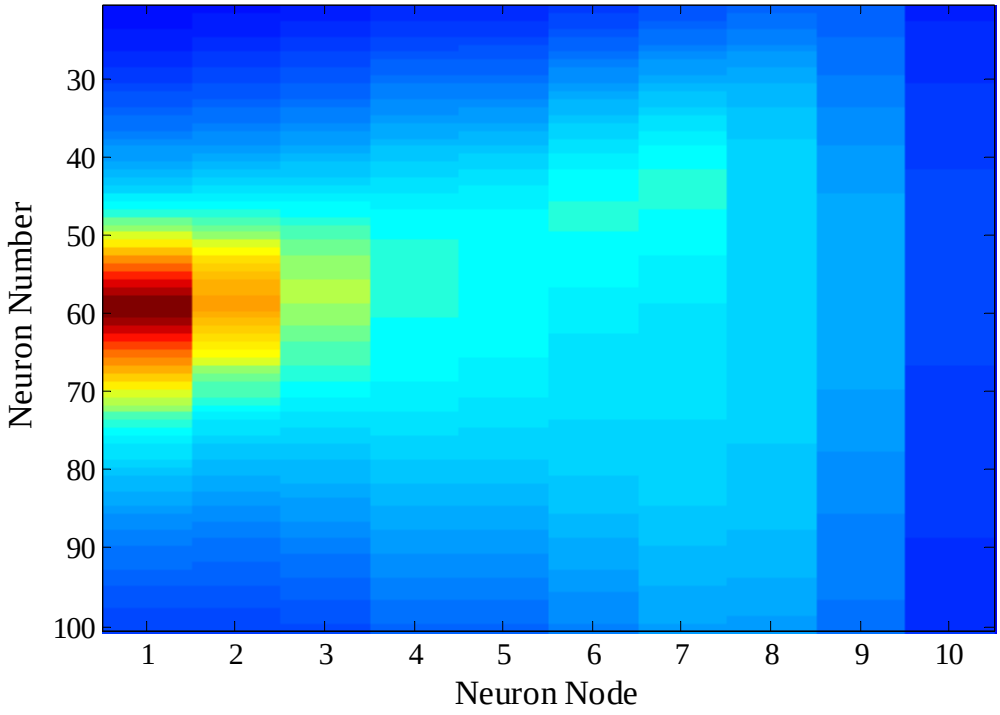

Figure 3.32. Potential distribution around neurons closest to electrode 5 using MP 5 stimulation.

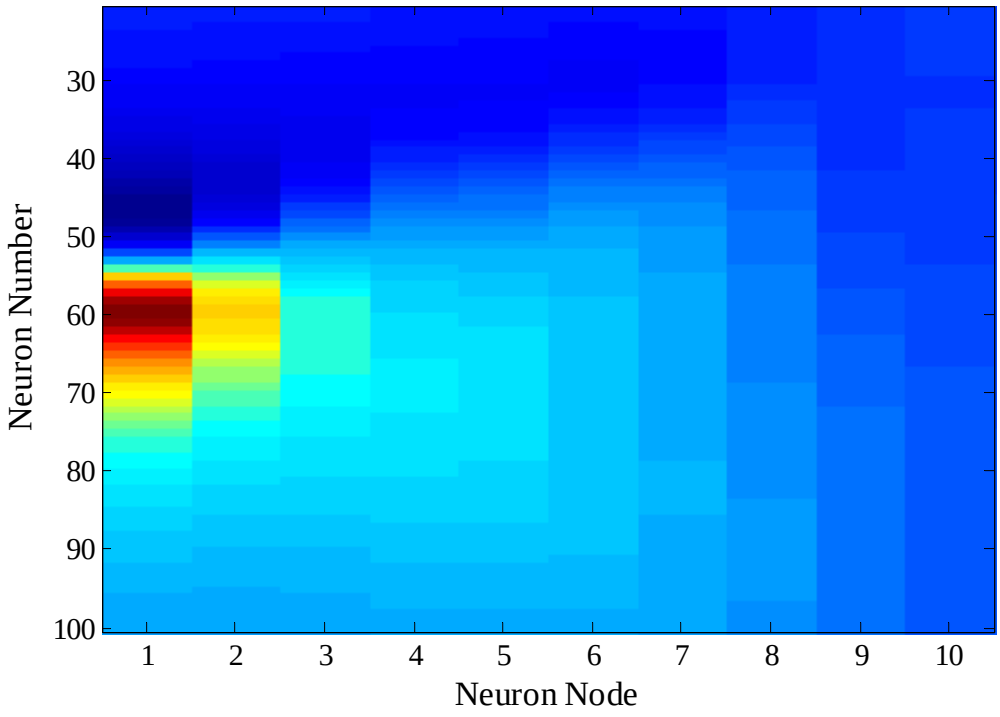

Figure 3.33. Potential distribution around neurons closest to electrode 5 using BP 5-6 stimulation.

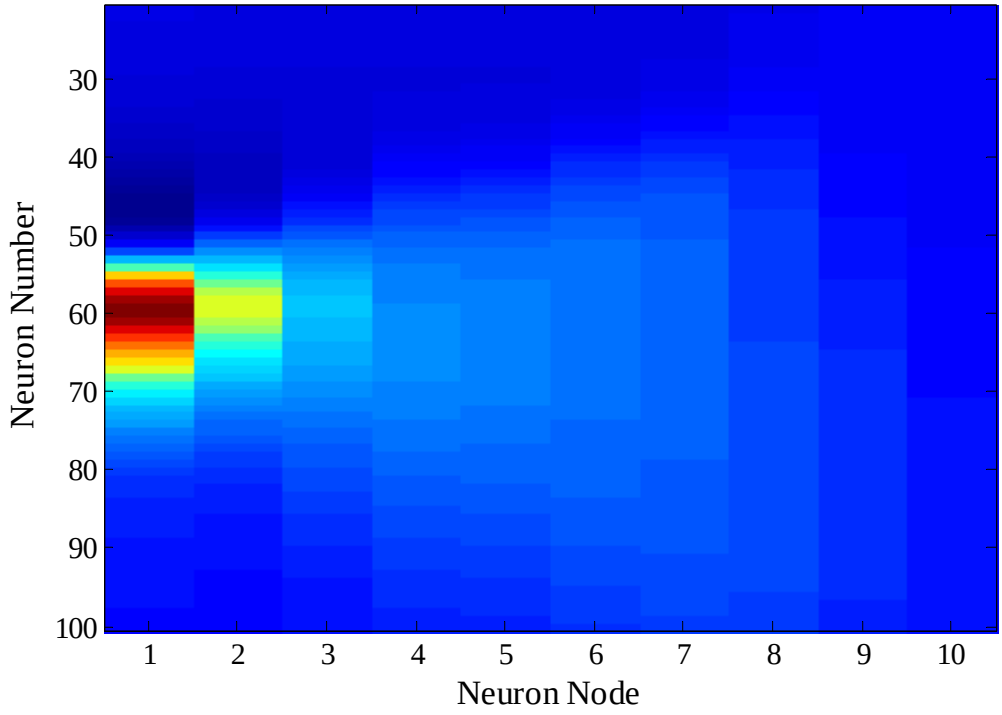

Figure 3.34. Potential distribution around neurons closest to electrode 5 using TP 4-5-6 stimulation. Note that tri-polar stimulation results in narrower current spread that using monopolar or bi-polar stimulation.

It is clear from the figures that monopolar (MP) stimulation produces a wider current spread than bi-polar (BP) or tri-polar (TP) stimulation with tri-polar stimulation producing the narrowest spread. This is consistent with literature (Black et. al., 1983). See section 4.2 for protocol definitions.

3.5 NEURON MODEL

3.5.1 Introduction

To predict the behaviour of the cochlear neurons, a neuron model was used. The Generalized Schwarz-Eikhof-Frijns (GSEF) model was implemented (Frijns et. al., 1995). This is a model of a guinea pig high spontaneous rate nerve fibre. The model implemented here has 16 internodal compartments to which the potentials calculated in the previous section were applied. A fibre with the first nine internodal compartments is shown in Figure 3.35. The dimensions shown are given in µm. The diameter of the fibre and soma is

3 µm and 10 µm respectively. The remaining 5 compartments not shown each has a length of 350 µm.

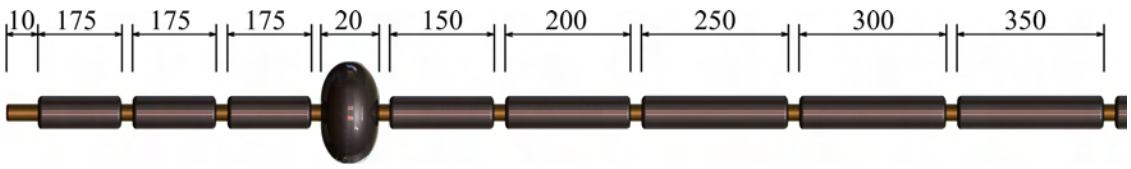

Figure 3.35. Illustration of the neuron modelled in the GSEF model. All dimensions are given in µm. The lengths of the internodes are 1 µm. The diameter of the fibre and soma is 3 µm and 10 µm respectively. Only the first ten internodes are shown.

The GSEF model is described in literature (Frijns et. al., 1995; Hanekom, 2001a) and is not described here. The parameters used in the model are given in Table 3.4.

Table 3.4. Parameters used in the GSEF model.

Parameter	Value	Unit
Nodal length	0.0001	cm
Axonal diameter	0.0003	cm
Axoplasm resistivity	0.07	kΩ-cm
Leak conductance	25.78	$k\Omega^{-1}/cm^2$
Potasium permeability	0.000067	Ωcm/s
Sodium permeability	0.00172	Ωcm/s
Intracellular potassium concentration	141	$mmol/cm^3$
Extracellular potassium concentration	4.2	$mmol/cm^3$
Intracellular sodium concentration	10	$mmol/cm^3$
Extracellular sodium concentration	142	$mmol/cm^3$
Simulation Temperature	310.15	K

The neuron model was implemented in a program written by T. Hanekom[1] in C++. This program determined the minimum threshold at which a neuron will fire. The same stimulus waveform was used for all the experiments. A cathodic first bi-phasic current pulse with a 0.2 ms phase duration and a 0.02 ms interphase gap was used (Figure 3.36).

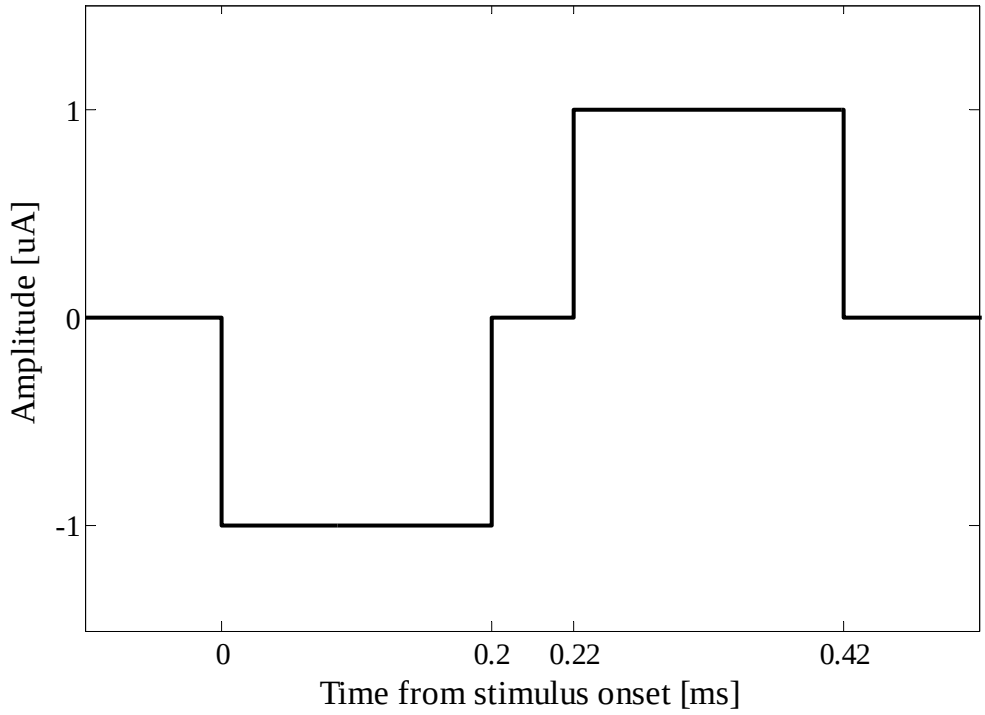

Figure 3.36. Cathodic first bi-phasic current pulse with a 0.2 ms phase duration and a 0.02 ms interphase gap used in all experiments. The amplitude was varied in the experiments.

The amplitude of the stimulus was varied systematically in the software to determine the minimum amplitude at which a neuron fires. This was determined for all 505 modelled neurons for different stimulation protocols. This produced threshold curves for each stimulation configuration. These threshold curves are the final output of the model and were used to investigate the effect of stimulation protocols on neuron excitation.

[1] Prof. Tania Hanekom - Department of Electrical, Electronic & Computer Engineering, University of Pretoria, Pretoria, South Africa

To validate the accuracy of the model output, it was compared to outputs from other 3D cochlear models and EABR data found in literature. The results were also compared to EABR data obtained from the specific guinea pig subject of which the model was constructed.

3.6 BRAIN STEM RESPONSE DATA

Electrically evoked auditory brain stem response (EABR) data was obtained from the live guinea pig by Bonham and colleagues in a similar way as in (Snyder et. al., 2008). This was done by inserting a 16 channel recording electrode array into the tonotopic section of the central nucleus of the inferior colliculus before cochlear implantation was performed. Pure audio tones with varying amplitudes were then played to the guinea pig. The resulting response data was then used to determine the characteristic frequencies at which the recording electrodes were located in the inferior colliculus. Figure 3.37 shows the resulting acoustic frequency response areas of each recording electrode. The characteristic frequency of each electrode derived from these plots is listed in Table 3.5.

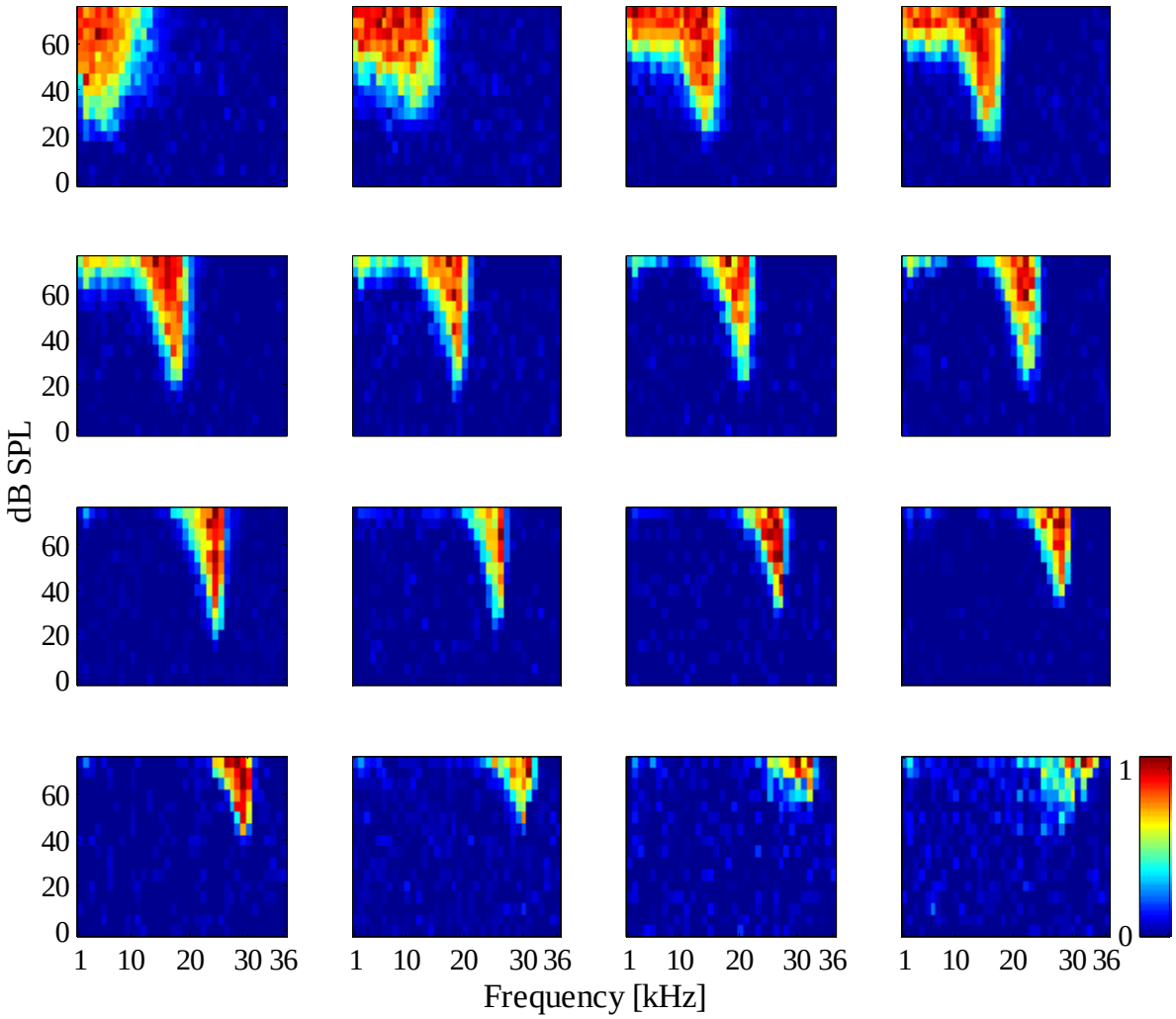

Figure 3.37. Acoustic frequency response areas of the 16 electrode contacts implanted in the inferior colliculus (unpublished data from B. Bonham via personal communication). The most superficial recording site is displayed top-left. The deepest recording site is displayed bottom-right.

Table 3.5. Characteristic frequencies of electrodes implanted in inferior colliculus measured from acoustic stimulation. Electrode 1 is the most superficial and 16 is the deepest.

Recording Electrode	Characteristic Frequency [kHz]
1	2.8
2	4.8
3	6.2
4	7.3
5	8.0
6	9.5
7	10.4
8	12.3
9	14.7
10	16.0
11	17.4
12	20.7
13	22.6
14	24.7
15	29.3
16	29.3

The guinea pig was then implanted with a cochlear implant. The spike rate responses to different stimulation configurations were recorded in the central nucleus of the inferior colliculus (IC) and plotted by colour as a function of depth and current level to these characteristic frequencies. Such a response is called a spatial tuning curve (STC).

The spike rate was recorded over a 5 to 30 ms interval after stimulation. Spontaneous neural activity was estimated as the average spike rate of the period before stimulation. The responses were normalized to the maximum spike rate so that the values are between 0 and 1. The following formula was used to normalize the response (Snyder et. al., 2008):

$$RN = \frac{R - S}{M - S} \tag{3.7}$$

Where RN is the normalized rate, R is the recorded rate, S the spontaneous rate and M is the maximum recorded rate for each stimulus presented.

The overall minimum threshold current of a stimulus configuration is the lowest current that elicits a neural response. Because of the interference of the spontaneous activity and the low spectral resolution of the EABR recordings, this threshold can be difficult to determine. To simplify this process, the threshold was defined as the minimum stimulus level that induces a normalized response of 0.2 (Snyder et. al., 2008).

Figure 3.38 to Figure 3.43 shows the normalized EABR responses with the estimated spontaneous activity subtracted. The colour legend indicates the normalized recorded firing rate. The dark blue indicates sub threshold activity, whereas dark red indicates the maximum recorded firing rate caused by a specific stimulus protocol.

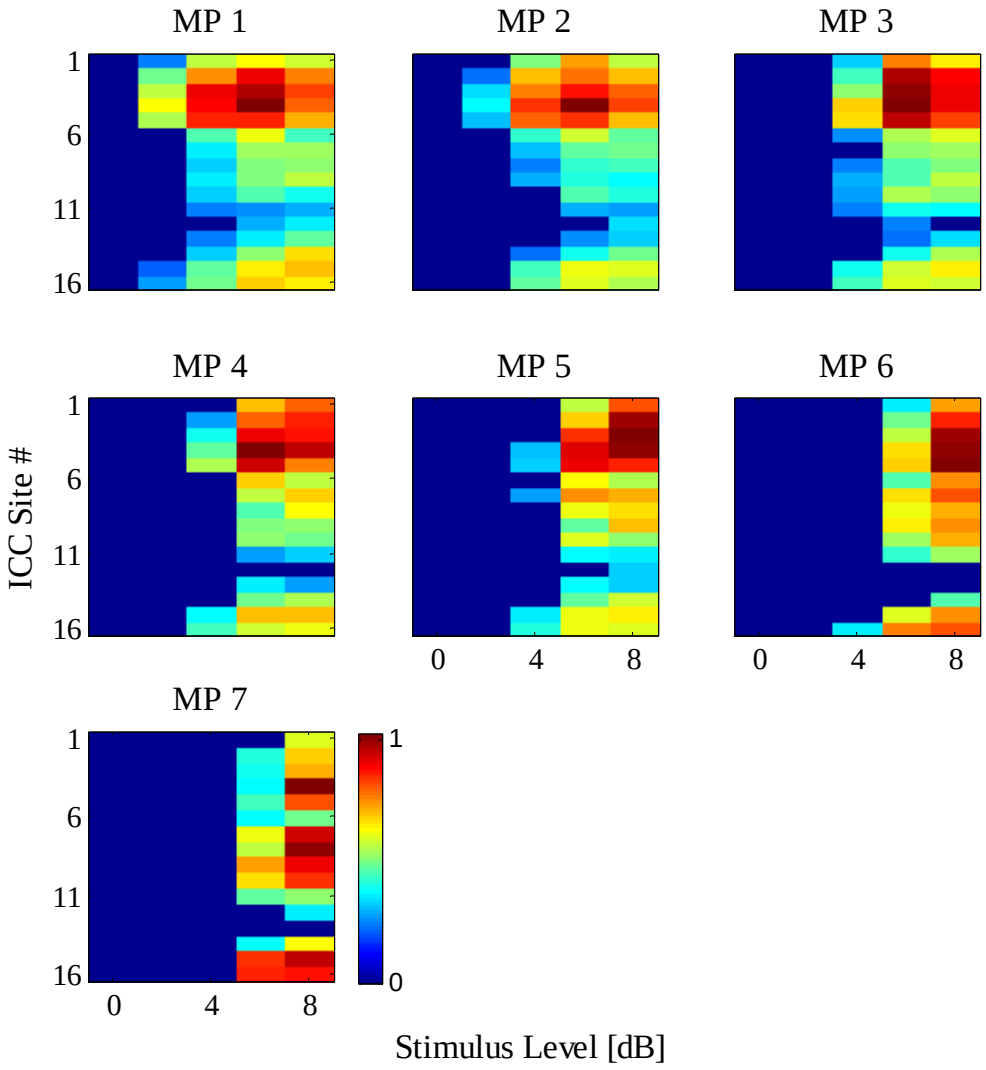

Figure 3.38. Normalized spatial tuning curves obtained from EABR recordings for MP 1 to MP 7 protocols. The vertical axis is the position of the recording electrode in the inferior colliculus (ICC). The reference current (I_{ref}) is 20 µA.

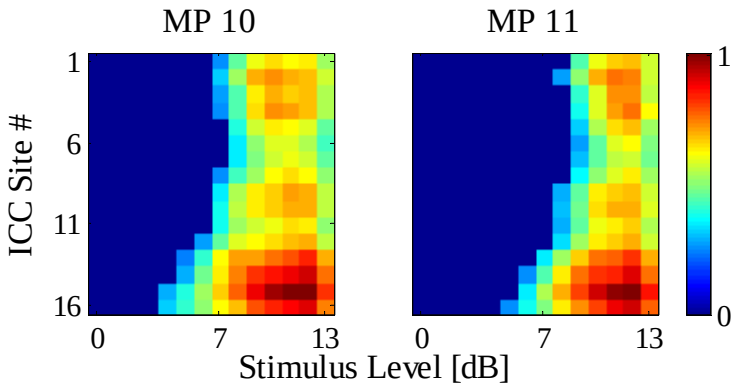

Figure 3.39. Normalized spatial tuning curves obtained from EABR recordings for MP 10 and MP 11 protocols (I_{ref} = 40 µA).

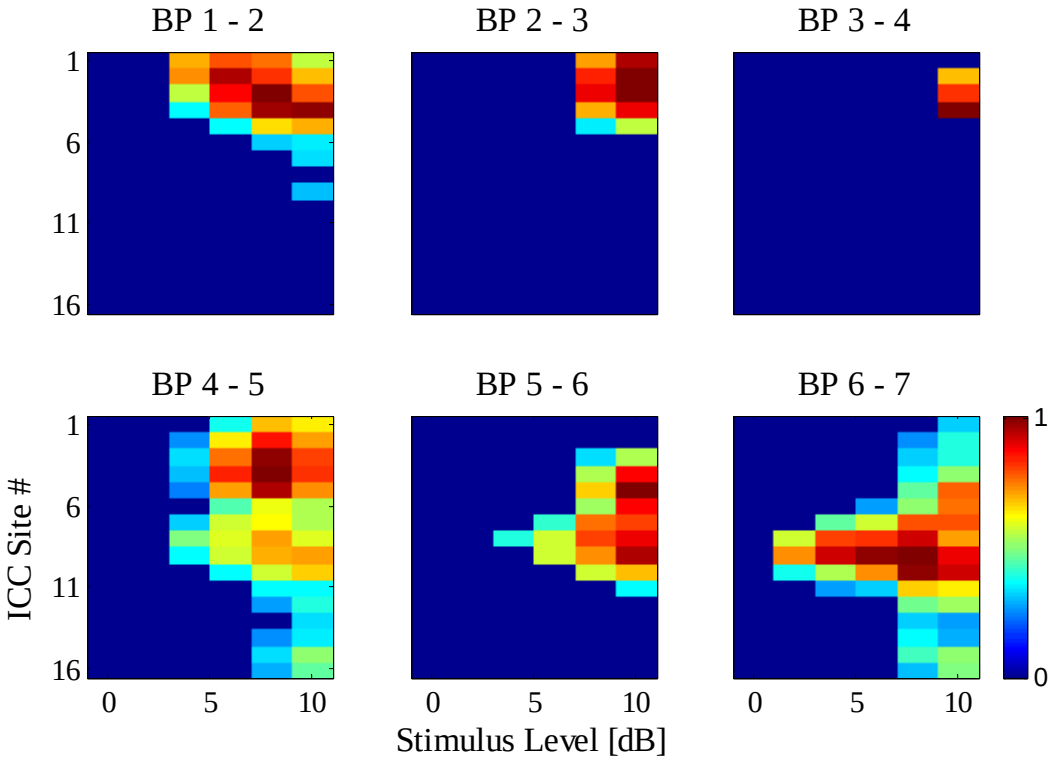

Figure 3.40. Spatial tuning curves obtained from EABR recordings for BP 1-2 to BP 6-7 protocols (I_{ref} = 100 µA).

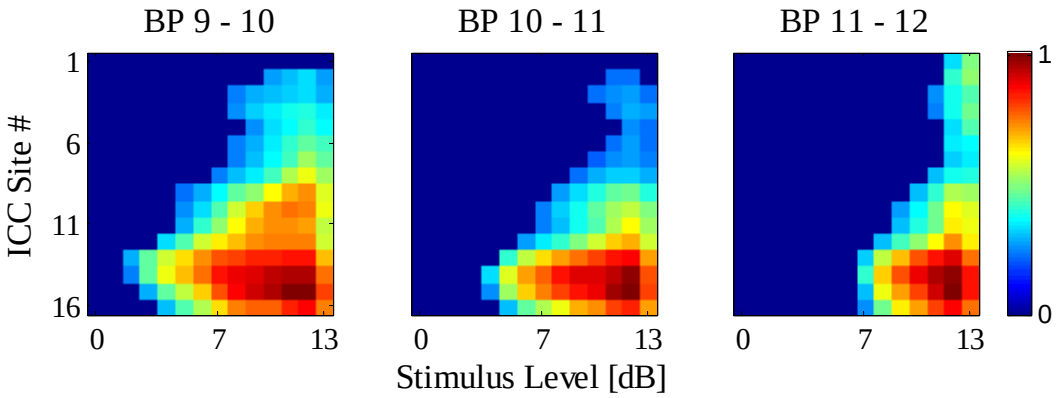

Figure 3.41. Spatial tuning curves obtained from EABR recordings for BP 9-10 to BP 11-12 protocols (I_{ref} = 112 µA).

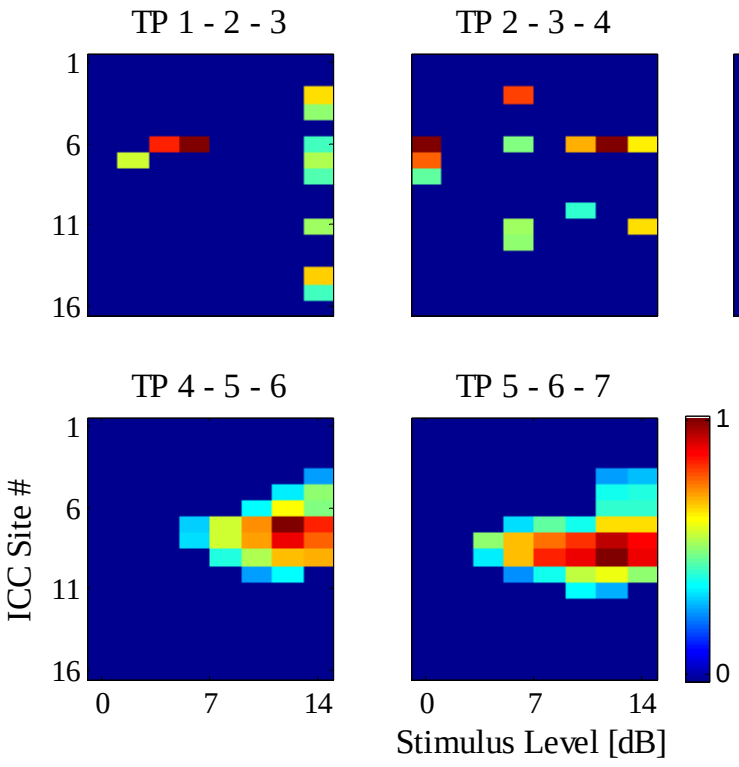

Figure 3.42. Spatial tuning curves obtained from EABR recordings for TP 1-2-3 to TP 5-6-7 protocols (I_{ref} = 100 µA).

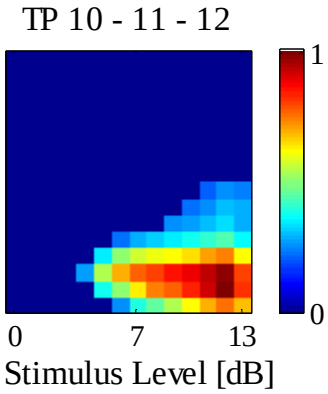

Figure 3.43. Spatial tuning curves obtained from EABR recordings for the TP 10-11-12 protocol (I_{ref} = 141 µA).

The spatial tuning curves for TP 1-2-3 and TP 2-3-4 (Figure 3.42) show only spontaneous activity because the maximum threshold tested exceeded the safety limit of the electrode.

The width of the STC was determined at a stimulus level 2 dB above the overall minimum threshold current. The width is the frequency range that the normalized response exceeds 0.2.

The frequency resolution of the EABR data is approximately 0.2 octaves per site for most of the 16 inferior colliculus recording sites. Each obtained response is the response of a small population of neurons with similar, but not identical characteristic frequencies. The STC width was characterized by two values describing the spread of activation consistent with the measured response described in Figure 3.44.

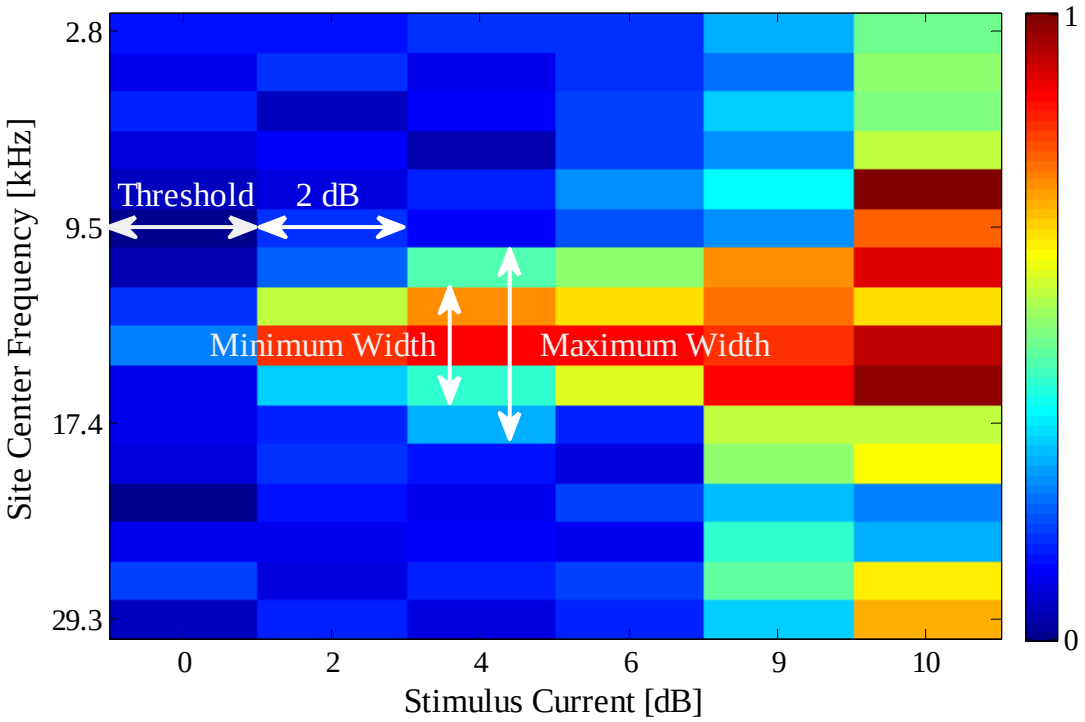

Figure 3.44. Estimation of the width of the spatial tuning curve. The stimulus current is given in dB with a reference of 100 µA. The width is determined at 2 dB above the threshold current. The colour bar on the right indicates the amplitude of the normalized response.

3.7 SUMMARY

This section described the method developed to construct a model of a specific guinea pig cochlea. The model can be set up to simulate different stimulation protocols applied to different electrodes. The output of the model is a threshold curve indicating the minimum stimulus current at which each neuron starts to fire (also referred to as a spatial tuning curve or STC). An STC was generated for each of the investigated stimulation criteria. The model output is discussed in the following chapter.

CHAPTER 4 RESULTS

4.1 INTRODUCTION

This chapter summarizes the results obtained from the model. Different stimulation configurations and electrode arrays were implemented and the resulting threshold curves were obtained. First, a simplified electrode array was modelled to validate the model. Second, the subject specific electrode array was modelled to investigate the extent to which the model output compares to brainstem responses obtained from the guinea pig subject.

4.2 TERMINOLOGY USED

Threshold curves were generated for three stimulus protocols namely monopolar (MP), bi-polar (BP) and tri-polar (TP) stimulation. These protocols were applied to different electrodes.

When referring to electrodes, the electrode number will be given. Electrodes are numbered from 1 to 12. 1 is the most apical electrode and 12 the most basal electrode. Monopolar stimulation is referred to as *MP electrode*, where *electrode* is the electrode to which current is applied. For example MP 1 means current was applied to electrode 1 and the return electrode is connected to the bone casing of the model. Bi-polar stimulation is referred to as *BP electrode 1 – electrode 2*, where *electrode 1* is the electrode to which a positive stimulus is applied and *electrode 2* is the electrode to which an inverse of the stimulus is applied. For example BP 1–2 means positive stimulus is applied to electrode 1 and the negative of the stimulus is applied to electrode 2. Tri-polar stimulation is referred to as *TP electrode 1 – electrode 2 – electrode 3*, where *electrode 2* is the electrode to which a positive stimulus is applied and *electrode 1* and *electrode 3* are the electrodes to which an inverse of the stimulus is applied. For example TP 1-2-3 means positive stimulus is applied to electrode 2 and the negative of the stimulus is applied to electrodes 1 and 3.

4.3 MODEL VALIDATION: RESPONSE THRESHOLDS COMPUTED FOR A CENTERED STIMULATING ARRAY

To ensure that the model behaves as expected, its output was compared to the output of other 3D cochlear models, EABR data, psychophysical and central nervous data found in literature. For this subject specific model to be comparable to models with a more general morphology and configuration, the detail thereof has to be reduced.

To achieve this, the subject specific electrode array was replaced with an array with electrodes that are located exactly in the centre of the scala tympani. This resembles an array with good, non-damaging insertion into the scala tympani, whereas the array of the modelled subject perforated the upper wall of the scala tympani. The electrodes were modelled as 110 µm spheres that do not contain any insulating material between them because no electrode carrier was modelled. This set up resembles banded electrode contacts because there is nothing restricting current flowing in radial directions. This setup does however allow current to be more easily shunted between adjacent electrode contacts, something that the insulating carrier restricts to an extent in conventional banded arrays. Figure 4.1 shows an illustration of the scala tympani with the electrodes placed on the centre line through the scala.

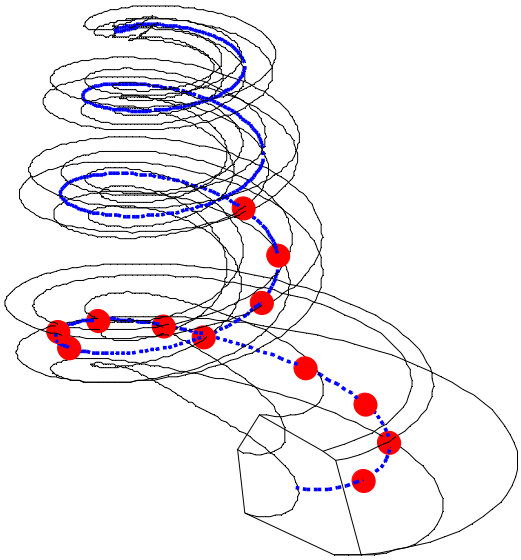

Figure 4.1. Electrode array placed in the middle of the scala tympani used for verification of the model. The black indicates the outline of the scala tympani. The red spheres are the electrode contacts and the blue line indicates the centre line of the scala tympani.

The threshold curves were obtained for various stimulation protocols and compared to outcomes commonly found in literature.

4.3.1 Thresholds of stimulation protocols

Studies indicate that thresholds using monopolar stimulation are consistently lower than thresholds using bi-polar and tri-polar stimulation (Bierer and Middlebrooks, 2002; Bierer and Middlebrooks, 2004; Brown, Abbas, Borland and Bertschy, 1996; Hartmann and Klinke, 1990; Kral et. al., 1998; Kwon and Van Den Honert, 2006; Snyder, Bierer and Middlebrooks, 2004; Snyder et. al., 2008; Snyder, Rebscher, Cao, Leake and Kelly, 1990; Van Den Honert and Stypulkowski, 1987). The thresholds obtained from the model confirm this. The thresholds for electrode 6 were determined with different stimulation protocols (MP 6, BP 6-7 and TP 5-6-7) and are given in Table 4.1.

Table 4.1. Comparison of thresholds of electrode 6 for modelled stimulation configurations. MP has a lower threshold than BP, whereas TP stimulation has the highest threshold.

Stimulus	Threshold [µA]
MP 6	130
BP 6-7	150
TP 5-6-7	194

Monopolar stimulation resulted in the lowest threshold whereas tri-polar stimulation resulted in the highest threshold current. This is consistent with literature and aids to validate the model.

4.3.2 Spatial spread of stimulation protocols

The spatial spread of a stimulation protocol gives an indication of the selectivity of the protocol. The spatial spread was measured as the maximum of the width range of the STC at a stimulus level of 6 dB above threshold. Determination of the width range is described in section 3.6. Spatial spread was measured in kHz. This was achieved by mapping frequencies to positions along the basilar membrane using Greenwood's equation (Greenwood, 1990). The procedure is described in section 4.5.1. The widths elicited by electrode 6 were measured for different stimulation protocols (MP 6, BP 6-7 and TP 5-6-7) and are shown in Table 4.2.

Table 4.2. Comparison of spatial spreads of electrode 6 for modelled stimulation protocols. Monopolar stimulation has a wider spread than bi-polar stimulation, whereas tri-polar stimulation has the narrowest spread. The characteristic frequency of electrode 6 is 7.88 kHz.

Stimulus	Max. width at 6 dB above threshold [kHz]
MP 6	5.386
BP 6-7	1.647
TP 5-6-7	1.167

It is evident that monopolar stimulation gives rise to the widest spread, where bi-polar and tri-polar stimulation elicit narrower spreads. This trend is also commonly found in literature (Bierer and Middlebrooks, 2002; Snyder et. al., 2008; Van Den Honert and Stypulkowski, 1987) and aids to verify the model.

4.3.3 Effect of bi-polar electrode separation

When using bipolar stimulation, the distance between the two electrodes has an effect on the threshold and current spread of the neural response. BP 6-7 and BP 6-8 stimulations were used to investigate this effect. The threshold currents and widths at 6 dB above threshold were determined and are shown in Table 4.3.

Table 4.3. Comparison of the threshold current and spatial spread when increasing the distance between bi-polar electrodes.

Stimulus	Threshold [µA]	6 dB Width [kHz]
BP 6-7	150	1.653
BP 6-8	122	1.998

It is evident that the wider electrode separation causes a lower threshold and wider spatial spread. This is consistent with EABR (Shepherd et. al., 1993; Snyder et. al., 2008) and psychophysical (Lim, Tong and Clark, 1989) studies. A study by Bierer and Middlebrooks that measured responses in the auditory cortex also found that thresholds decrease as electrode separation increases (Bierer and Middlebrooks, 2004). This also aids in the validation of the model.

4.3.4 Effect of electrode position in the scala on threshold current

Studies have indicated that there is a trend whereby the thresholds increase as the electrodes are located more basally (Shepherd et. al., 1993; Snyder et. al., 2008). This is ascribed to the widening of the cochlea towards the base that results in electrodes being further away from the neurons. Another reason may be that more current is shunted between electrodes because the resistivity of the perilymph decreases as the cross sectional area of the scala increases. By approximating the scala as a cylinder, this may be described by the following equation:

$$R = \frac{\rho L}{A}. \tag{4.1}$$

Where R is the resistivity of the cylinder of perilymph between the electrodes, ρ is the conductivity of the perilymph, L is the distance between the electrodes and A is the area of the scala.

This was investigated by comparing the thresholds of all 12 electrodes of the validation array using monopolar stimulation to their positions in the cochlea. As seen in Figure 4.2, there is a trend for thresholds to increase as the electrodes are located more basally.

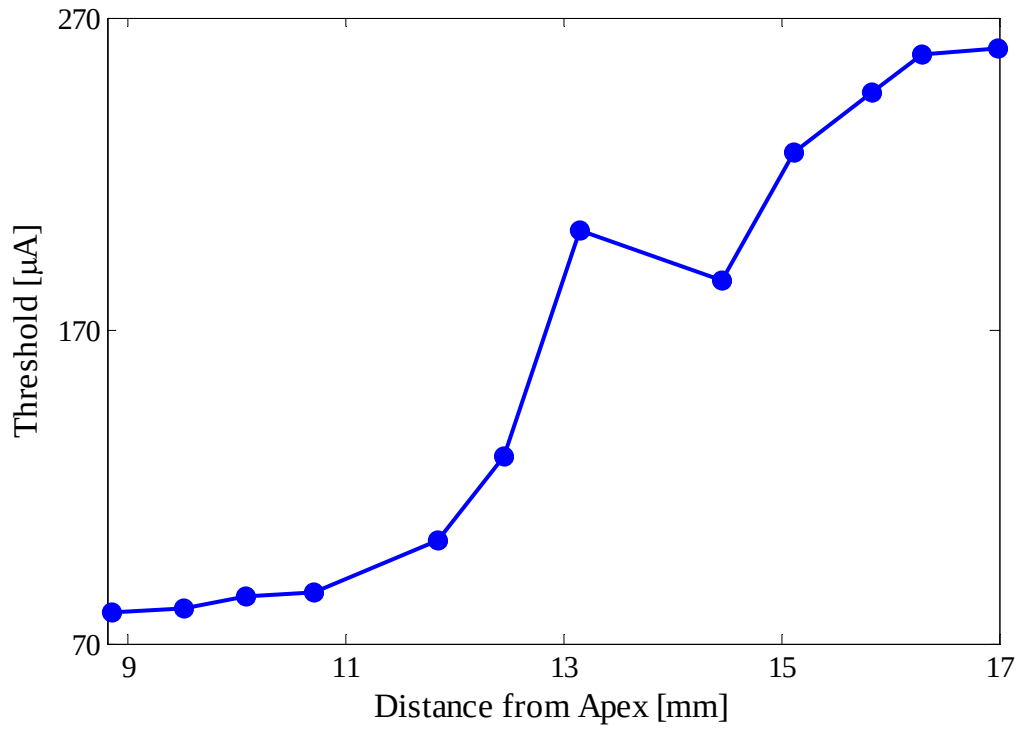

Figure 4.2. Modelled thresholds of the validation electrode array placed in the centre of the scala tympani. Note that there is a trend for thresholds to increase basally.

It was investigated if this effect is due to the distance between the electrodes and neurons that increases as the electrodes are situated more basally. The thresholds were plotted as a function of the distance between an electrode and the first node of the nearest neuron (node N1 in Figure 3.29) in Figure 4.3.

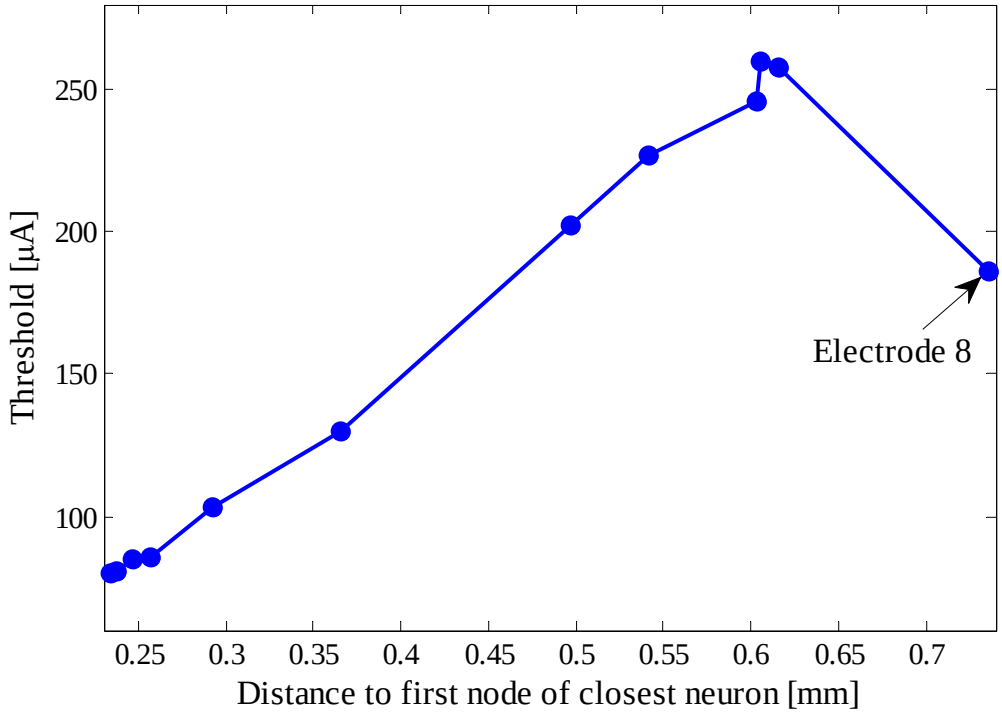

Figure 4.3. Modelled threshold current of the validation electrodes increases as the distance between the electrode and the nearest N1 node increases. Electrode 8 does not follow this trend as it stimulates axons in the modiolus.

There is a trend for thresholds to increase as the distance to the tip of the nearest neuron increases. Electrode 8 is located the furthest from the neuron tip, but has a low threshold value. When looking at the potential distribution caused by electrode 8, it was found that a large potential peak occurred in the axons located in the modiolus. It can be assumed that the low threshold is caused by an action potential that was induced in the neuron axon, whereas the other electrodes induced action potentials in the dendrites of the neurons.

Clinical, model and animal studies show that an electrode array placed closer to the modiolus has lower thresholds (Briaire and Frijns, 2006; Firszt, Wackym, Gaggl, Burg and Reeder, 2003; Frijns et. al., 2001; Frijns et. al., 1995; Shepherd et. al., 1993). This is consistent with the findings of this study as a position closer to the modiolus will decrease the distance between the electrodes and neuron dendrites or axons. Neurons with degenerated dendrites will be stimulated in the remaining axonal part and not in the dendrite.

4.3.5 Summary

The model is capable of predicting outcomes commonly found in literature. This serves as validation that this model does predict outcomes as expected. This also shows that this model is valid as a research tool and that it may be used to investigate neural responses of different electrode positions and stimuli.

4.4 RESPONSE THRESHOLDS COMPUTED FOR ARRAY POSITIONED USING µ-CT DATA

To investigate the extent to which this model can predict responses predicted by EABR data obtained from the subject, the subject specific electrode array was modelled. The threshold curves for the different electrodes and configurations were obtained and are given here. Only configurations for which EABR data were available were simulated.

4.4.1 Monopolar stimulation

Monopolar stimulation was applied to electrodes 1, 2, 3, 4, 5, 6, 7, 10 and 11. The threshold curves obtained from the model are shown in Figure 4.4 to Figure 4.8.

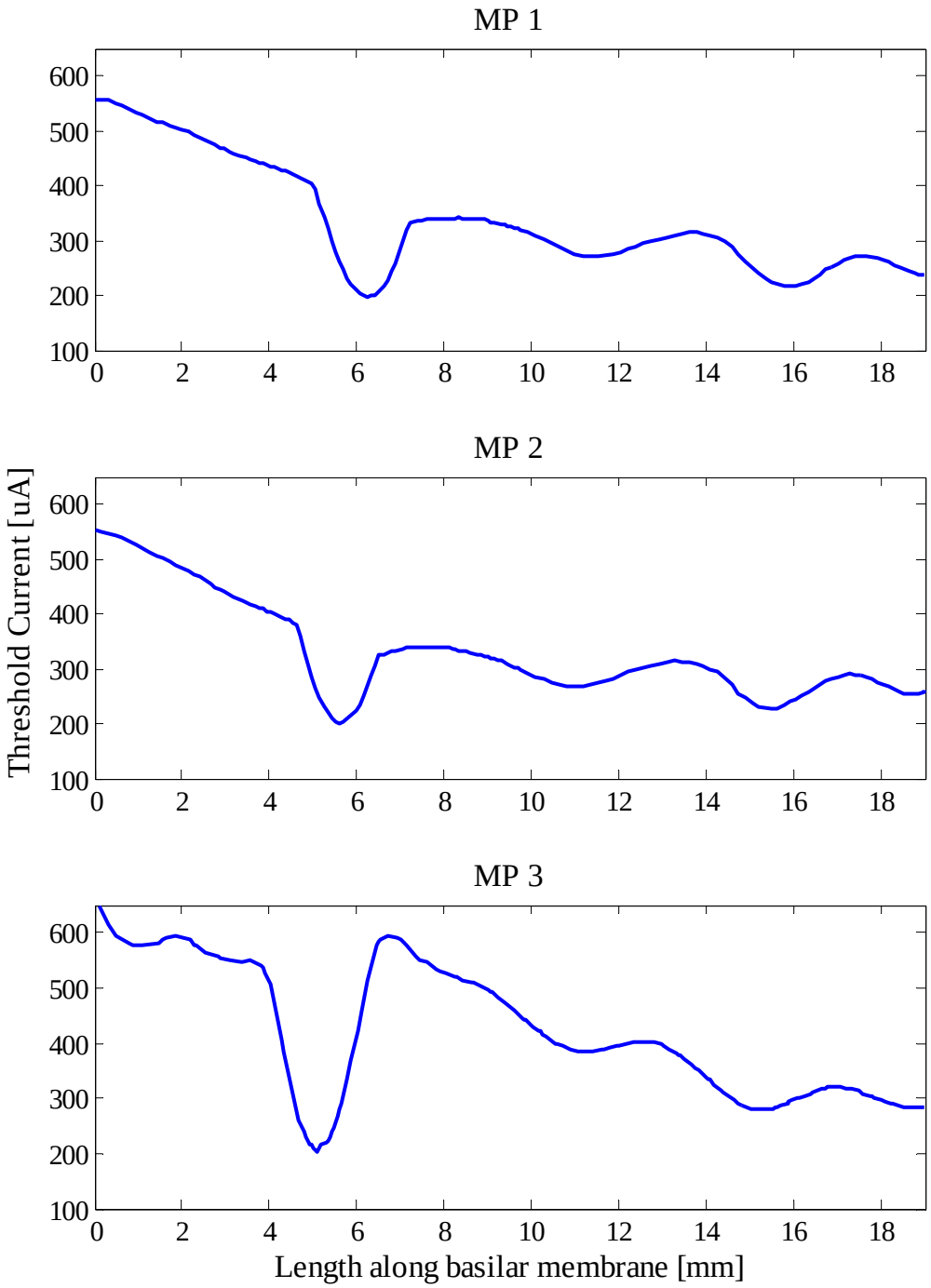

Figure 4.4. Threshold curves obtained from the model using MP1, MP2 and MP3 stimulation measured along the length of the basilar membrane from the base.

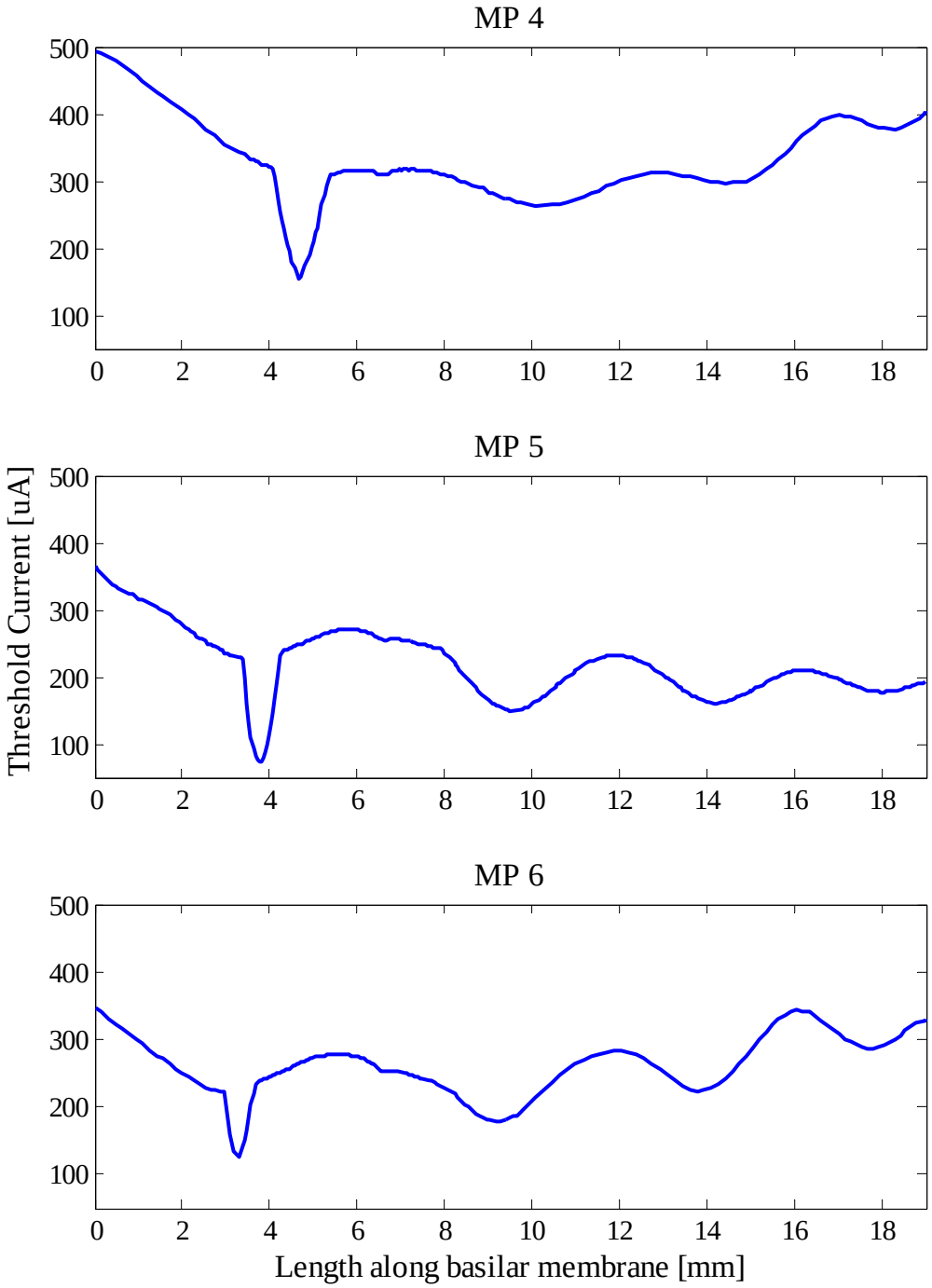

Figure 4.5. Threshold curves obtained from the model using MP4, MP5 and MP3 stimulation measured along the length of the basilar membrane from the base.

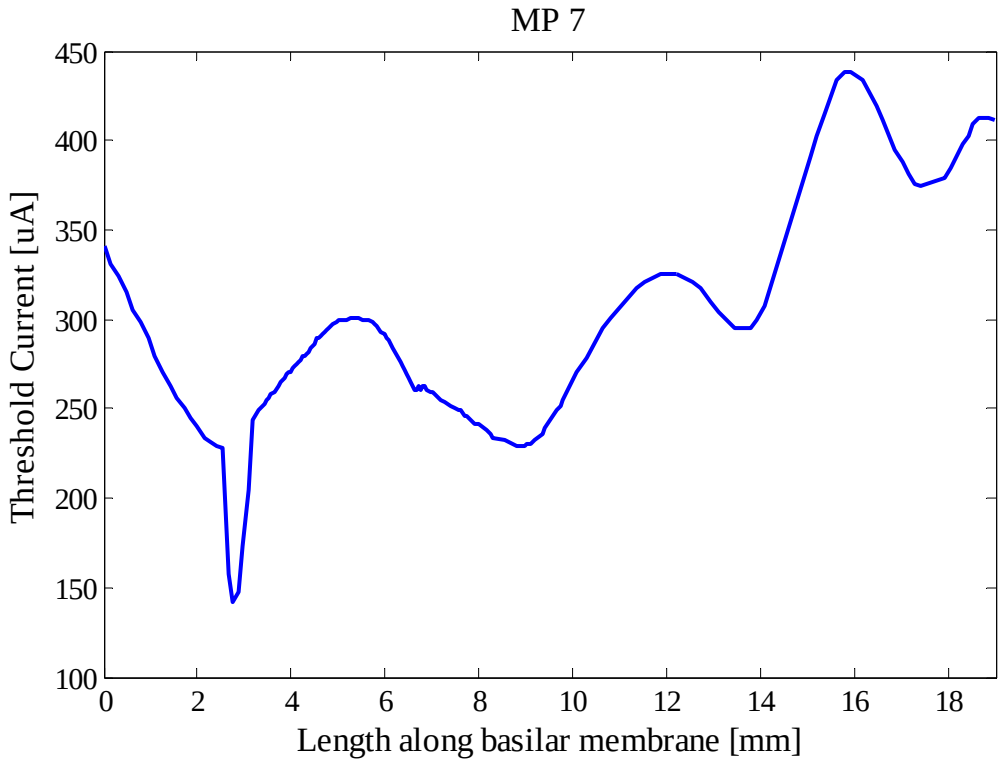

Figure 4.6. Threshold curve obtained from the model using MP7 stimulation measured along the length of the basilar membrane from the base.

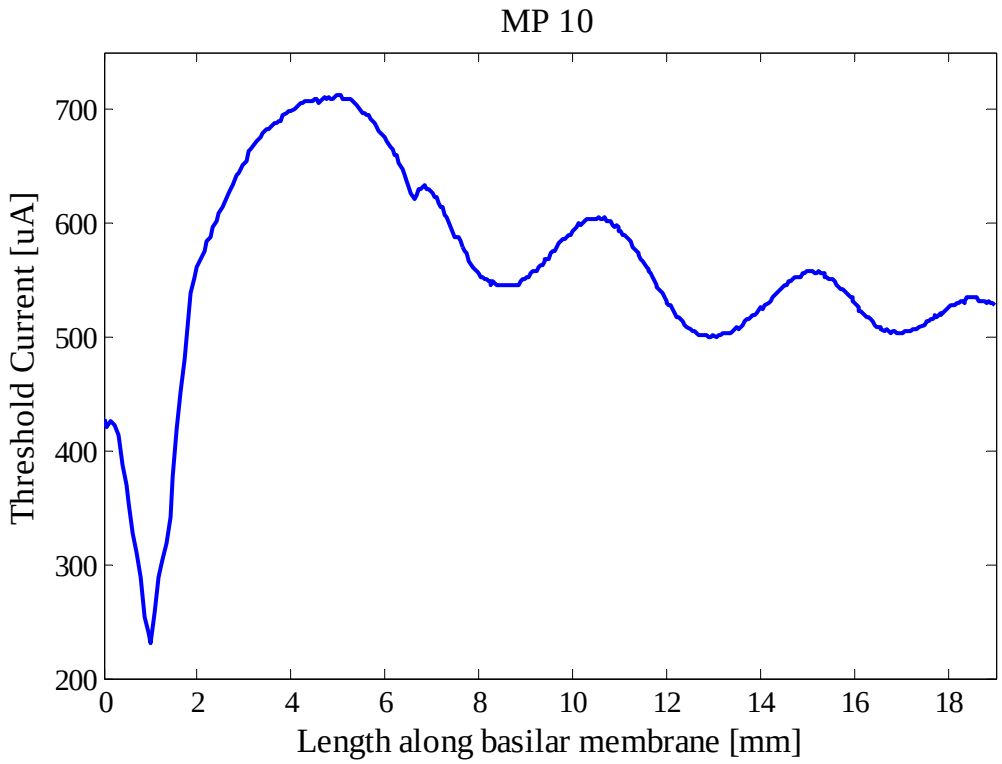

Figure 4.7. Threshold curve obtained from the model using MP10 stimulation measured along the length of the basilar membrane from the base.

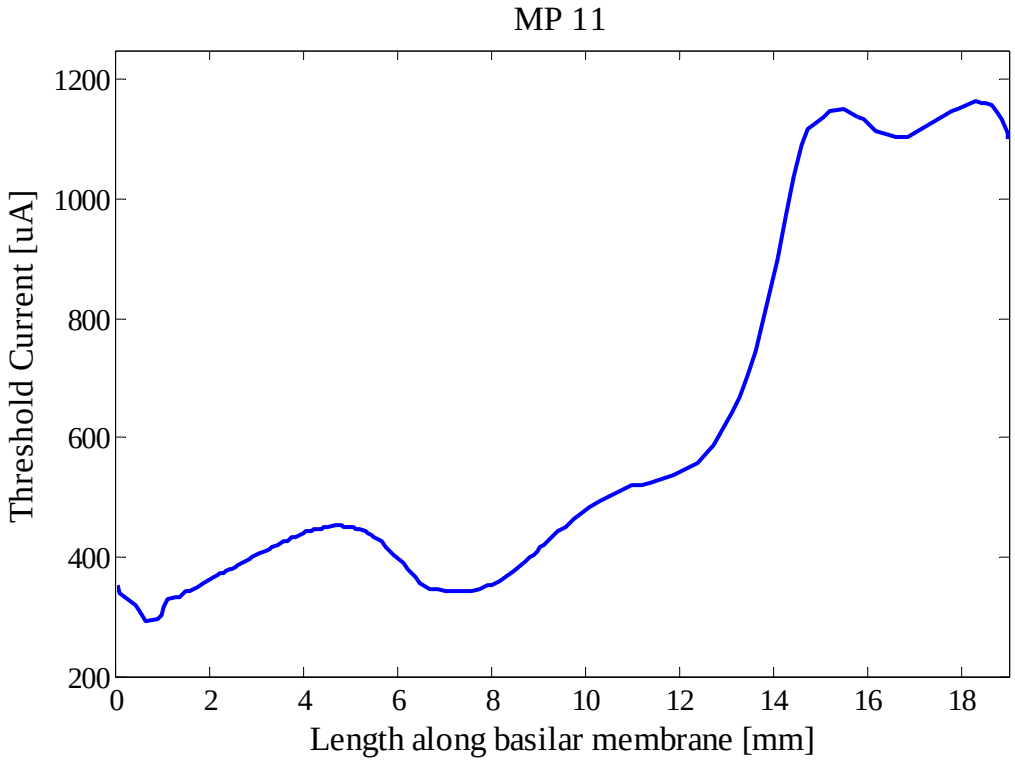

Figure 4.8. Threshold curve obtained from the model using MP11 stimulation measured along the length of the basilar membrane from the base.

A clear minimum can be seen in all monopolar cases. This minimum indicates the location along the basilar membrane where a very low threshold is required to cause a neural response. The position of the minima increased along the length of the basilar membrane as the position of the electrode increased along the length of the basilar membrane. This is intuitive if it is assumed that the neurons closest to the electrode will have the smallest threshold.

To investigate this assumption, the positions of the electrodes were compared to the positions of the minima. The positions of the electrodes were measured from the model. Table 4.4 lists these positions and indicates the error.

Table 4.4. Comparison of electrode position vs. minima position. Positions are given as the distance along the basilar membrane measured from the model base.

Electrode Number	Electrode position [mm]	Position of minimum [mm]	% Error
1	6.0512	6.2339	2.93
2	5.5057	5.5960	1.61
3	5.0153	5.1036	1.73
4	4.6664	4.6664	0.00
5	3.7994	3.7548	1.19
6	3.2377	3.2873	1.51
7	2.7587	2.7587	0.00
10	0.9412	1.0194	7.67
11	0.7055	0.7448	5.27

The trend of these results is that the site with a minimum threshold is very close to the electrode position. As can be seen from the errors, it is not located exactly at the location of the electrode. This is most likely because of the non-uniform geometry of the cochlea.

Other local minima periodically occurring along the cochlea are seen in all the results. These local minima all occur at the same angle around the modiolus. This implies that the stimulating electrode also elicits a response in cochlear turns other that the one it is located in. This is referred to as ectopic or cross-turn stimulation. This usually happens when the axons of neurons are stimulated in the modiolus where the axons of neuron from other turns lie at the same angle as the neurons from the stimulated turn.

4.4.2 Bi-polar Stimulation

Bi-polar stimulation was applied to electrode pairs 1-2, 2-3, 3-4, 4-5, 5-6, 6-7, 9-10 and 10-11. The threshold curves obtained from the model are shown in Figure 4.9 to Figure 4.11.

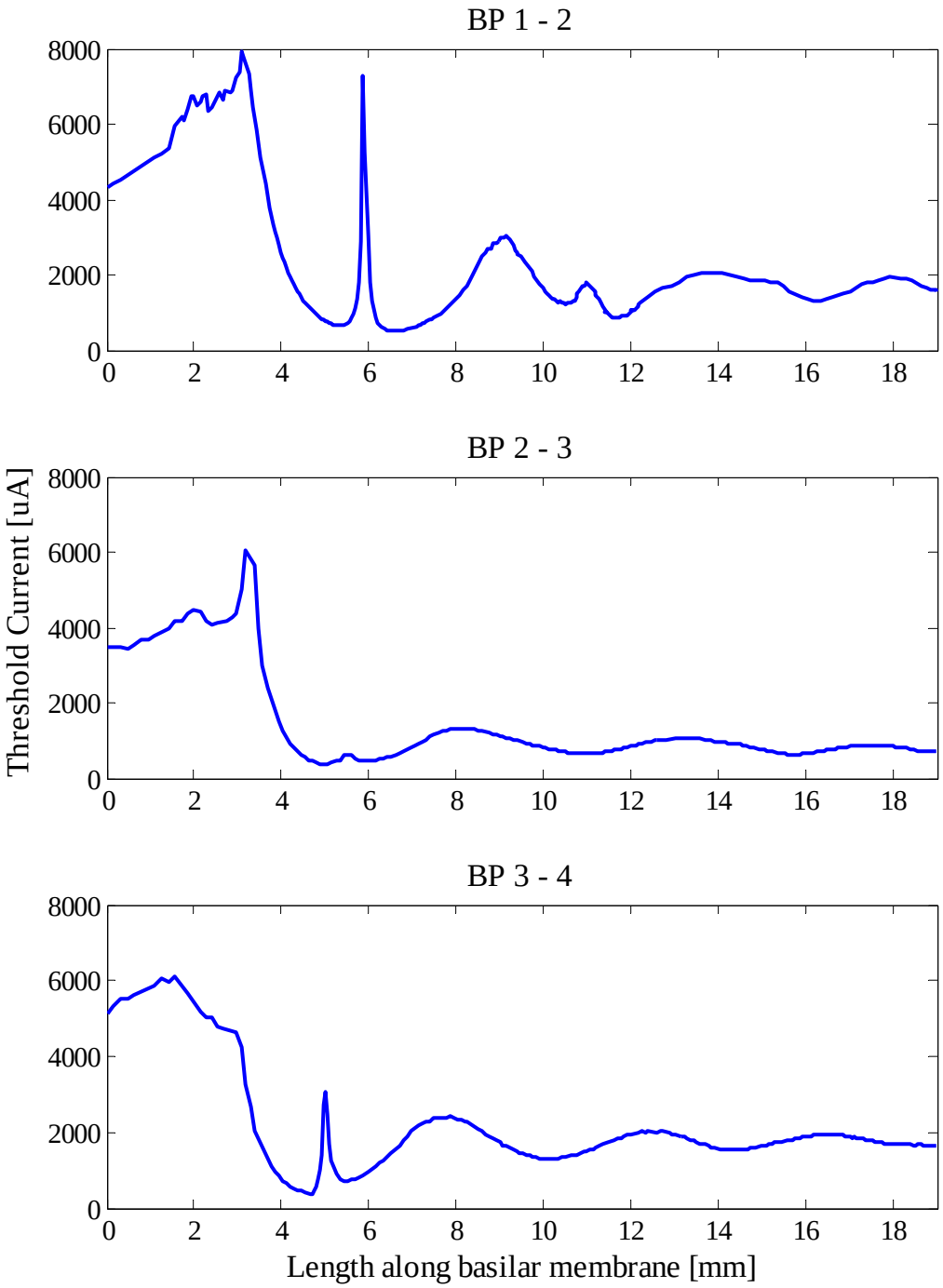

Figure 4.9. Threshold curves obtained from the model using BP 1-2, BP 2-3 and BP 3-4 stimulation measured along the length of the basilar membrane from the base.

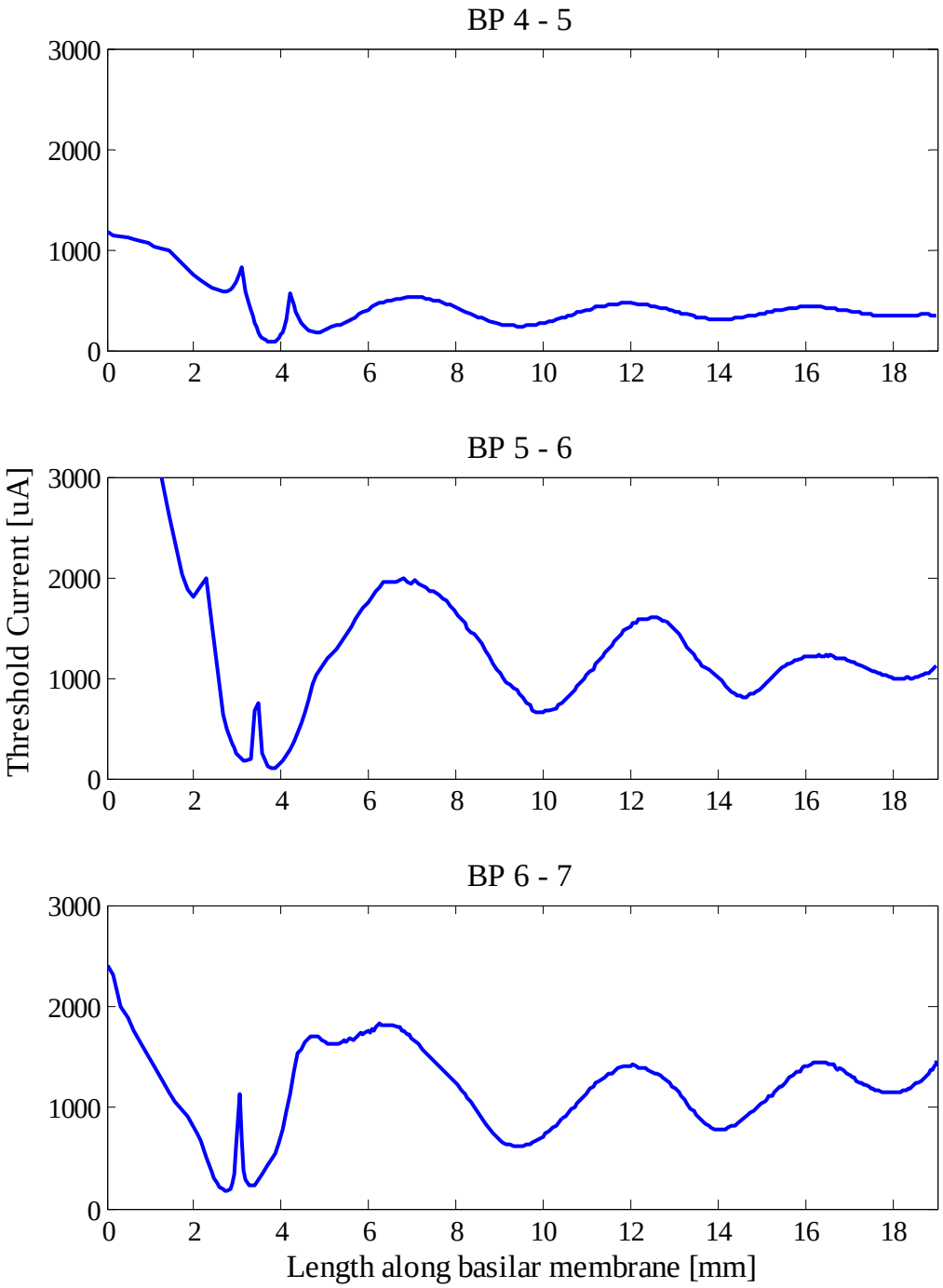

Figure 4.10. Threshold curves obtained from the model using BP 4-5, BP 5-6 and BP 6-7 stimulation measured along the length of the basilar membrane from the base.

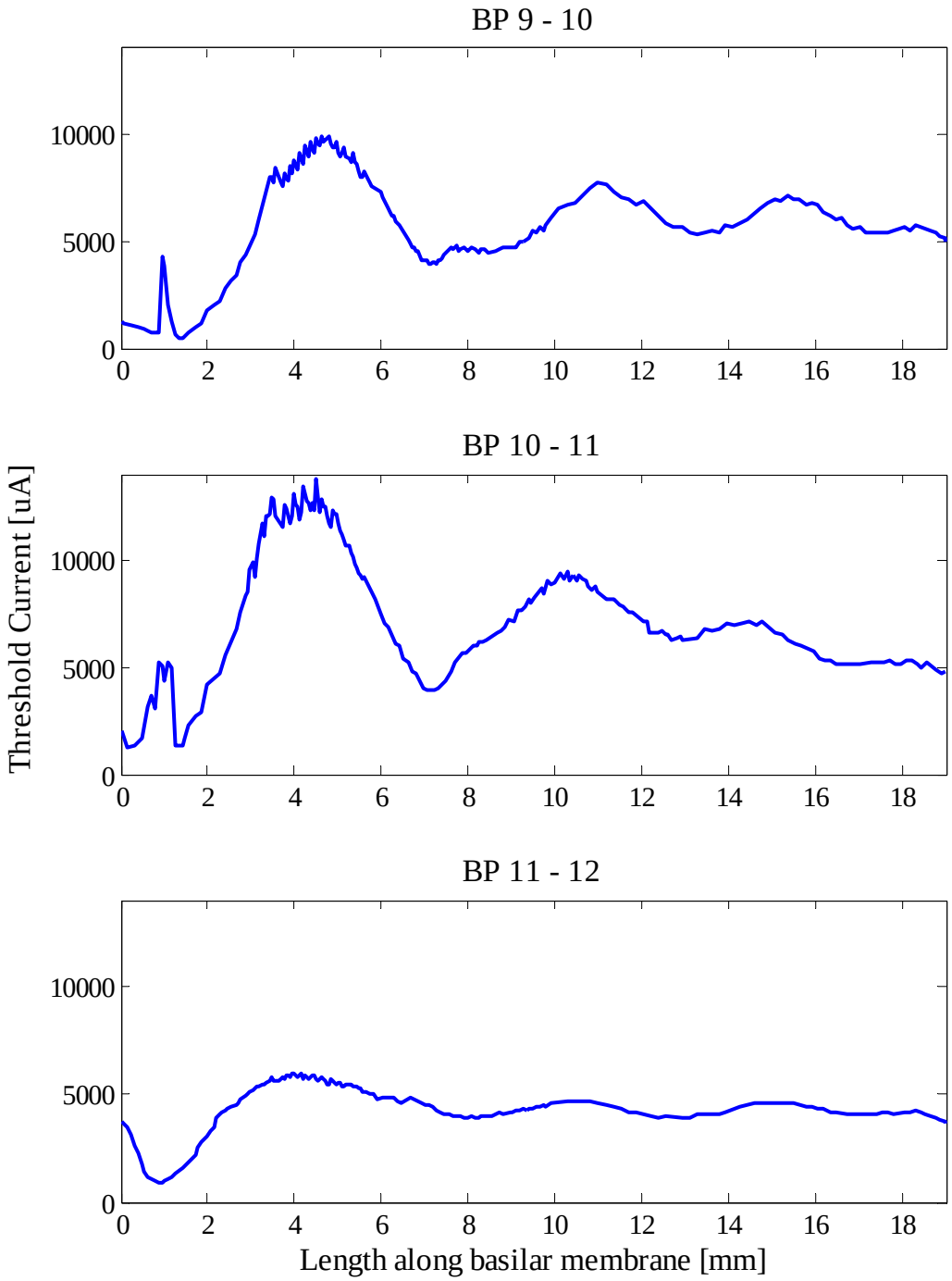

Figure 4.11. Threshold curves obtained from the model using BP 9-10, BP 10-11 and BP 11-12 stimulation measured along the length of the basilar membrane from the base.

As in the case with monopolar stimulation, a clear minimum can be observed in all bi-polar cases. In some cases, double minima with a large positive peak are observed (Figure 4.9 and Figure 4.10). The large positive peak may be caused by the presence of a null

isopotential surface between the two stimulating electrodes. This surface may be aligned with the neurons in its vicinity causing equal potentials on the nodes of these neurons that results in them not firing. Similar results are seen in modelled responses by Frijns et. al. (Frijns et. al., 2000). Large positive peaks are not seen when using BP 9-10, BP 10-11, BP 11-12. This may be because the electrodes in these pairs are found further away from the neurons than in the case of the other electrode pairs. This may cause the null isopotential surface not to be planar as the larger cochlear geometry bends the electric fields. The null isopotential surface may also not line up perfectly with the nodes of a neuron due to the cochlear geometry.

Ectopic stimulation is clearly seen in all the threshold curves. The positive peak does not occur in the ectopic responses except in BP 1-2. Electrodes 1 and 2 are located more apically where the cochlear ducts are narrower. The narrower geometry places the electrode closer to the axons of neurons. This shorter distance will cause the electrical fields not to be warped that much. The ground plane will then still be in place to cause a positive threshold peak ectopically.

4.4.3 Tri-polar stimulation

Tri-polar stimulation was applied to electrode sets 1-2-3, 2-3-4, 3-4-5, 4-5-6, 5-6-7 and 10-11-12. The threshold curves obtained from the model are shown in Figure 4.12 to Figure 4.15.

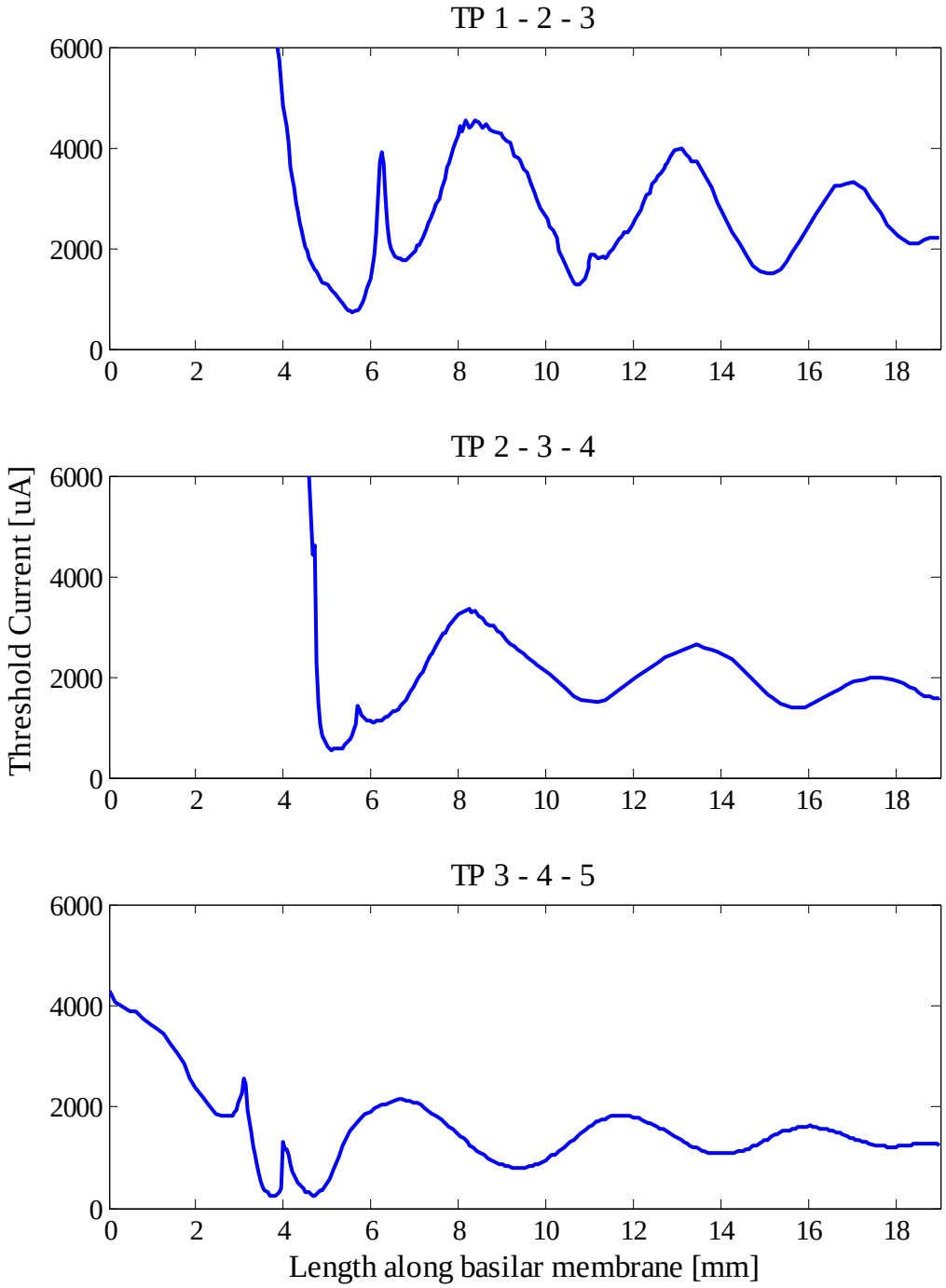

Figure 4.12. Threshold curves obtained from the model using TP 1-2-3, TP 2-3-4 and TP 3-4-5 stimulation measured along the length of the basilar membrane from the base.

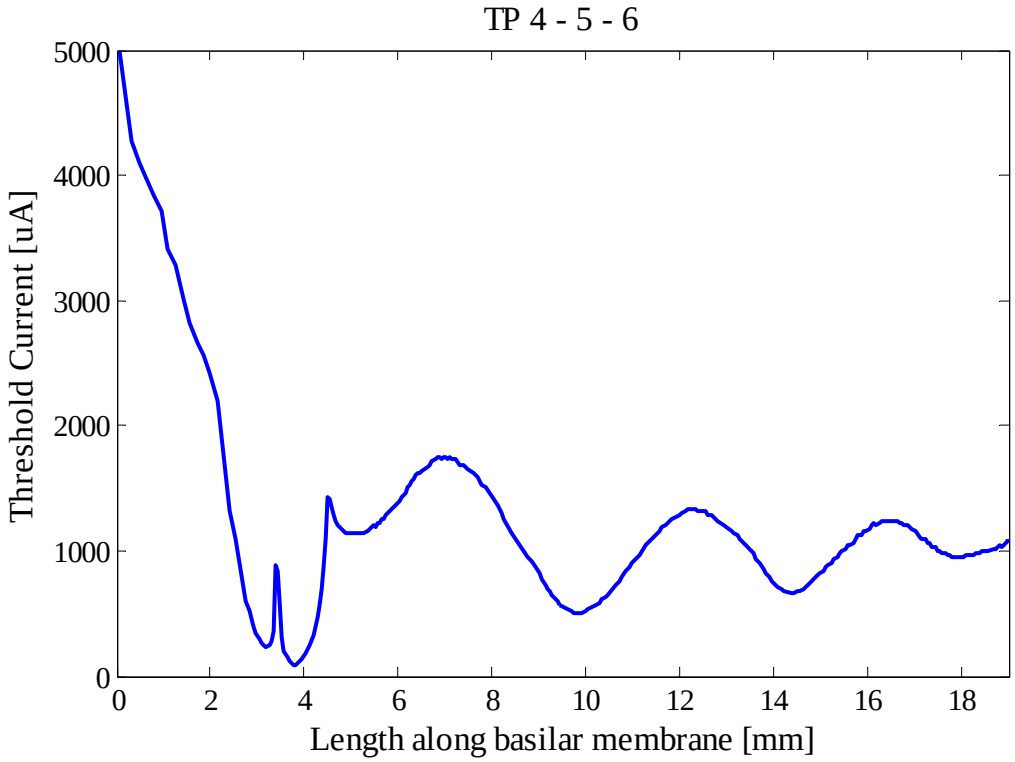

Figure 4.13. Threshold curves obtained from the model using TP 4-5-6 stimulation.

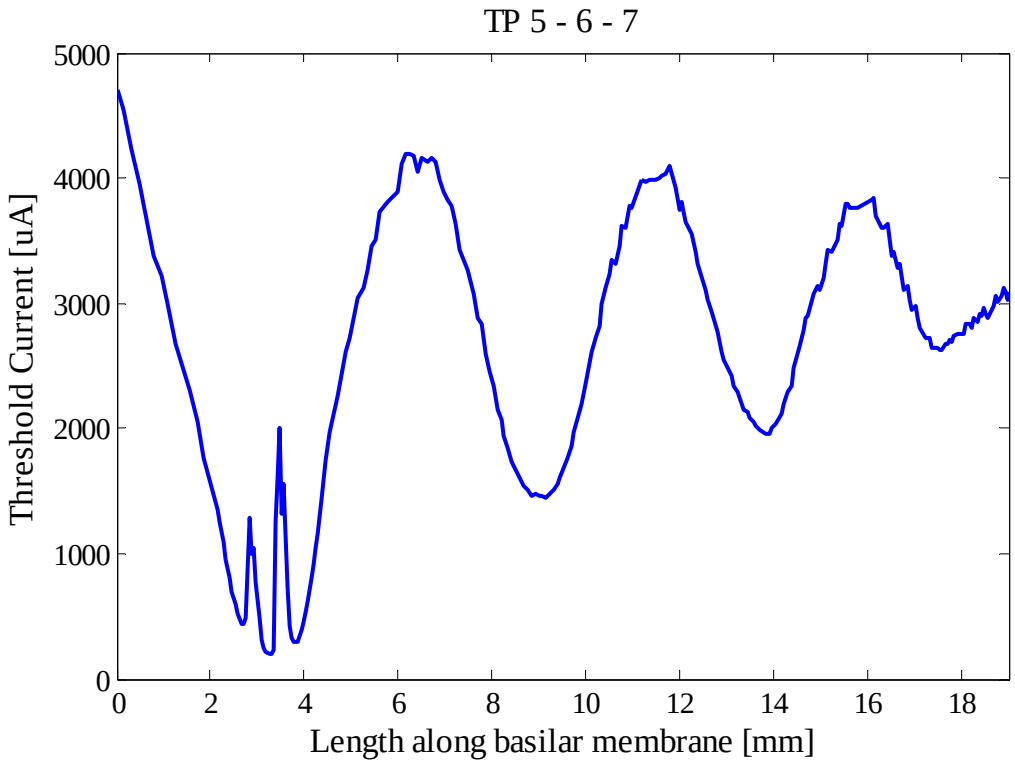

Figure 4.14. Threshold curves obtained from the model using TP 5-6-7 stimulation.

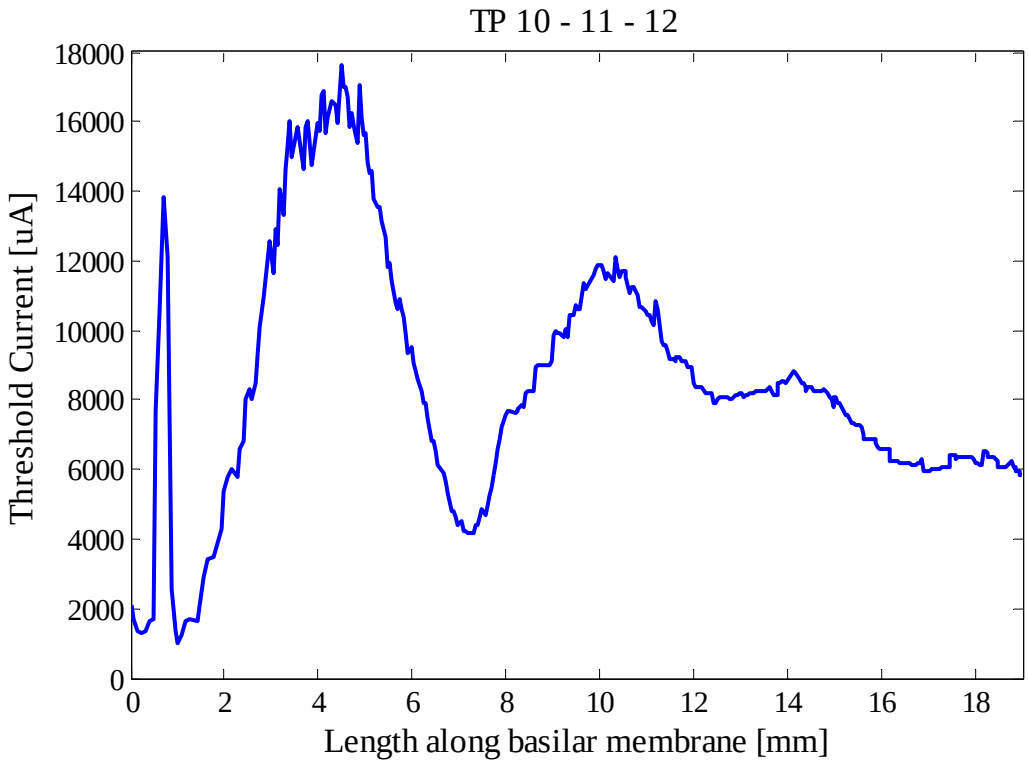

Figure 4.15. Threshold curves obtained from the model using TP 10-11-12 stimulation.

As is the case with monopolar and bi-polar stimulation, clear minima can be seen near the locations of the electrodes. All the threshold curves except TP 10-11-12 exhibit triple minima with positive peaks between them. These positive peaks are caused by the null isopotential surfaces forming due to the dipoles formed between the electrodes. This is similar to the bi-polar case. Only TP 10-11-12 has double minima with one positive peak in between. This may be because the electrodes are located further away from the neurons which may cause the one null isopotential surface not to be aligned with the neurons.

4.5 COMPARISON WITH BRAINSTEM RESPONSE DATA

Recorded EABR data was compared to the output data of the model. This was done to verify if the subject specific model is able to predict certain outcomes normally obtained using EABR recordings.

4.5.1 Frequency mapping

To compare the model data to the EABR data, the model threshold curves were plotted as a function of frequency and not as a function of the length along the basilar membrane (as it is plotted in Figure 4.4 to Figure 4.15).

To achieve this, the characteristic frequencies of the basilar membrane at locations along the length of the basilar membrane were determined using Greenwood's equation (Greenwood, 1990):

$$\begin{aligned} F &= A\left(10^{ax} - k\right) \\ &= 0.35 \times \left(10^{0.1135x} - 0.85\right) \end{aligned} \tag{4.2}$$

where F is the characteristic frequency in Hertz. The constants A, a and k were set to values found for the Guinea pig cochlea (Greenwood, 1990). x is the distance along the basilar membrane measured from the apex in mm.

Because the original cochlea from which the model was constructed was damaged near the apex, the position of the most apical part of the model was estimated. This has an influence on the measured length x. To compensate for this, an offset was added to x. This offset was varied until a good fit occurred between the estimated frequencies and the measured frequencies. An offset of 2 mm was subtracted from the distance measured from the modelled apex to ensure a good fit.

Strictly speaking a deafened animal does not have areas in the cochlea that are sensitive to acoustic frequencies. The frequencies mentioned here refer to the frequencies that the cochlea was sensitive to before deafening and aids in the comparison between EABR data and modelled data.

4.5.2 Threshold frequency location

The minimum stimulation current at which any neuron fires in a stimulation protocol is called the threshold current. The location along the basilar membrane at which that threshold occurs is mapped to frequency and called the threshold frequency.

The threshold frequencies obtained from the model and EABR results are compared in Table 4.5. The ratios between the EABR threshold frequencies to the model frequencies are shown. The mean and standard deviation of each protocol are also shown. The mean ratios are close to 1. This shows that the model can accurately predict the threshold frequency as a result of a specific stimulus. The slight deviation from unity that occurs may be due to the low frequency resolution of the EABR data and inaccuracies occurring when applying Greenwood's equation to this specific cochlea.

Table 4.5. Comparison of threshold frequencies between model and EABR data. There is a close match between the results from the model and EABR data.

Protocol	Distance from apex [mm]	Model Frequency [kHz]	EABR Frequency [kHz]	Ratio (EABR/Model)
Monopolar				
MP 1	10.75	5.52	7.30	1.32
MP 2	11.39	6.57	7.30	1.11
MP 3	11.88	7.51	7.30	0.97
MP 4	12.32	8.46	8.00	0.95
MP 5	13.23	10.81	8.00	0.74
MP 6	13.70	12.26	8.00	0.65
MP 7	14.23	14.12	14.70	1.04
MP 10	15.97	22.41	29.30	1.31
MP 11	16.24	24.10	29.30	1.22
Mean +- S.D.				1.03 ±0.23

Bi-polar				
BP 1-2	12.39	4.98	4.80	0.96
BP 2-3	13.93	7.60	6.20	0.82
BP 3-4	14.32	8.45	7.30	0.86
BP 4-5	15.23	10.81	12.30	1.14
BP 5-6	15.23	10.81	12.30	1.14
BP 6-7	16.28	14.33	14.70	1.03
BP 9-10	17.58	20.22	22.60	1.12
BP 10-11	18.83	28.15	24.70	0.88
BP 11-12	18.12	23.35	24.70	1.06
Mean +- S.D.				1.00 ±0.13
Tri-polar				
TP 1-2-3	13.43	6.65	--	--
TP 2-3-4	13.88	7.51	--	--
TP 3-4-5	15.23	10.81	12.30	1.14
TP 4-5-6	15.23	10.81	12.30	1.14
TP 5-6-7	15.75	12.41	12.30	0.99
TP 10-11-12	18.99	22.40	24.70	1.10
Mean +- S.D.				1.09 ±0.07

4.5.3 Absolute Overall Thresholds

The absolute overall thresholds of the modelled and brain stem responses were obtained and are listed in Table 4.6. The ratios between the thresholds from the model relative to the EABR data are compared. The mean ratios are also shown. The thresholds obtained from protocols involving the first seven electrodes are significantly different from the ratios of protocols involving the last four electrodes. Their means are calculated separately to show this difference. It is also evident that the ratios between bi-polar and tri-polar are somewhat similar. The average monopolar ratios are almost double that of the bi-polar and tri-polar cases. Overall there is, however, no consistent ratio between all the thresholds from the model and EABR data.

A consistent conclusion that can be made from this data is that the mean thresholds of the bi-polar and tri-polar protocols are higher than the mean threshold of the monopolar protocol. This is true for both the modelled and EABR data and is consistent with literature (Bierer and Middlebrooks, 2002; Brown et. al., 1996; Hartmann and Klinke, 1990; Kral et. al., 1998; Snyder et. al., 2004; Snyder et. al., 2008; Snyder et. al., 1990; Van Den Honert and Stypulkowski, 1987).

Table 4.6. Comparison of absolute minimum thresholds of stimulation protocols. Monopolar stimulation has the lowest thresholds on average compared to bi-polar and tri-polar stimulation.

Protocol	**Model Threshold [uA]**	**EABR Threshold [uA]**	**Ratio (model/EABR)**
Monopolar			
MP 1	198	25.18	7.86
MP 2	201	25.18	7.98
MP 3	204	31.70	6.44
MP 4	153	31.70	4.83
MP 5	75	31.70	2.37
MP 6	126	31.70	3.98
MP 7	142	39.91	3.56
MP 10	231	63.40	3.64
MP 11	293	71.13	4.12
Mean ± S.D. (All)	180.33 ± 64.05	39.06 ± 16.67	4.97 ± 2.00
Mean ± S.D. (MP 1 to MP 7)	157.00 ± 47.87	31.01 ± 4.98	5.29 ± 2.19
Mean ± S.D. (MP 10 to MP 11)	262.00 ± 43.84	67.26 ± 5.47	3.88 ± 0.34

Bi-polar			
BP 1-2	503	158.49	3.17
BP 2-3	376	251.19	1.50
BP 3-4	352	316.23	1.11
BP 4-5	82	158.49	0.52
BP 5-6	100	158.49	0.63
BP 6-7	178	125.89	1.41
BP 9-10	444	141.00	3.15
BP 10-11	1286	177.51	7.24
BP 11-12	906	250.74	3.61
Mean ± S.D. (All)	469.67 ± 395.79	193.11 ± 64.15	2.48 ± 2.13
Mean ± S.D. (BP 1-2 to BP 6-7)	265.17 ± 170.19	194.80 ± 72.98	1.39 ± 0.96
Mean ± S.D. (BP 10-11 to BP 11-12)	878.67 ± 421.67	189.75 ± 55.88	4.67 ± 2.24
Tri-polar			
TP 1-2-3	736	--	--
TP 2-3-4	528	--	--
TP 3-4-5	233	316.23	0.74
TP 4-5-6	95	251.19	0.38
TP 5-6-7	199	158.49	1.26
TP 10-11-12	1006	223.47	4.50
Mean ± S.D. (All)	383.25 ± 355.40	237.34 ± 65.38	1.72 ± 1.89
Mean ± S.D. (TP 3-4-5 to TP 5-6-7)	175.67 ± 265.45	241.97 ± 79.27	0.79 ± 0.44

To compare the trends between the data, the absolute thresholds for each stimulation configuration were normalized to values between 0 and 1 and are plotted in Figure 4.16 to Figure 4.18.

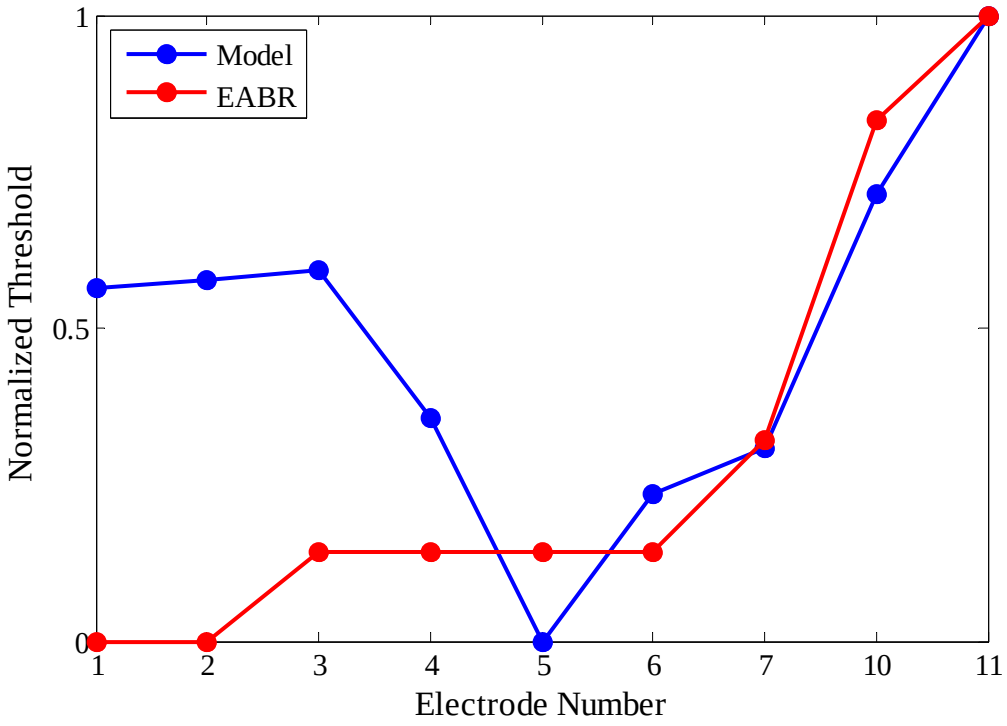

Figure 4.16. Normalized model thresholds (blue) and EABR thresholds (red) of each electrode using monopolar stimulation.

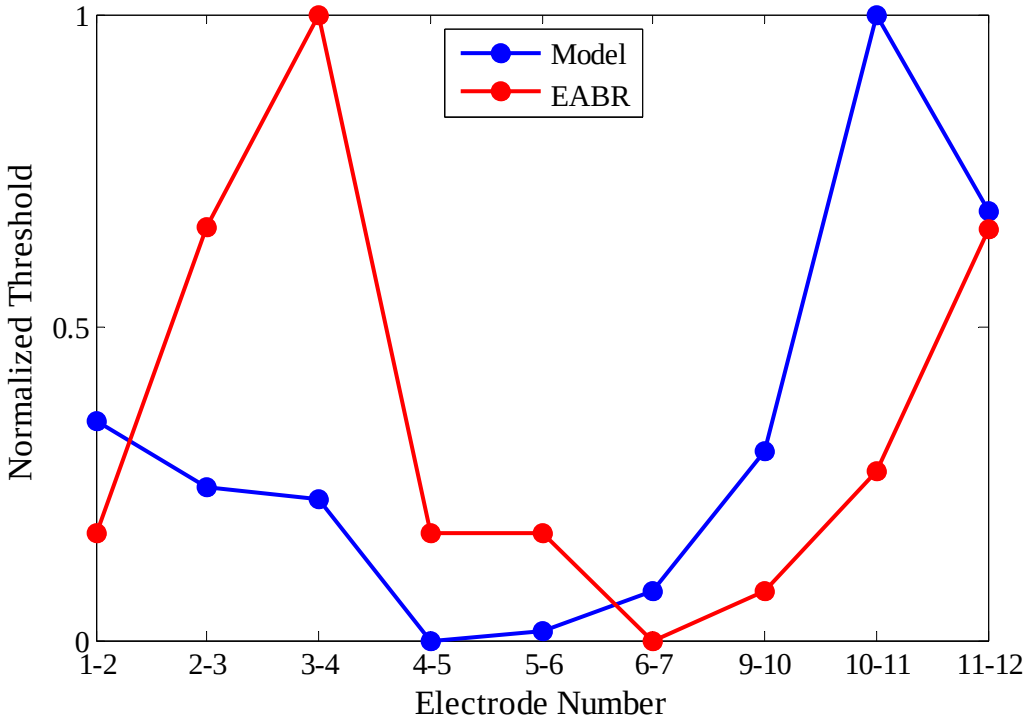

Figure 4.17. Normalized model thresholds (blue) and EABR thresholds (red) of each electrode pair using bi-polar stimulation.

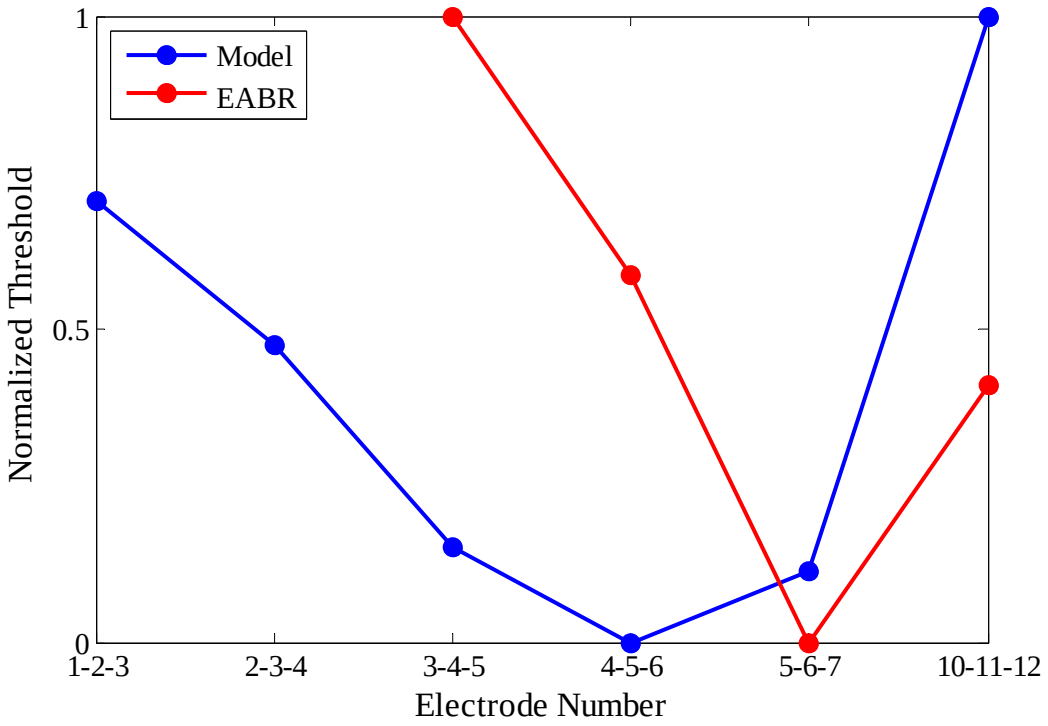

Figure 4.18. Normalized model thresholds (blue) and EABR thresholds (red) of each electrode set using tri-polar stimulation. Note that data is not available for EABR responses TP 1-2-3 and TP 2-3-4.

For all three configurations there is a slight trend for the model thresholds (blue) to decrease from electrode 1 (located apically in the cochlea) to electrode 5 and then increase towards electrode 12 (located basally).

It is expected that there would be a consistent trend between different stimulation configurations as the positions of the electrodes involved stay the same. A study by Snyder et. al. (Snyder et. al., 2008) confirms this where a trend was found for the thresholds to increase basally for MP, BP and TP stimulation.

The EABR data of the present study does not follow the same trend across all the stimulation modes. There is a trend for thresholds of the more basal electrodes to increase more basally, but the more apical electrodes show no such trend. There are a few differences between the model and EABR thresholds. They can be explained in light of the electrode position in the cochlea as well as the possible damage caused to cochlear structures and neurons during insertion.

Electrode 4 is located in the scala media. This shows that the electrode array perforated the upper wall of the scala tympani during insertion. This may have caused a change in resistance of the structures near the damaged area. Also potassium-rich endolymph may have leaked from the scala media which is neurotoxic. Damage was also likely caused to the organ of Corti and the neurons near electrode 4. This neural damage will cause the measured response to differ from the response predicted by the model because neural damage was not incorporated in the model.

The EABR thresholds of electrodes 1 and 2 using monopolar stimulation are lower than the EABR thresholds of the other electrodes. This may be because they create a current path to the monopolar return electrode where neurons are easily excited. This current path is not formed in the model data because the return electrode was not modelled as a single electrode but rather by setting the boundary of the bone conductor to ground. This was done because the exact position of the return electrode in the subject was not known. Electrode 5 is located the closest to the neurons (Figure 3.25). This should cause it to have the lowest threshold. This is the case in the modelled data. It also has a low threshold in the EABR data. Electrodes 3, 4 and 6 are spaced almost as close to the neurons but have the same EABR threshold as electrode 5. This may be due to the limited amplitude resolution of the EABR data. Also the distance that the electrodes are located from the neurons has the smallest effect when using monopolar stimulation because current is more widely spread. The orientation of the electrodes to the return electrode may play a role in this current spread. The EABR thresholds of electrodes 7, 10 and 11 follow the same trend as the modelled thresholds.

Using bi-polar stimulation, electrode pairs 4-5, 5-6 and 6-7 have the lowest thresholds for both EABR and modelled data. This is expected as they are located closest to the neurons. EABR thresholds of electrode pairs containing electrode 4 are higher than the modelled thresholds. This may be because of the neuron damage that occurred near these electrodes during insertion which was not incorporated in the model. The effect of local neuron damage on thresholds will be less pronounced for monopolar stimulation as stimulation is less local.

Bi-polar EABR thresholds of electrode pairs containing electrodes 10 and 11 are lower than the modelled thresholds. This may be because these electrodes were modelled surrounded by the intact spiral ligament. In the actual animal this may not be the case. The spiral ligament may have been pushed aside by the electrode carrier. This should cause a lower resistance path between the electrodes and the neurons which will cause lower thresholds.

Tri-polar EABR thresholds are higher than the modelled thresholds when electrode 4 is involved. If it is assumed that neurons were damaged during insertion, this result is valid as damaged neurons near electrode 4 will show higher thresholds as less spikes are recorded.

The absence of the electrode carrier will have an effect on the thresholds. This is because it displaces conducting perilymph in the scala tympani and scala vestibuli. This causes a higher impedance in the cochlear ducts. This causes less current to be shunted between electrodes and more current to flow through the neurons. This higher impedance may cause thresholds to be lower (Hanekom, 2005).

During insertion of the electrode carrier, holes may be made in membranes. These holes may not be perfectly sealed by the carrier and may cause current to leak through to other structures. This will also influence the measured thresholds.

These results show that it cannot always be assumed that thresholds increase towards the base of the cochlea. Aspects such as the location of an electrode inside other cochlear structures and insertion damage may lead to different results. It is therefore essential to model the morphology and electrode position of a cochlea accurately to be able to model these differences.

4.5.4 Electrode Distance from Neurons

It is presumed that electrodes placed closer to the neurons would cause lower threshold currents. Model and animal studies confirm that an electrode array placed closer to the modiolus has lower thresholds (Briaire and Frijns, 2006; Firszt et. al., 2003). The electrode

array of the present subject is not located entirely in the scala tympani as in these studies. It is located partially in the scala tympani, scala media, scala vestibuli and extracochlear space outside the round window as it was inserted through the side of the cochlear wall and perforated the upper wall of the scala tympani. The electrodes of the array are thus located in different areas of the cochlea that have different conductivities.

To investigate the effect that distance from the neurons has on threshold values, the monopolar thresholds were normalized and plotted as a function of distance from the modiolus in Figure 4.19. Data was normalized between 0 and 1 where 1 corresponds to the maximum value of all the data points. Electrodes located in the same cochlear structures were connected. The electrode numbers are indicated at the top of the graph.

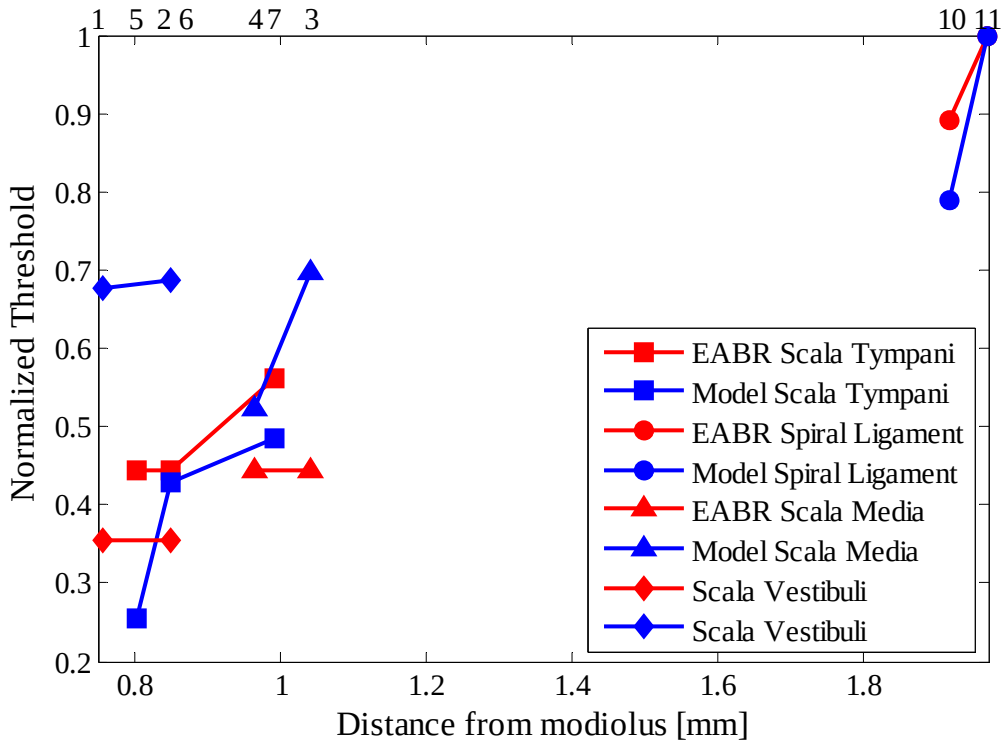

Figure 4.19. Normalized monopolar threshold values as the distance of the electrodes from the modiolus is increased. The EABR threshold values are shown in red whereas the thresholds from the model are shown in blue. The electrode numbers are shown at the top of the graph. Electrodes located in the same cochlear structures are connected.

The thresholds do not increase linearly as the distance between the electrodes and modiolus increases (as in the case of the verification array). This is because the electrodes are located in different cochlear structures with different material properties. There is a trend for thresholds of electrodes placed in the same cochlear structure to increase as the distance from the modiolus is increased. E.g. electrodes 5, 6 and 7 are all located in the scala tympani and their corresponding thresholds increase or stay the same as the distance from the modiolus is increased. This is true for both the model and the EABR data. This shows that the model is capable of predicting threshold trends within cochlear structures.

The model predicts lower thresholds for the electrodes located in the scala tympani (electrodes 5, 6 and 7) than the EABR data suggests in relation to other electrodes. This may be because modelled neural responses are mostly activated at the dendrites of the neurons, whereas the actual subject neurons may have been activated in the axons and have higher threshold values. The silastic carrier was not modelled. Such a carrier may have an influence on current spread inside the cochlea and have an effect on measured thresholds.

4.5.5 Spatial tuning curve width

The width of the spatial tuning curve at a certain stimulus intensity gives an indication of the current spread in the cochlea. Certain stimulus protocols like bi-polar and tri-polar stimulation are used instead of monopolar stimulation because of the more focused current spread it elicits.

The widths of the threshold curves obtained from the model were compared to the spatial tuning curves obtained from the brain stem response data. Widths were measured at a stimulus level of 2 dB above the absolute minimum threshold. This value was used because some EABR responses (like BP 2-3 see Figure 3.40) do not have data available for higher stimulus intensities. The widths of the brain stem responses are given as frequency ranges to account for the low frequency resolution of the EABR data. The method used to obtain these ranges is described in section 3.6 (p.65).

Some of the modelled bi-polar and tri-polar threshold curves have sharp positive spikes near the thresholds as described in sections 4.4.2 and 4.4.3. These spikes make determination of the width difficult as they split the width to be measured into 2 or three parts. If present, these spikes would not be visible in the brain stem response data because of the low spatial resolution of the EABR recording method. They may not be present the EABR data if the null potential isosurfaces are not parallel to the neuronal processes. This causes the brain stem response widths to be larger because the gaps caused by the spikes are not subtracted from the measured widths. To compensate for this effect, the spikes in the modelled responses were removed. This was done by interpolating the threshold curve between the values where the spikes are using spline interpolation. This was implemented using the 'interp' function in Matlab set up to use the 'spline' method. An example is shown in Figure 4.20. The red line indicates the interpolated data. The blue line is the original threshold curve.

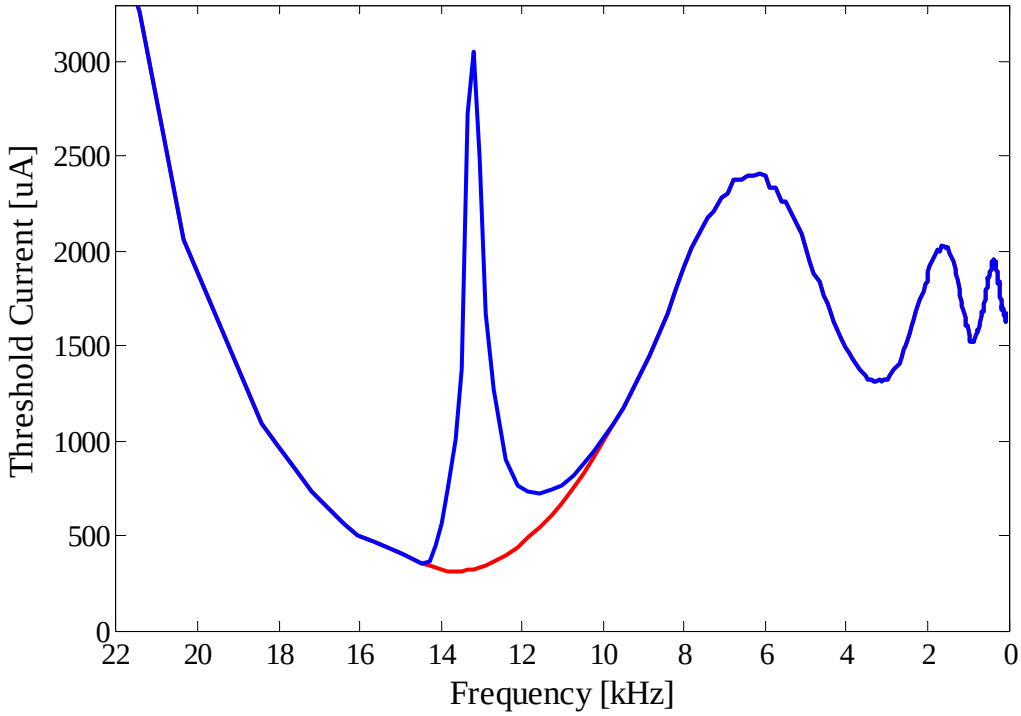

Figure 4.20. Example of spike removal from the modelled response to assist in width determination. The original threshold response is shown in blue and the new interpolated data is shown in red. The new data is used to determine the STC width. This is done to assist in the comparison with EABR data that does not show spikes because of its low resolution.

The widths of the various stimulation protocols are listed in Table 4.7. Errors are also indicated. An error of 0 was obtained when the modelled width fell within the range of the EABR width.

The errors indicate that about half of the modelled bi-polar and most of the tri-polar STC widths fall within the width ranges of the EABR data. The monopolar widths obtained with the model are a lot narrower than the EABR widths. This may be in part because the modelled cochlea was entirely encased in bone, whereas a guinea pig cochlea is surrounded by a thin layer of bone surrounded by an air-filled bulla. The ground electrode was placed in this bone. This may cause monopolar currents to spread differently than expected. Another reason for the discrepancy in widths between the model and EABR data may be due to the inherent differences between the thresholds of single fibre responses (as was modelled) and spike rate thresholds of neural populations containing activity of the ICC not related to cochlear stimulation (obtained from EABR data).

Table 4.7. Comparison of modelled widths to EABR widths. Bi-polar and Tri-polar widths closely match EABR data whereas monopolar widths are a lot narrower than in the EABR data.

Protocol	EABR Width Range [kHz]	Model Width [kHz]	Error [%]
Monopolar			
MP 1	11.2 - 14.6	1.75	84.33
MP 2	7.5 - 11.9	1.85	75.34
MP 3	24.5 - 26.5	1.67	93.20
MP 4	11.2 - 14.6	1.08	90.35
MP 5	11.2 - 14.6	0.86	92.36
MP 6	11.2 - 14.6	1.22	89.09
MP 7	12.6 - 17.9	1.46	88.39
MP 10	6.7 - 8.6	2.47	63.19
MP 11	4.6 - 6.7	2.26	50.93
Bi-polar			
BP 1-2	2.5 - 5.2	2.63	0.00
BP 2-3	2.5 - 5.2	2.79	0.00
BP 3-4	--	1.81	--
BP 4-5	1.4 - 4.5	2.47	0.00
BP 5-6	0 - 4.3	2.16	0.00
BP 6-7	3.7 - 7	2.73	26.18
BP 9-10	6.7 - 8.6	3.13	53.33
BP 10-11	6.7 - 8.6	8.78	2.07
BP 11-12	11.9 - 13.3	3.22	72.91
Tri-polar			
TP 1-2-3	--	1.47	--
TP 2-3-4	--	1.98	--
TP 3-4-5	1.9 - 5.2	2.98	0.00
TP 4-5-6	0 - 4.3	1.63	0.00
TP 5-6-7	2.4 - 5.6	2.63	0.00
TP 10-11-12	6.7 - 8.6	6.01	10.33

4.5.6 I/O Curves

Another method to determine the measure of the excitation spread (width) is to generate an I/O curve of the threshold curve.

An I/O curve gives the number of excited neurons for each stimulus current. The slope of this curve gives an indication of the spatial spread of excitation. A steep slope indicates that a small increase in stimulus current causes a lot of fibres to be activated. This is thus an indication of a wide excitation spread. The slope changes abruptly where ectopic excitation occurs. Such an I/O curve is shown in Figure 4.21.

The I/O curves were only generated for the part of the model that falls within the frequency range of the EABR data (2.8 kHz to 29.3 kHz). The number of neurons is given as a percentage of the total number of neurons in this reduced model.

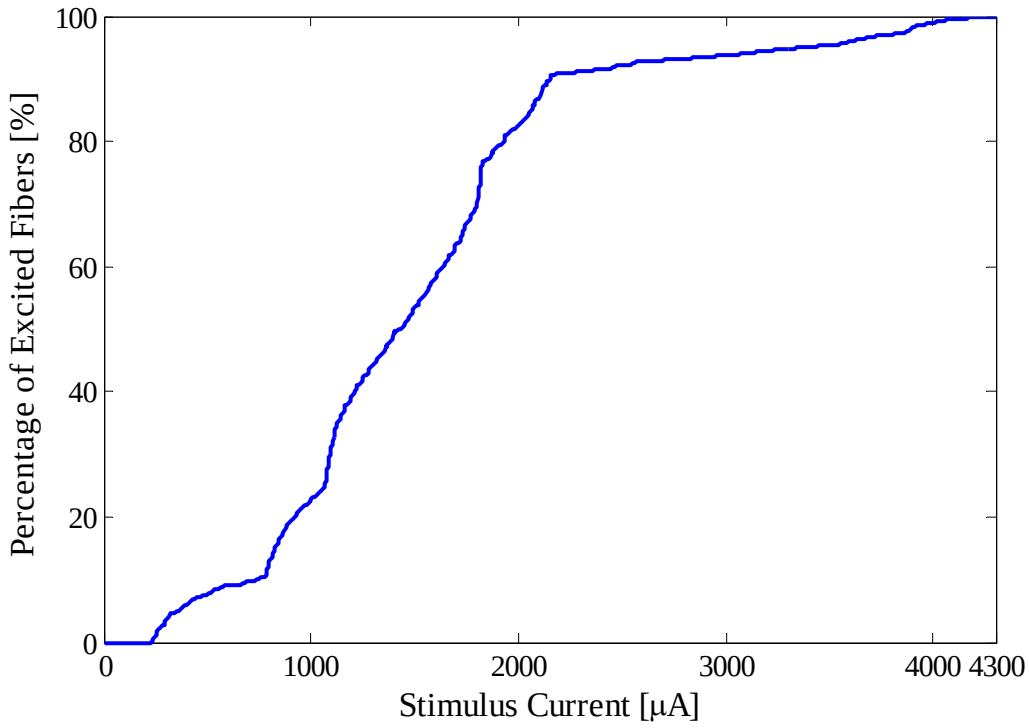

Figure 4.21. I/O curve from model (TP 3-4-5). The number of excited neurons is plotted as a function of the stimulus current. Note that abrupt changes in slope indicate the currents at which ectopic stimulation occurs.

I/O curves of the EABR data were also generated. To compare the model data to EABR data, the slope of the first 2 dB of the I/O curves were compared. In this stimulus range the slope is fairly constant because ectopic stimulation does not occur. This slope should thus give an indication of the width of the threshold curve.

In the EABR data the number of excited neurons is not known. The EABR data does however indicate the total number of spikes recorded. If it is assumed that each neuron contributes equally to the spike total when stimulated (Frijns et. al., 2000) and that the thresholds of all the neurons are the same, a relative measure of the total stimulated neurons can be obtained. The ratio between the slope from the model data and the slope from the EABR data was determined. This ratio is, however, only useful in determining the relative widths of the protocols as one does not know the number of spikes that a single neuron emits and therefore cannot determine the absolute width in frequency. Table 4.8 lists the results.

Table 4.8. Comparison of the slope of the first 2 dB of the I/O curves. The ratio between the EABR and model data is fairly constant for the bi-polar and tri-polar cases.

Protocol	**EABR Gradient [spikes / dB]**	**Model Gradient [% / dB]**	**Ratio [% / spikes]**
Monopolar			
MP 1	84.3	3.73	0.044
MP 2	90.08	3.43	0.038
MP 3	82.08	2.84	0.035
MP 4	108.45	1.64	0.015
MP 5	111.79	1.04	0.009
MP 6	88.03	1.04	0.012
MP 7	38.72	1.04	0.027
MP 10	442.23	0.9	0.002
MP 11	409.38	10.75	0.026
Mean ± S.D. (All)			0.023 ± 0.014
Mean ± S.D. (MP 1 to MP 7)			0.026 ± 0.014
Mean ± S.D. (MP 10 to MP 11)			0.014 ± 0.017

Bi-polar			
BP 1 – 2	23.72	2.84	0.120
BP 2 – 3	12.07	2.84	0.235
BP 3 – 4	--	1.04	--
BP 4 – 5	59.74	0.9	0.015
BP 5 – 6	12.36	0.9	0.073
BP 6 – 7	17.36	0.9	0.052
BP 9 – 10	1361.95	0.45	0.0002
BP 10 – 11	620.8	1.04	0.002
BP 11 – 12	610.2	1.04	0.002
Mean ± S.D. (All)			0.062 ± 0.082
Mean ± S.D. (BP 1 - 2 to BP 6 - 7)			0.099 ± 0.085
Mean ± S.D. (BP 10 - 11 to BP 11 - 12)			0.001 ± 0.001
Tri-polar			
TP 1 – 2 – 3	--	1.64	--
TP 2 – 3 – 4	--	1.34	--
TP 3 – 4 – 5	11.43	1.34	0.117
TP 4 – 5 – 6	9.39	0.9	0.096
TP 5 – 6 – 7	13.77	0.75	0.054
TP 10 – 11 – 12	399.62	0.3	0.001
Mean ± S.D. (All)			0.067 ± 0.051
Mean ± S.D. (TP 3 - 4 - 5 to TP 5 - 6 - 7)			0.089 ± 0.032

The mean of the ratios are similar for the bi-polar and tri-polar cases. If the spatial spreads of the model perfectly match the spatial spreads of the EABR data, the ratios should be constant for all stimulation protocols. When viewing the monopolar ratios in isolation, the low standard deviation leads one to the conclusion that the spatial spread is predicted correctly by the model. However, by comparing the results to the absolute widths (calculated in section 4.5.5), one finds that this assumption is incorrect. The modelled monopolar widths are constantly narrower than the EABR data. This leads to the ratio being lower than the bi-polar and tri-polar cases.

4.6 SUMMARY

This section summarized some of the results obtained using the model. A more general electrode array was firstly modelled. The output was compared to data found in literature to verify the model. The subject specific array was also modelled and compared to EABR data from the guinea pig subject. Some of the conclusions that can be drawn from these comparisons were discussed. The final discussion of all the results is given in the following chapter.

CHAPTER 5 DISCUSSION

5.1 INTRODUCTION

In this study, a method was developed to create a model of a specific cochlea for use in electric hearing research. This method was used to create a model of the cochlea of a specific guinea pig subject. The model was validated by modelling an electrode array with a more general shape and position in the cochlea and comparing its output to data found in literature. The extent to which the model output compares to EABR data obtained from the subject was also investigated. The findings of this study are discussed in this chapter. The research questions are also answered from these findings.

5.2 DISCUSSION OF RESEARCH QUESTIONS

The research questions are listed here and answered in the light of the results obtained from this study.

5.2.1 Is it possible to construct a subject specific cochlear model using available technology?

Yes, a subject specific cochlear model was successfully constructed using readily available technology. A µ-CT scanner was used to obtain the morphology of the cochlea. This method provided sufficient resolution and detail to image the outer and bony parts of the cochlea. The positions of the smaller inner parts of the cochlea were estimated using photomicrographs of cochleae from other subjects. This reduces the degree to which the model is subject specific. Photomicrographs of the subject used in this study were not available. If such data is available it will increase the accuracy of the model with regards to its subject specific structure.

All calculations and modelling were done using readily available software. FEM was used to obtain the current distribution inside the cochlea and was implemented using the commercial software package Comsol Multiphysics. The neuron model was implemented

in the widely used programming language C++. Other mathematical functions were implemented using Matlab which is also widely used as a research tool.

5.2.2 Is such a subject specific model able to predict neural responses in more detail than generic models?

Yes, in cases where the electrode array is located in different cochlear structures. When modelling the generic electrode array, with all the electrodes located in the scala tympani, there was a clear tendency for the absolute thresholds to increase as the distance between the stimulating electrode and the neurons increased. This is also predicted by models based on a non-subject specific geometry (Frijns et. al., 2000). When the subject specific electrode array was modelled, thresholds did not increase according to distance from the neurons. This was because the electrodes are found in different cochlear structures because the array perforated the upper wall of the scala tympani during insertion. This result was made possible by placing the modelled electrodes in the same cochlear structures in which they occur in the subject. This can only be done accurately by modelling the specific cochlear morphology of the subject.

5.2.3 To what extent does the output of this model compare to brain stem response data obtained from the guinea pig subject of which it was constructed?

Characteristic frequencies of electrodes obtained from EABR data were accurately predicted by the model. Relative spatial and threshold values within a stimulus protocol were estimated accurately, but absolute thresholds and spatial spread were not estimated correctly. This was investigated for an array with electrodes situated in different cochlear structures (subject specific cochlea used in this study). The extent to which the modelled data compares to the EABR data of a subject with an array with electrodes situated in one cochlear structure was not investigated. To accurately predict absolute threshold values and spatial spreads of electrodes, the accuracy of the model has to be refined. This is described in section 5.6. Further comparisons between EABR data and model data are discussed in section 5.4.

5.3 COMPARISON WITH LITERATURE

To validate the model, its output was compared to outcomes commonly found using other mathematical and animal models. To make this comparison, the detail of the model was reduced. An electrode array located in centre of the scala tympani was modelled. This reduced the detail of the model with regards to electrode placement. The morphology of the model was still kept the same as the specific subject.

Using this configuration, the model was able to predict outcomes generally found in literature.

The model predicted that monopolar stimulation yielded lower thresholds than bi-polar or tri-polar stimulation. This trend was also found in other studies (Bierer and Middlebrooks, 2002; Bierer and Middlebrooks, 2004; Brown et. al., 1996; Hartmann and Klinke, 1990; Kral et. al., 1998; Kwon and Van Den Honert, 2006; Snyder et. al., 2004; Snyder et. al., 2008; Snyder et. al., 1990; Van Den Honert and Stypulkowski, 1987).

The model also predicted that monopolar stimulation yields a wider spatial spread than bi-polar or tri-polar stimulation with tri-polar stimulation yielding the narrowest spatial spread. This result is also found in other studies (Bierer and Middlebrooks, 2002; Snyder et. al., 2008; Van Den Honert and Stypulkowski, 1987).

The effect of electrode separation during bi-polar stimulation was also investigated. The model predicted that a wider electrode separation yielded a wider spatial spread and had a lower threshold than bi-polar stimulation using adjacent electrodes. This finding is also consistent with other studies (Bierer and Middlebrooks, 2004; Lim et. al., 1989; Shepherd et. al., 1993; Snyder et. al., 2008).

Finally, the model predicted that electrode thresholds increased as the distance between the electrode and the neural elements increased. This is also consistent with literature (Briaire and Frijns, 2006; Firszt et. al., 2003; Frijns et. al., 2001; Frijns et. al., 1995; Shepherd et. al., 1993).

Based on these findings, it was concluded that the model output is valid and that it can be used as a research tool for investigating the effects that electrode position and stimulation protocol has on spatial spread and threshold values.

5.4 COMPARISON WITH SUBJECT EABR DATA

The subject specific electrode array was modelled to assess the extent to which the model can be used to predict EABR responses from the subject.

The model accurately predicted the characteristic frequencies at which the electrodes are located. This was done by mapping the positions of the electrodes along the basilar membrane to frequencies using Greenwood's equation (Greenwood, 1990). An offset was added to the length along the basilar membrane to account for modelling errors in the damaged apical region of the subject cochlea. These results show that the positions of the electrodes along the basilar membrane were modelled correctly and that the model may be used to predict EABR characteristic frequencies.

The absolute thresholds of electrodes were determined for monopolar, bi-polar and tri-polar stimulation protocols. In all cases, the modelled threshold values were higher than the EABR thresholds. Monopolar stimulation yielded thresholds that were on average 4.97 times higher than EABR data. Modelled bi-polar and tri-polar thresholds were on average 2.48 and 1.72 times higher than EABR thresholds respectively. The absence of the electrode carrier in the model may have an effect on these values as it influences the current spread in the cochlea.

The modelled thresholds followed a slight trend to decrease from electrode 1 towards electrode 5 and then increase to electrode 12 in all the protocols. This trend is however not visible in the EABR data. It is intuitive that the trend should stay the same across protocols. This is because the electrode positions do not change and threshold is a function of the distance to the neurons (sections 4.3.4 and 4.5.4). A study using similar EABR recording techniques found the same threshold trend across all three stimulation protocols

(Snyder et. al., 2008). There the trend was for the thresholds to increase basally. In this study the electrodes are however located in different cochlear structures. This fact combined with the possible neuron damage incurred during insertion, has an effect on the thresholds of electrodes.

The effect that the distance between an electrode and the neurons has on threshold values was investigated for the monopolar case. It was found that the thresholds of electrodes found in the same cochlear structures followed the trend to increase as distance from the neurons increased. This was true for the modelled as well as the EABR thresholds. No trend was however found across electrodes placed in different cochlear structures. This may explain why there is no common threshold trend between stimulus protocols. In bi-polar and tri-polar protocols, electrodes in different cochlear structures may be employed. This may result in relative thresholds being different from the monopolar case.

The spatial spread of each electrode using each stimulation protocol was obtained at 2 dB above the threshold. The EABR monopolar widths were on average eight times wider than the modelled widths. This may in part be ascribed to the monopolar return electrode and surrounding bone that was not modelled exactly as it is in the subject. The bi-polar and tri-polar EABR widths were on average 1.5 and 1.1 times wider than the modelled widths respectively. The most of the modelled bi-polar and tri-polar widths compared well to the EABR widths. The EABR widths were estimated as a range of frequencies to compensate for the low frequency resolution at which it was obtained (responses were measured at 16 discrete frequency sites).

To compensate for this frequency resolution inaccuracy, I/O curves were also generated. These curves also give an indication of the spatial spread. An I/O curve shows the total number of recorded spikes as a function of stimulation current. The resolution of these curves is not limited by frequency resolution of the recordings, but rather by the resolution of the stimulus current. The slope of the I/O curves gives an indication of the relative spatial spread of an electrode. The slopes of the I/O curves over the first 2 dB of stimulus currents were measured. It was found that the average ratio between the slopes of the modelled and EABR data were comparable for the bi-polar and tri-polar cases. This ratio

was a lot smaller for the monopolar case. This corresponds to the finding that the modelled monopolar widths were a lot narrower than EABR widths. The ratios are, however, fairly constant within a protocol. This shows that the model accurately predicts relative spatial spread within a protocol.

Some of the discrepancies in threshold values and spatial spreads between the EABR data and model data may be ascribed to the inherent differences between the EABR and modelled thresholds. EABR thresholds were obtained from normalized spike rates recorded from a population of neurons, whereas the model thresholds are obtained from single modelled auditory neurons. The modelled responses were obtained from modelled neurons coming directly from the cochlea whereas the EABR results were recorded in the inferior colliculus which is a more central process. Also the EABR thresholds are difficult to estimate because the EABR data includes spontaneous neural activity. Other discrepancies may also be due to the limited frequency and stimulus current resolution of the available neurophysiological data where stimulus was in some cases applied in 2 dB steps. The omission of an electrode carrier in the model also influences the results. An insulating carrier will cause lower thresholds because current shunting between electrodes is limited. Stimulus widths and electrode directionality will also be affected as current spreading perilymph is displaced. The holes made in some membranes through which the carrier protrudes may also not be perfectly sealed. This will cause current to be shunted to other structures and may also have an effect on measured thresholds.

The model is a valuable research tool for accurately estimating EABR characteristic frequencies of electrodes. Relative spatial and threshold values within the same electrode configuration may also be estimated, but estimating absolute thresholds and spatial spread may lead to incorrect results. This was investigated for an array with electrodes situated in different cochlear structures. The extent to which the modelled data compares to the EABR data of a subject with an array with electrodes situated in one cochlear structure was not investigated.

5.5 GENERAL DISCUSSION

It was shown that the method described in this study can be successfully used to create a model of a subject specific cochlea. When the electrodes of the subject are all within one cochlear structure (such as the scala tympani), the model predicts outcomes commonly found in literature. This includes the relative threshold values and spatial spread between stimulation protocols. This shows that the model may be used as a valid research tool. The model is also able to predict responses in more detail than models based on a generic cochlear morphology. This proves the hypothesis.

The extent to which the model can predict EABR responses of a specific subject with abnormal electrode insertion was also investigated. In this case the subject electrode array was located in different cochlear structures. It was found that the model predicted electrode characteristic frequencies accurately. Absolute thresholds between protocols were predicted higher by the model than was found using the EABR recordings. The model predicted threshold trends for electrodes located in the same cochlear structures correctly. No trends could be predicted between electrodes located in different cochlear structures. Absolute spatial spread was predicted relatively well for bi-polar and tri-polar stimulation protocols, where monopolar spatial spread was predicted a lot narrower than was found with the EABR recordings.

The initial results obtained from the model are promising. To further improve the extent to which the model can predict EABR data of a specific subject, refinements can be made to the model. This is described in the next section.

5.6 FUTURE WORK

The method developed in this study proved to be well suited to the modelling of a subject specific model. Future work includes the refinement of the model and the comparison of model outputs between different subjects.

5.6.1 Model refinement

Further refinements can be made to improve the accuracy of the predictions made by the model. To do this, the detail of the model geometry may be further improved to match the geometry of the subject cochlea more accurately.

The current model encases the entire cochlea in bone, whereas an actual guinea pig cochlea is surrounded by a thin bone layer inside the air-filled middle ear space on one side and fairly conductive neural tissue on the other side. This may have an effect on the potential distribution inside the cochlea. The results obtained from monopolar stimulation may be especially influenced as the return electrode is connected to the bone encasing. This may explain the wide monopolar spatial spreads elicited by the model. To investigate whether this is the case and what the effect of the shape of the bone has on the results, the bone should be modelled as it is found in the cochlea.

The hook area was not modelled to simplify the modelling process. This area may have an influence on current spread elicited by basal electrodes. Incorporating the hook area may increase the accuracy of the model.

The cochlear neurons were modelled at equal angles around the modiolus. In reality, the density of the cochlear neurons varies along the length of the cochlea. Rosenthal's canal is also abbreviated in the apical part of the cochlea (in humans) resulting a very few spiral ganglion cells present in that area. Incorporating the correct neuron densities in the model may lead to better comparisons of neural responses to EABR data.

The positions of the smaller interior cochlear structures were estimated from photomicrographs from other guinea pig subjects. To improve the accuracy of the model, histological sections should be obtained from the specific subject that is being modelled.

The electrode carrier was not modelled in the present study because its shape was not known. Modelling of the carrier will have an effect on the output of the model because it influences current flow inside the cochlea. A study by Snyder et. al. (2008) found that space filling arrays with carriers that match the shape of the scala, elicited more selective currents at lower thresholds than a non space filling array. This was because the carrier limited shunting of current between the contacts. By modelling the shape of the carrier, a more accurate current distribution inside the cochlea could be obtained. Capacitive effects between the electrode wires inside the carrier and the cochlear fluids may also have an effect on currents when short stimulus pulses are used and may also be incorporated into the model for more accurate results.

The present study assumed that when stimulated above threshold, each neuron contributed equally to the recorded EABR spike rate. This is not the case in a real subject as a neuron may produce increasing spike rates if the stimulus current is increased above threshold (Rattay, 1990). This is problematic since responses of neural populations are recorded. In these populations some neurons may be stimulated just above threshold and others far above threshold. As thresholds are determined as the current where a certain total spike rate is recorded, this may lead to incorrect assumptions as to which neurons are activated. Ideally single neuron responses should be recorded to accurately compare the EABR responses to the model output (single neurons were modelled). A model could also be incorporated to statistically determine the spread that would be recorded from a neural population in the inferior colliculus given the activated cochlear neurons.

During insertion of the electrode array, neurons were damaged where the array perforated the scala media. This has an effect on the neural response measured near the damaged area. The model assumes that all neurons are healthy. An accurate assessment of neuron damage and the implementation thereof in the model should increase the accuracy of the model response. Holes are also present in the membranes through which the carrier protrudes.

These holes may not perfectly seal around the carrier. This will cause current to be shunted to other cochlear structures and influence the current distribution in the cochlea. Modelling of these leaky holes may also improve the accuracy of the model output.

Defining subject specific impedance values of cochlear structures may improve the accuracy of the predicted current spread in the cochlea. Accuracy may also be improved my incorporating the anisotropic conductivities of structures such as the nerve fibres.

5.6.2 Modelling more subjects

In this study the cochlea of a single subject was modelled. To fully ascertain the strengths and weaknesses of the modelling method, more subjects should be modelled. This will allow a more objective measure of the validity of the modelling method as a research tool.

REFERENCES

Aschendorff, A., Kubalek, R., Hochmuth, A., Bink, A., Kurtz, C., Lohnstein, P., Klenzner, T. and Laszig, R. (2004). Imaging procedures in cochlear implant patients - Evaluation of different radiological techniques, *Acta Oto-Laryngologica, Supplement* **124**(552): 46-49.

Aschendorff, A., Kubalek, R., Turowski, B., Zanella, F., Hochmuth, A., Schumacher, M., Klenzner, T. and Laszig, R. (2005). Quality control after cochlear implant surgery by means of rotational tomography, *Otology and Neurotology* **26**(1): 34-37.

Balkany, T. J., Eshraghi, A. A. and Yang, N. (2002). Modiolar proximity of three perimodiolar cochlear implant electrodes, *Acta Otolaryngol* **122**: 363-369.

Bettman, R., Beek, E., Van Olphen, A., Zonneveld, F. and Huizing, E. (2004). MRI versus CT in assessment of cochlear patency in cochlear implant candidates, *Acta Oto-Laryngologica* **124**(5): 577-581.

Bierer, J. A. and Middlebrooks, J. C. (2004). Cortical Responses to Cochlear Implant Stimulation: Channel Interactions, *JARO - Journal of the Association for Research in Otolaryngology* **5**(1): 32-48.

Bierer, J. A. and Middlebrooks, J. C. (2002). Auditory cortical images of cochlear-implant stimuli: Dependence on electrode configuration, *Journal of Neurophysiology* **87**(1): 478-492.

Black, R. C., Clark, G. M. and Patrick, J. F. (1981). Current distribution measurements within the human cochlea, *IEEE Transactions on Biomedical Engineering* **28**(10): 721-725.

Black, R. C., Clark, G. M., Tong, Y. C. and Patrick, J. F. (1983). Current distributions in cochlear stimulation, *Annals of the New York Academy of Sciences* **405**: 137-145.

Blamey, P., Arndt, P., Bergeron, F., Bredberg, G., Brimacombe, J., Facer, G., Larky, J., Lindström, Nedzelski, J., Peterson, A., Shipp, D., Staller, S. and Whitford, L. (1996). Factors Affecting Auditory Performance of Postlinguistically Deaf Adults Using Cochlear Implants, *Audiology and Neuro-Otology* **1**(5): 293-306.

REFERENCES

Bonham, B. H. and Litvak, L. M. (2008). Current focusing and steering: Modeling, physiology, and psychophysics, *Hearing Research* **242**(1-2): 141-153.

Bouchard, M. E., Ouellet, C. and Cohen, H. (2009). Speech development in prelingually deaf children with cochlear implants, *Linguistics and Language Compass* **3**(1): 1-18.

Brackmann, D. E. (1976). The cochlear implant; basic principles, *Laryngoscope* **86**(3): 373-388.

Briaire, J. J. and Frijns, J. H. M. (2000). 3D mesh generation to solve the electrical volume conduction problem in the implanted inner ear, *Simulation Practice and Theory* **8**(1-2): 57-73.

Briaire, J. J. and Frijns, J. H. M. (2006). The consequences of neural degeneration regarding optimal cochlear implant position in scala tympani: A model approach, *Hearing Research* **214**(1-2): 17-27.

Brown, C. J., Abbas, P. J., Borland, J. and Bertschy, M. R. (1996). Electrically evoked whole nerve action potentials in ineraid cochlear implant users: Responses to different stimulating electrode configurations and comparison to psychophysical responses, *Journal of Speech, Language, and Hearing Research* **39**(3): 453-467.

Burnett, D. S. (1987). *Finite Element Analysis: From concepts to applications*, Addison-Wesley Publishing Company.

Caldemeyer, K. S., Sandrasegaran, L., Shinaver, C. N., Mathews, V. P., Smith, R. R. and Kopecky, K. K. (1999). Temporal Bone: Comparison of Isotropic Helical CT and Conventional DirectAxial and Coronal CT, *Americal Journal of Radiology* **172**: 1675-1682.

Chaturvedi, A., Mohan, C., Mahajan, S. B. and Kakkar, V. (2006). Imaging of cochlear implants, *Indian Journal of Radiology and Imaging* **16**(3): 385-392.

Chen, J. M., Farb, R., Hanusaik, L., Shipp, D. and Nedzelski, J. M. (1999). Depth and quality of electrode insertion: A radiologic and pitch scaling assessment of two cochlear implant systems, *American Journal of Otology* **20**(2): 192-197.

REFERENCES

Cheng, A. H. D. and Cheng, D. T. (2005). Heritage and early history of the boundary element method, *Engineering Analysis with Boundary Elements* **29**(3): 268-302.

Chiu, S. Y., Richie, J. M., Rogart, R. B. and Stagg, D. (1979). A quantitative description of membrane currents in rabbit myelinated nerve, *J.Physiol.* (292): 149-166.

Choi, C. T. M., Lai, W. D. and Chen, Y. B. (2004). Optimization of cochlear implant electrode array using genetic algorithms and computational neuroscience models, *IEEE Transactions on Magnetics* **40**(2 II): 639-642.

Chou, C. K. (2007). Thirty-five years in bioelectromagnetics research, *Bioelectromagnetics* **28**(1): 3-15.

Clough, R. W. (1990). Original formulation of the finite element method, *Finite Elements in Analysis and Design* **7**(2): 89-101.

Cohen, L. T., Saunders, E., Knight, M. R. and Cowan, R. S. C. (2006). Psychophysical measures in patients fitted with Contour and straight Nucleus electrode arrays, *Hearing Research* **212**(1-2): 160-175.

Cohen, L. T., Saunders, E. and Richardson, L. M. (2003). Spatial spread of neural excitation in cochlear implant recipients: comparison of improved ECAP method and psychophysical forward masking, *Hearing Research* **179**: 72-87.

Cohen, L. T., Xu, J., Xu, S. A. and Clark, G. M. (1996). Improved and simplified methods for specifying positions of the electrode bands of a cochlear implant array, *American Journal of Otology* **17**(6): 859-865.

Dawson, P. W., Blamey, P. J., Rowland, L. C., Dettman, S. J., Clark, G. M., Busby, P. A., Brown, A. M., Dowell, R. C. and Rickards, F. W. (1992). Cochlear implants in children, adolescents, and prelinguistically deafened adults: Speech perception, *Journal of Speech and Hearing Research* **35**(2): 401-417.

Drullman, R. and Bronkhorst, A. W. (2004). Speech perception and talker segregation: Effects of level, pitch, and tactile support with multiple simultaneous talkers, *Journal of the Acoustical Society of America* **116**(5): 3090-3098.

Fankhauser, D. B. (12-9-2008). Histology of the inner ear. http://biology.clc.uc.edu/fankhauser/Labs/Anatomy_&_Physiology/A&P202/Special_Senses/Ear/cochlear_nerve_40x_P2182170.JPG. Last accessed on 20 July 2009.

Fernandez, C. (1952). Dimensions of the Cochlea (Guinea Pig), *The Journal of the Acoustical Society of America* **24**(5): 519-523.

Finley, C. C., Holden, T. A., Holden, L. K., Whiting, B. R., Chole, R. A., Neely, G. J., Hullar, T. E. and Skinner, M. W. (2008). Role of electrode placement as a contributor to variability in cochlear implant outcomes, *Otology & neurotology : official publication of the American Otological Society, American Neurotology Society [and] European Academy of Otology and Neurotology* **29**(7): 920-928.

Firszt, J. B., Wackym, P. A., Gaggl, W., Burg, L. S. and Reeder, R. M. (2003). Electrically evoked auditory brain stem responses for lateral and medial placement of the Clarion HiFocus electrode, *Ear and Hearing* **24**(2): 184-190.

Fitzburg, R. (1969). Mathematical models of excitaions and propagation in nerve, *Biological Engineering* : 1-85.

Frankenhaeuser, B. and Huxley, A. F. (1964). The action potential in the myelinated nerve fiber of Xenopus laevis as computed on the basis of voltage clamp data, *J.Physiol.* (171): 302-315.

Friedland, D. R., Venick, H. S. and Niparko, J. K. (2003). Choice of ear for cochlear implantation: The effect of history and residual hearing on predicted postoperative performance, *Otology and Neurotology* **24**(4): 582-589.

Frijns, J. H. M., Briaire, J. J. and Grote, J. J. (2001). The importance of human cochlear anatomy for the results of modiolus-hugging multichannel cochlear implants, *Otology and Neurotology* **22**(3): 340-349.

Frijns, J. H. M., Briaire, J. J. and Schoonhoven, R. (2000). Integrated use of volume conduction and neural models to simulate the response to cochlear implants, *Simulation Practice and Theory* **8**(1-2): 75-97.

Frijns, J. H. M., de Snoo, S. L. and Schoonhoven, R. (1995). Potential distributions and neural excitation patterns in a rotationally symmetric model of the electrically stimulated cochlea, *Hearing Research* **87**(1-2): 170-186.

Geers, A., Tobey, E., Moog, J. and Brenner, C. (2008). Long-term outcomes of cochlear implantation in the preschool years: From elementary grades to high school, *International Journal of Audiology* **47**(SUPPL. 2).

Geuzaine, C. and Remacle, J. F. (2009). Gmsh: a three-dimensional finite element mesh generator with built-in pre- and post-processing facilities, *International Journal for Numerical Methods in Engineering* .

Ghiz, A. F., Salt, A. N., DeMott, J. E., Henson, M. M., Henson, J. and Gewalt, S. L. (2001). Quantitative anatomy of the round window and cochlear aqueduct in guinea pigs, *Hearing Research* **162**(1-2): 105-112.

Girzon, G. (1987). *Investigation of current flow in the inner ear during electrical stimulation of intracochlear electrodes*, Master's thesis, M.I.T.

Gray, H. and Lewis, W. H. (1918). *Anatomy of the human body*, 20 edn, Lea & Febiger, Philadelphia.

Greenwood, D. D. (1990). A cochlear frequency-position function for several species - 29 years later, *Journal of the Acoustical Society of America* **87**(6): 2592-2605.

Gupta, R., Bartling, S. H., Basu, S. K., Ross, W. R., Becker, H., Pfoh, A., Brady, T. and Curtin, H. D. (2004). Experimental Flat-Panel High-Spatial-Resolution Volume CT of the Temporal Bone, *Americal Journal of Neuroradiology* **25**: 1417-1424.

Hanekom, T. (2001b). Three-dimensional spiraling finite element model of the electrically stimulated cochlea, *Ear and Hearing* **22**(4): 300-315.

Hanekom, T. (2005). Modelling encapsulation tissue around cochlear implant electrodes, *Medical and Biological Engineering and Computing* **43**(1): 47-55.

Hanekom, T. (2001a). *Modelling of the eletrode-auditory nerve fibre interface in cochlear prosthesis*, PhD thesis, University of Pretoria.

Hartmann, R. and Klinke, R. (1990). Impulse patterns of auditory nerve fibres to extra- and intracochlear electrical stimulation, *Acta Oto-Laryngologica, Supplement* (469): 128-134.

Hartmann, R., Topp, G. and Klinke, R. (1984). Discharge patterns of cat primary auditory fibers with electrical stimulation of the cochlea, *Hearing Research* **13**: 47-62.

Hassanzadeh, S., Farhadi, M., Daneshi, A. and Emamdjomeh, H. (2002). The effects of age on auditory speech perception development in cochlear-implanted prelingually deaf children, *Otolaryngology - Head and Neck Surgery* **126**(5): 524-527.

Hodgkin, A. L. and Huxley, A. F. (1952). A quantitative description of membrane current and its application to conduction and excitation in nerve, *J.Physiol.* (117): 500-544.

Hofman, R., Segenhout, J. M. and Wit, H. P. (2009). Three-dimensional reconstruction of the guinea pig inner ear, comparison of OPFOS and light microscopy, applications of 3D reconstruction, *Journal of Microscopy* **233**(2): 251-257.

Jiang, M., Wang, G., Skinner, M. W., Rubinstein, J. T. and Vannier, M. W. (2003). Blind deblurring of spiral CT images, *IEEE transactions on medical imaging* **22**(7): 837-845.

Jolly, C. N., Spelman, F. A. and Clopton, B. M. (1996). Quadrupolar stimulation for cochlear prostheses: Modeling and experimental data, *IEEE Transactions on Biomedical Engineering* **43**(8): 857-865.

Kaste, S. C., Young, C. W., Holmes, T. P. and Baker, D. K. (1997). Effect of helical CT on the frequency of sedation in pediatric patients, *Americal Journal of Radiology* **168**(4): 1001-1003.

Ketten, D. R., Skinner, M. W., Wang, G., Vannier, M. W., Gates, G. A. and Neely, G. J. (1998). In vivo measures of cochlear length and insertion depth of nucleus cochlear implant electrode arrays, *Ann Otol Rhinol Laryngol* **107**: 1-16.

Kim, H. N., Shim, Y. J., Chung, M. H., Chang, M. S. and Choi, H. S. (1997). Comparison of speech discrimination scores between SPEAK and MPEAK speech-processing strategies, *Advances in oto-rhino-laryngology* **52**: 110-112.

Klop, W. M. C., Briaire, J. J., Stiggelbout, A. M. and Frijns, J. H. M. (2007). Cochlear implant outcomes and quality of life in adults with prelingual deafness, *Laryngoscope* **117**(11): 1982-1987.

Koizuka, I., Seo, Y., Murakami, M., Seo, R. and Kato, I. (1997). Micro-magnetic resonance imaging of the inner ear in the guinea pig, *NMR in Biomedicine* **10**(1): 31-34.

Kral, A., Hartmann, R., Mortazavi, D. and Klinke, R. (1998). Spatial resolution of cochlear implants: The electrical field and excitation of auditory afferents, *Hearing Research* **121**(1-2): 11-28.

Kunisue, K., Fukushima, K., Kawasaki, A., Maeda, Y., Nagayasu, R., Kataoka, Y., Kariya, S., Fukutomi, Y., Takami, H. and Nishizaki, K. (2007). Comprehension of abstract words among hearing impaired children, *International journal of pediatric otorhinolaryngology* **71**(11): 1671-1679.

Kwon, B. J. and Van Den Honert, C. (2006). Effect of electrode configuration on psychophysical forward masking in cochlear implant listeners, *Journal of the Acoustical Society of America* **119**(5): 2994-3002.

Lane, J. I., Driscoll, C. W. L., Witte, R. J., Primak, A. and Lindell, E. P. (2007). Scalar Localization of the Electrode Array After Cochlear Implantation: A Cadaveric Validation Study Comparing 64-Slice Multidetector Computed Tomography With Microcomputed Tomography, *Otology & Neurotology* **28**: 191-194.

Lim, H. H., Tong, Y. C. and Clark, G. M. (1989). Forward masking patterns produced by intracochlear electrical stimulation of one and two electrode pairs in the human cochlea, *Journal of the Acoustical Society of America* **86**(3): 971-980.

Lim, S. L., Park, S., Kim, Y. H., Oh, S. H. and Kim, S. J. (2005). Three-dimensional analysis of electrode behavior in a human cochlear model, *Medical Engineering & Physics* **27**(8): 695-703.

Liu, B., Gao, X. L., Yin, H. X., Luo, S. Q. and Lu, J. (2007). A detailed 3D model of the guinea pig cochlea, *Brain Structure and Function* **212**(2): 223-230.

Loizou, P. C., Stickney, G., Mishra, L. and Assmann, P. (2003). Comparison of speech processing strategies used in the Clarion implant processor, *Ear and Hearing* **24**(1): 12-19.

Luker, G. D., Lee, B. C. P. and Erickson, K. K. (2007). Spiral CT of the temporal bone in unsedated pediatric patients, *Americal Journal of Neuroradiology* **14**: 1145-1150.

Majdani, O., Leinung, M., Rau, T., Akbarian, A., Zimmerling, M., Lenarz, M., Lenarz, T. and Labadie, R. (2008). Demagnetization of cochlear implants and temperature changes in 3.0T MRI environment, *Otolaryngology - Head and Neck Surgery* **139**(6): 833-839.

McCreery, D., Lossinsky, A. and Pikov, V. (2007). Performance of multisite silicon microprobes implanted chronically in the ventral cochlear nucleus of the cat, *IEEE Transactions on Biomedical Engineering* **54**(6): 1042-1052.

Michelson, R. P., Merzenich, M. M., Pettit, C. R. and Schindler, R. A. (1973). A cochlear prosthesis: Further clinical observations; preliminary results of physiological studies, *Laryngoscope* **83**(7): 1116-1122.

Middlebrooks, J. C. and Snyder, R. L. (2007). Auditory prosthesis with a penetrating nerve array, *JARO - Journal of the Association for Research in Otolaryngology* **8**(2): 258-279.

Middlebrooks, J. C. and Snyder, R. L. (2008). Intraneural stimulation for auditory prosthesis: Modiolar trunk and intracranial stimulation sites, *Hearing Research* **242**(1-2): 52-63.

Mosnier, I., Sterkers, O., Bebear, J. P., Godey, B., Robier, A., Deguine, O., Fraysse, B., Bordure, P., Mondain, M., Bouccara, D., Bozorg-Grayeli, A., Borel, S., Ambert-Dahan, E. and Ferrary, E. (2009). Speech performance and sound localization in a complex noisy environment in bilaterally implanted adult patients, *Audiology and Neurotology* **14**(2): 106-114.

Nadol Jr., J. B. (1990). Degeneration of cochlear neurons as seen in the spiral ganglion of man, *Hearing Research* **49**: 141-154.

Nadol Jr., J. B. and Eddington, D. K. (2004). Histologic evaluation of the tissue seal and biologic response around cochlear implant electrodes in the human, *Otology and Neurotology* **25**(3): 257-262.

O'Leary, S. J., Black, R. C. and Clark, G. M. (1985). Current distributions in the cat cochlea: A modelling and electrophysiological study, *Hearing Research* **18**(3): 273-281.

Plonsey, R. and Barr, R. C. (2000). *Bioelectricity A Quantitative Approach*, Second edn, Kluwer Academic/Plenum Publishers, New York.

Postnov, A., Zarowski, A., De Clerck, N., Vanpoucke, F., Offeciers, F. E., Van Dyck, D. and Peeters, S. (2006). High resolution micro-CT scanning as an innovatory tool for evaluation of the surgical positioning of cochlear implant electrodes, *Acta Oto-Laryngologica* **126**(5): 467-474.

Poznyakovskiy, A. A., Zahnert, T., Kalaidzidis, Y., Schmidt, R., Fischer, B., Baumgart, J. and Yarin, Y. M. (2008). The creation of geometric three-dimensional models of the inner ear based on micro computer tomography data, *Hearing Research* **243**(1-2): 95-104.

Rattay, F. (1990). *Electrical Nerve Stimulation*, Springer-Verlag Wien.

Rattay, F., Leao, R. N. and Felix, H. (2001). A model of the electrically excited human cochlear neuron. II. Influence of the three-dimensional cochlear structure on neural excitability, *Hearing Research* **153**(1-2): 64-79.

Rattay, F., Lutter, P. and Felix, H. (2001). A model of the electrically excited human cochlear neuron I. Contribution of neural substructures to the generation and propagation of spikes, *Hearing Research* **143**: 43-63.

Rebscher, S. J., Hetherington, A. M., Snyder, R. L., Leake, P. A. and Bonham, B. H. (2007). Design and fabrication of multichannel cochlear implants for animal research, *Journal of Neuroscience Methods* **166**(1): 1-12.

REFERENCES

Rebscher, S. J., Snyder, R. L. and Leake, P. A. (2001). The effect of electrode configuration and duration of deafness on threshold and selectivity of responses to intracochlear electrical stimulation, *Journal of the Acoustical Society of America* **109**(5 I): 2035-2048.

Roland, J. T., Fishman, A. J., Alexiades, G. and Cohen, N. L. (2000). Electrode to modiolus proximity: a fluoroscopic and histologic analysis, *American Journal of Otolaryngology* **21**: 218-225.

Rose, J. E., Greenwood, D. D., Goldberg, J. M. and Hind, J. E. (1963). Some Discharge Characteristics of Single Neurons in the Inferior Colliculus of the Cat. I. Tonotopical Organization, Relation of Spike-Counts to Tone Intensity, and Firing Patterns of Single Elements, *Journal of Neurophysiology* **26**(2): 294-320.

Rübenkönig, O. (2007). The Finite Volume Method (FVM) - An introduction. http://www.imtek.uni-freiburg.de/simulation/mathematica/IMSweb/imsTOC/Lectures and Tips/Simulation I/FVM_introDocu.html. Last accessed on 19 June 2009.

Rubinstein, J. T., Parkinson, W. S., Tyler, R. S. and Gantz, B. J. (1999). Residual speech recognition and cochlear implant performance: Effects of implantation criteria, *American Journal of Otology* **20**(4): 445-452.

Sakata, M., Hareyama, M., Heil, T. A., Henson, M. M., Henson Jr., O. W., Webber, R. L., Nair, M. K. and Smith, D. W. (2007). High-Resolution in situ Imaging of Cochlear Implant Electrode Arrays in Cat Temporal Bones Using Tuned Aperture Computed Tomography (TACT®), *Ear and Hearing* **28**: 435-443.

Salt, A. N., Henson, M. M., Gewalt, S. L., Keating, A. W., DeMott, J. E. and Henson, J. (1995). Detection and quantification of endolymphatic hydrops in the guinea pig cochlea by magnetic resonance microscopy, *Hearing Research* **88**(1-2): 79-86.

Schorr, E. A., Roth, F. P. and Fox, N. A. (2009). Quality of life for children with cochlear implants: Perceived benefits and problems and the perception of single words and emotional sounds, *Journal of Speech, Language, and Hearing Research* **52**(1): 141-152.

Schuknecht, H. F. (1993). *Pathology of the Ear,* Lea & Febiger, Philadelphia.

Schwartz, J. R. and Eikhof, G. (1987). Na currents and action potentials in rat myelinated nerve fibres at 20 and 37 degrees C, *Pflug.Arch.* (409): 469-577.

Seemann, M. D., Seemann, O., Bon, H., Suckfüll, M. and Englmeier, K. H. (1999). Evaluation of the middle and inner ear structures: comparison of hybrid rendering, virtual endoscopy and axial 2D source images, *European Radiology* **9**: 1851-1858.

Seeram, E. (2001). *Computed Tomography: Physical principles, clinical applications and quality control*, 2nd edn, Saunders, Philadelphia.

Shepherd, R. K., Hatsushika, S. and Clark, G. M. (1993). Electrical stimulation of the auditory nerve: The effect of electrode position on neural excitation, *Hearing Research* **66**(1): 108-120.

Shibata, T., Matsumoto, S., Agishi, T. and Nagano, T. (2009). Visualization of Reissner membrane and the spiral ganglion in human fetal cochlea by micro-computed tomography, *American Journal of Otolaryngology - Head and Neck Medicine and Surgery* **30**(2): 112-120.

Shivdasani, M. N., Mauger, S. J., Rathbone, G. D. and Paolini, A. G. (2008). Inferior colliculus responses to multichannel microstimulation of the ventral cochlear nucleus: Implications for auditory brain stem implants, *Journal of Neurophysiology* **99**(1): 1-13.

Simmons, F. B. (1966). Implants, *Archives of Otolaryngology* **84**(2).

Skinner, M. W., Holden, L. K., Whitford, L. A., Plant, K. L., Psarros, C. and Holden, T. A. (2002a). Speech recognition with the Nucleus 24 SPEAK, ACE, and CIS speech coding strategies in newly implanted adults, *Ear and Hearing* **23**(3): 207-223.

Skinner, M. W., Ketten, D. R., Holden, L. K., Harding, G. W., Smith, P. G., Gates, G. A., Neely, G. J., Kletzker, G. R., Brunsden, B. and Blocker, B. (2002b). CT-Derived Estimation of Cochlear Morphology and Electrode Array Position in Relation to Word Recognition in Nucleus-22 Recipients, *Journal of the Association of Research in Otolaryngology* **3**: 332-350.

Skpizner, B. A., Holliday, R. A., Roland, J. T., Cohen, N. L., Waltzman, S. B. and Shapiro, W. H. (1995). Postoperative Imaging of the Multichannel Cochlear Implant.pdf, *Americal Journal of Neuroradiology* **16**: 1517-1524.

Snyder, R. L., Bierer, J. A. and Middlebrooks, J. C. (2004). Topographic spread of inferior colliculus activation in response to acoustic and intracochlear electric stimulation, *JARO - Journal of the Association for Research in Otolaryngology* **5**(3): 305-322.

Snyder, R. L., Middlebrooks, J. C. and Bonham, B. H. (2008). Cochlear implant electrode configuration effects on activation threshold and tonotopic selectivity, *Hearing Research* **235**(1-2): 23-38.

Snyder, R. L., Rebscher, S. J., Cao, K., Leake, P. A. and Kelly, K. (1990). Chronic intracochlear electrical stimulation in the neonatally deafened cat. I: Expansion of central representation, *Hearing Research* **50**(1-2): 7-34.

Sorn, P. M. and Curtin, H. D. (1996). *Head and neck imaging*, 3 edn, Mosby-Year Book, St. Louis.

Spahr, A. J., Litvak, L. M., Dorman, M. F., Bohanan, A. R. and Mishra, L. N. (2008). Simulating the effects of spread of electric excitation on musical tuning and melody identification with a cochlear implant, *Journal of Speech, Language, and Hearing Research* **51**(6): 1599-1606.

Strelioff, D. (1973). A computer simulation of the generation and distribution of cochlear potentials, *Journal of the Acoustical Society of America* **54**(3): 620-629.

Suesserman, M. F. and Spelman, F. A. (1993). Lumped-parameter model for in vivo cochlear stimulation, *IEEE Transactions on Biomedical Engineering* **40**(3): 237-245.

Sun, Q., Chang, K. H., Dormer, K. J., Dyer, J. and Gan, R. Z. (2002). An advanced computer-aided geometric modeling and fabrication method for human middle ear, *Medical Engineering and Physics* **24**(9): 595-606.

Swartz, J. D. (1989). Current imaging approach to the ternporal bone, *Radiology* **171**: 309-317.

Sweeney, J. D., Mortimer, J. T. and Durand, D. (1987). Modeling of mammilian myelinated nerve for functional neuromuscular electrostimulation, *IEEE 9-th ann.conf.Eng.Med.Biol.Soc.Boston* : 1577-1578.

Teufert, K. B., Linthicum, J. and Connell, S. S. (2006). The effect of organ of Corti loss on ganglion cell survival in humans, *Otology and Neurotology* **27**(8): 1146-1151.

Thorne, M., Salt, A. N., DeMott, J. E., Henson, M. M., Henson, J. and Gewalt, S. L. (1999). Cochlear fluid space dimensions for six species derived from reconstructions of three-dimensional magnetic resonance images, *Laryngoscope* **109**(10): 1661-1668.

Van Den Honert, C., Finley, C. C. and Xue, S. (1997). Microstimulation of auditory nerve for estimating cochlear place of single fibers in a deaf ear, *Hearing Research* **113**(1-2): 140-154.

Van Den Honert, C. and Kelsall, D. C. (2007). Focused intracochlear electric stimulation with phased array channels, *Journal of the Acoustical Society of America* **121**(6): 3703-3716.

Van Den Honert, C. and Stypulkowski, P. H. (1987). Single fiber mapping of spatial excitation patterns in the electrically stimulated auditory nerve, *Hearing Research* **29**(2-3): 207-222.

Verbist, B. M., Frijns, J. H. M., Geleijns, J. and van Buchem, M. A. (2005). Multisection CT as a Valuable Tool in the Postoperative Assessment of Cochlear Implant Patients, *Americal Journal of Neuroradiology* **26**: 424-429.

Vincent, C., Ruzza, I., Vaneecloo, F. M. and Dubrulle, F. (2008). Magnetic resonance imaging with the Digisonic SP Neurelec cochlear implant, *European Archives of Oto-Rhino-Laryngology* **265**(9): 1043-1046.

Voie, A. H. (2002). Imaging the intact guinea pig tympanic bulla by orthogonal-plane fluorescence optical sectioning microscopy, *Hearing Research* **171**(1-2): 119-128.

Voie, A. H. and Spelman, F. A. (1995). Three-dimensional reconstruction of the cochlea from two-dimensional images of optical sections, *Computerized Medical Imaging and Graphics* **19**(5): 377-384.

Voie, A. H. and Spelman, F. A. (1990). Analysis of the guinea pig cochlea using a general cylindrical coordinate system, *Proceedings of the Annual Conference on Engineering in Medicine and Biology, 1 November 1990, Seattle*, IEEE, pp. 206-207.

Vollmer, M., Beitel, R. E., Snyder, R. L. and Leake, P. A. (2007). Spatial selectivity to intracochlear electrical stimulation in the inferior colliculus is degraded after long-term deafness in cats, *Journal of Neurophysiology* **98**(5): 2588-2603.

Wada, H., Sugawara, M., Kobayashi, T., Hozawa, K. and Takasaka, T. (1998). Measurement of guinea pig basilar membrane using computer-aided three- dimensional reconstruction system, *Hearing Research* **120**(1-2): 1-6.

Wang, G., Vannier, M. W., Skinner, M. W., Cavalcanti, G. P. and Harding, G. W. (1998). Spiral CT Image Deblurring for Cochlear Implantation, *IEEE transactions on medical imaging* **17**(2): 251-262.

Wang, G., Vannier, M. W., Skinner, M. W., Kalender, W. A., Polacin, A. and Ketten, D. R. (1996). Unwrapping Cochlear Implants by Spiral CT, *IEEE Transactions on Biomedical Engineering* **43**(9): 891-900.

Wang, H., Northrop, C., Burgess, B., Liberman, M. C. and Merchant, S. N. (2006). Three-dimensional virtual model of the human temporal bone: A stand-alone, downloadable teaching tool, *Otology and Neurotology* **27**(4): 452-457.

Whiting, B. R., Bae, K. T. and Skinner, M. W. (2001). Cochlear Implants: Three-dimensional Localization by Means of Coregistration of CT and Conventional Radiographs, *Radiology* **221**: 543-549.

Xu, J., Stevenson, A. W., Gau, D., Tykocinski, M., Lawrence, D., Wilkins, S. W., Clark, G. M., Saunders, E. and Cowan, R. S. (2001). The role of radiographic phase-contrast imaging in the development of intracochlear electrode arrays, *Otol Neurotol* **22**: 862-868.

Xu, J., Xu, S. A., Cohen, L. T. and Clark, G. M. (2000). Cochlear view: Postoperative radiography for cochlear implantation, *American Journal of Otology* **21**(1): 49-56.

Yang, S., Wang, G., Skinner, M. W., Rubinstein, J. T. and Vannier, M. W. (2000). Localization of cochlear implant electrodes in radiographs, *Medical Physics* **27**(4): 775-777.

Yin, H. X., Zhao, T., Liu, B., Shu, H., Huang, Z. F., Gao, X. L., Zhu, P. P., Wu, Z. Y. and Luo, S. Q. (2007). Visualization of guinea pig cochleae with computed tomography of diffraction enhanced imaging and comparison with histology, *Journal of X-Ray Science and Technology* **15**(2): 73-84.

ADDENDUM A

A.1. GMSH PARAMETERS

GMSH 2.3.0 was used to create the cochlear mesh. The cochlear structure was implemented using GMSH code and saved as a .geo file. GMSH was set up using the settings in Table A.1. to handle the geometry. Table A.2 lists the settings used to set up the meshing routine in GMSH.

Table A.1. Geometry settings used in GMSH.

General settings	
Geometry tolerance	1E-06
Remove duplicate entities in GEO models	Checked
Remove small edges in OpenCascade models	Checked
Remove small faces in OpenCascade models	Checked
Sew faces in OpenCascade models	Unchecked

Table A.2. Settings used in GMSH to set up the meshing routine.

General settings	
2D algorithm	MeshAdapt+Delaunay
3D algorithm	Netgen
Subdivision algorithm	None
Smoothing steps	1
Element size factor	1.00
Minimum element size	0
Maximum element size	1E+22
Element order	1
Use incomplete high order elements	Checked
Advanced settings	
Compute elements sizes using point values	Checked
Compute element sizes from curvature	Unchecked
Extend element sizes from boundary	Checked
Optimize quality of tetrahedra	Unchecked
Optimize quality of tetrahedra with Netgen	Unchecked
Optimize high order mesh (2D-plane only)	Unchecked
Impose C1 continuity (2D-plane only)	Unchecked

A.2. COMSOL PARAMETERS

After meshing with GMSH, the mesh was saved in the Nastran format and imported into Comsol. Comsol Multiphysics 3.5a was used to perform the FEM analysis.

The parameters used to import the mesh into Comsol are listed in Table A.3. The solver was set up using the parameters listed in Table A.4.

Table A.3. Parameters used in Comsol to import the mesh.

Import file type	NASTRAN
General settings	
Partition mesh according to material information	Checked
Face partitioning settings	
Max angle between boundary elements	360°
Max angle between neighboring boundary elements	20.053°
Remove small faces	0.01

Table A.4. Solver parameters used in Comsol.

Solver type	Stationary
General settings	
Linear system solver	Conjugate gradients
Preconditioner	Algebraic multigrid
Quality of multigrid hierarchy	3
Matrix symmetry	Automatic
Stationary settings	
Linearity	Automatic
Relative tolerance	1.0E-6
Maximum number of iterations	25
Method	Damped Newton
Advanced settings	
Constraint handling method	Elimination
Null-space function	Automatic
Assembly block size	Auto
Stop if error due to undefined operation	Checked
Solution form	Automatic
Type of scaling	Automatic
Row equilibration	On